PREDICTION AND INTERPRETATION OF INFRARED SPECTRA

BY

KUHALIM B. KUBULAT

A DISSERTATION PRESENTED TO THE GRADUATE SCHOOL
OF THE UNIVERSITY OF FLORIDA IN
PARTIAL FULFILLMENT OF THE REQUIREMENTS
FOR THE DEGREE OF DOCTOR OF PHILOSOPHY

UNIVERSITY OF FLORIDA

1989

TO MY LATE MOTHER DERYAH BTE ABDULLAH
MY FATHER KU BULAT B KU ALI
MY SISTER MINAH BTE ISHAK
MY BROTHER KU AZLAN B KU BULAT
AND
MY WIFE SURAYA BTE IBRAHIM

ACKNOWLEDGEMENTS

I would like to express my sincerest appreciation to the chairman of my supervisory committee, Dr. Willis B. Person, for his guidance and suggestions which have contributed much to the formulation and performance of the research. His inspiration and persuasion have been the foundation of this study. Without his untiring help and encouragement this dissertation would not have been possible. Thanks are extended also to Dr. Alan Katritzky, Dr. William Weltner, Jr., Dr. Robert J. Hanrahan, and Dr. Thomas Bailey for their friendly help and for their participation on the supervisory committee.

I owe an extreme debt of gratitude to Dr. Carlos Sosa of the Quantum Theory Project (University of Florida) for the provision of the *ab initio* force constants and polar tensors for the whole series of molecules used in this study, and for his friendship and his priceless help over the years.

I would like to thank the past and present members of Dr. Person's research group and my colleagues in the Chemistry Department for their friendship and support. In doing this work I have also had the privilege of working with some of the leading experts of the world in theoretical and experimental physical chemistry: Dr. J. S. Kwiatkowski, Dr. K. Szczepaniak, Dr. M. Szczesniak, and Dr. R. J. Bartlett. It was Dr. J. S.

Kwiatkowski who taught me to use the GAUSSIAN programs. Dr. K. Szczepaniak has always providing helpful suggestions and encouragement. Each and every one of them in their own special way have assisted me in understanding the "heart and soul" of physical chemistry.

We are grateful for computer support provided jointly by the Center for Instructional and Research Computing Activities (CIRCA) and Northeast Regional Data Center (NERDC), which made the implementation of this study possible.

I extend my sincere appreciation to the Government of Malaysia and University Kebangsaan Malaysia, especially the Department of Chemistry, for providing part of the financial support and for granting the leave of absence required for the program. In addition, financial support from several different research grants is gratefully acknowledged. These grants include: GPA Project No. 831; CRDEC Contract DAAA15-85-C-0034; and especially NIH Research Grant No. 32988.

Thanks are also due to all the friends I made in Gainesville for making my graduate education at the University of Florida the happiest and most satisfying time of my life.

I am deeply grateful for the loving support and understanding given to me by my wife, Suraya, and by my parents - who stood behind me patiently during the long period of my graduate studies.

TABLE OF CONTENTS

Page

ACKNOWLEDGEMENTS.................................... iii

ABSTRACT.. ix

CHAPTER

1 INTRODUCTION.................................. 1

1.1 Perspective.......................... 1

1.2 Historical Perspective of the Molecules Studied.................. 4

1.3 Theoretical Determination of Vibrational Frequencies............ 9

1.4 Theoretical Determination of Vibrational Intensities............ 11

1.5 Preview of the Present Study......... 12

2 TECHNIQUES.................................... 15

2.1 Ab Initio Calculations............... 16
2.1.1 Geometry Optimizations........ 16
2.1.2 Calculation of Harmonic Force Constants............. 17
2.1.3 Calculation of Polar Tensors.. 21

2.2 Determination of Vibrational Frequencies........................ 22
2.2.1 Using Mass-Weighted Cartesian Coordinates................. 23
2.2.2 Using Symmetrized-Internal Coordinates................. 24

2.3 Determination of Vibrational Intensities........................ 29
2.3.1 Using Mass-Weighted Cartesian Coordinates................. 29

2.3.2 Using Symmetrized-Internal Coordinates.................. 32
2.4 Potential Energy Distribution Analysis........................... 32

2.5 Contribution to Intensities.......... 34

3 SYSTEMATIC SUMMARY OF RESULTS............... 37

3.1 Geometries........................... 39

3.2 Effect of Basis Set on the Prediction of Vibrational Spectra of Molecules in the XCH_2CH_2SH series............................ 45
3.2.1 trans-Ethanethiol............. 45
3.2.2 trans-Chloroethanethiol....... 54

3.3 Comparison of Vibrational Spectra Predicted for trans-Ethanethiol with that for gauche-Ethanethiol... 61

3.4 Prediction of Infrared Spectra of Molecules in the $XCH_2CH_2SCH_2CH_2X$ Series............................ 68

4 DIRECT TRANSFER OF VIBRATIONAL PARAMETERS... 117

4.1 Choosing the Vibrational Coordinates for Force Constants................ 119

4.2 Procedure for Transferring Force Constants and Atomic Polar Tensors............................ 122

4.3 Comparison of Vibrational Spectra Predicted by Transfer of Parameters with those Predicted from Direct Ab Initio Calculations. 124
4.3.1 Diethyl Sulfide............... 124
4.3.2 2,2'-Dichlorodiethyl Sulfide.. 128

5 SCALING OF THE QUANTUM MECHANICAL FORCE FIELD..................................... 151

5.1 Scaling Procedure................... 152

5.2 Survey of Results................... 153

6 PREDICTION OF INFRARED SPECTRA USING A SCALED-TRANSFERABLE FORCE FIELD WITH DIRECT TRANSFER OF POLAR TENSORS.......... 162

6.1 Diethyl Sulfide..................... 163

6.2 2,2'-Dichlorodiethyl Sulfide......... 165

7 PARTITION OF POLAR TENSOR INVARIANTS........ 183

7.1 Introduction to Principal Component Analysis........................... 183

7.2 Definitions of the Invariants........ 186

7.3 Application of Principal Component Analysis in Partitioning the Invariants.......................... 189
7.3.1 Carbon Invariants............. 190
7.3.2 Hydrogen Invariants........... 193

7.4 Similarities and Differences of Polar Tensors Calculated at Two Different Levels................... 196
7.4.1 Carbon Polar Tensors.......... 196
7.4.2 Hydrogen Polar Tensors........ 198

7.5 Comments on the Atom Anisotropy, Effective Charges, and Mean Dipole Moment Derivatives in Vibrational Intensity Analysis..... 200

8 SUMMARY.................................... 213

APPENDICES

A FLOWCHARTS OF ICA1 PROGRAM.................. 220

B FLOWCHARTS OF ICA2 PROGRAM.................. 224

C COMPONENTS OF DIPOLE MOMENT DERIVATIVES WITH RESPECT TO INTERNAL COORDINATE (P_R) FOR 2-CHLOROETHANETHIOL CALCULATED AT THE 6-31G** LEVEL........................ 229

D INVARIANTS OF ATOMIC POLAR TENSORS.......... 230

E MULLIKEN NET ATOMIC CHARGES................. 243

F VALUES OF ALPHA [OR $(\sqrt{2/3})\beta/X$].............. 246

G VALUES OF GAMMA (OR $\bar{P}/X$).................... 249

REFERENCES.. 252

BIOGRAPHICAL SKETCH................................. 258

Abstract of Dissertation Presented to the Graduate School of
the University of Florida in Partial Fulfillment of the
Requirements for the Degree of Doctor of Philosophy

PREDICTION AND INTERPRETATION OF INFRARED SPECTRA

BY

KuHalim B. KuBulat

May 1989

Chairman: Willis B. Person
Major Department: Chemistry

Ab initio self-consistent field molecular orbital methods with a split-valence basis set (3-21G) were used by Carlos Sosa of the Quantum Theory Project, University of Florida, to calculate the geometrical parameters, atomic polar tensors, and vibrational force constants for the XCH_2CH_2SH and $XCH_2CH_2SCH_2CH_2X$ (X = H, Cl) series of molecules. He had also performed additional calculations at a higher level (a 6-31G** basis set, which includes polarization functions on all atoms) for the XCH_2CH_2SH series of molecules.

Because these calculations have been so successful in predicting the values for these parameters, it was believed to be worth while to examine the predicted vibrational parameters in much more detail. In order to do so, normal coordinate programs were used to obtain the potential energy distributions (PEDs) as well as the contributions to vibrational frequencies and infrared intensities for all the normal modes. The calculated results were calibrated by comparison with experimental data whenever possible.

Since a heavy atom, S, isolates the two halves of the large molecules, the transferability of vibrational parameters such as internal coordinate force constants and atomic polar tensors from smaller model compounds to the larger molecules worked very well for this system.

The systematic disagreement between the calculated frequencies and the experimental values led us to propose a set of nine scaling factors to be applied to calculated force constants for each basis set. The proposed scaling factors, remarkably, reproduce the experimental frequencies within less than 1%.

Techniques for analysis of the intensity contribution were developed and then were used through out the dissertation to examine the disagreements in the intensities predicted with two different basis sets.

Principal component analysis (PCA) methods were introduced to summarize the similarities and differences between the polar tensor invariants for the small model compounds and for the larger molecules, and also to extract the invariants whose value are sensitive to changes in the basis sets.

CHAPTER 1
INTRODUCTION

1.1 Perspective

The infrared spectrum of a compound may supply two principal types of information relative to the structure of the molecule and the forces between the atoms: the values of the fundamental frequencies and the intensities of the associated bands in this spectrum.

The values of the frequencies have been and are still extensively used in the investigation of the vibrational dynamics of the molecule. The potential energy is usually expressed as a function of parameters (force constants) which can be evaluated from the experimental frequencies or, under particular conditions, can be transferred from other molecules. In many cases it is possible to derive a common force field which accounts for the fundamental frequencies of a whole series of compounds (overlay technique) (1).

Just as the frequencies are functions of the force constants, the intensities can be thought of as a functions of parameters which represent the electrical behavior of the molecule during the vibrational motion. There are at least two kinds of parameters that can be chosen to represent this phenomenon, including (i) the change in the total dipole moment with a change in the internal or symmetry coordinates (dipole moment derivatives) or (ii) the change of the total dipole moment with respect to displacements of each atom expressed in its cartesian coordinates (atomic polar tensors). These intensity parameters are then interpreted in terms of bond moment parameters (2) extended perhaps to "charge" and "charge flux" contributions (3-6). Another approach to the interpretation of intensity parameters has been given by the Soviet workers (7). The concept of atomic polar tensors (APTs) was first introduced by Biarge, Herranz, and Morcillo (8), and later reformulated by Person and Newton (9); a review of the use of these parameters has been published by Person (2). Since one advantage of the APT parameters is that they are calculated directly from ab initio quantum mechanical calculations of the vibrational spectra, we shall adopt their use here.

In recent years the implementation of analytic gradient techniques for quantum mechanical self-consistent field (SCF) and correlated energies as well as other ground state molecular properties has proven invaluable for prediction also of vibrational frequencies and infrared intensities. At the present time calculations of harmonic frequencies at a level that includes correlation effects are generally limited to small and medium size molecules (10). Calculations at the SCF level with a reasonable basis set such as 3-21G, 3-21G* or

6-31G** (11) generally gives predicted frequencies (wavenumbers) about 10% greater than experimental values. The agreement between the predicted and experimental frequencies can be improved by scaling the theoretical values (12). The scale factor (usually about 0.89 (13)) approximates the effects of correlation corrections as well as the effects of anharmonicity. This allows the prediction of vibrational frequencies for large polyatomic systems such as the $XCH_2CH_2SCH_2CH_2X$ series of molecules (13) and provides a guide to the interpretation of vibrational spectra for such complicated molecules.

We shall see that quantum chemical data, if used judiciously, can significantly improve our knowledge of force fields. Nevertheless, the accuracy of the calculations for the dominant force constants is still poor if compared to the high accuracy of spectroscopic measurements. Less dominant force constants are, however, usually more accurately determined from theory than from experiment (12). This complementarity of the theoretical and experimental information suggests the joint use of both if there is at least some experimental information available.

The predicted infrared intensities depend not only on the intensity parameters (APTs) as discussed above, but also on the normal coordinates determined from the calculated force constants. One of our purposes in this work is to examine these two effects separately and try to determine the magnitude of each error in contributing to the errors in the final calculated intensities.

1.2 Historical Perspective of the Molecules Studied

Chemical warfare (15) began in 1915 during World War I when chemicals such as chlorine, phosgene and later mustard gas were used against the British forces. During World War II, although nerve agents containing phosphorus such as tabun, sarin and soman were developed by the Germans, they were not used because it was thought that the Allies also had them for retaliation. Following World War II, mustard and tabun have been reported to have been used in the Iraq/Iran conflict. Currently there are some 15 countries believed to possess the capability for chemical warfare.

The molecules that we shall discuss in this thesis are mustard gas and a number of closely related model compounds. The precise cause of the toxicity of the sulphur mustard agent has not yet been identified. The physiological target of mustard agent is predominantly the skin. Many of the effects on skin from sulphur mustard result from the ability of its vapor to penetrate clothing and then remain trapped next to the skin. Burns are commonly found in the arm pits and groin where the skin is warm and moist, and where the increased hydration of the skin aggravates the lesion. The proportion of affected people that succumbs to the lethal effects of sulphur mustard is relatively small. Most of the deaths that occur from the exposure to mustard result from inhaling the vapor. Mustard is believed (16) to alkylate DNA and protein, both monofunctionally and by cross-linking chains and is mutagenic; some of its effects are similar to those produced by exposure to ionizing radiation.

Since mustard gas is a lethal gas, it is difficult to analyze, detect or measure experimentally. Hence, it would be a great help if one could predict theoretically the characteristic spectroscopic properties for this gas. However, mustard gas and its related model compounds are interesting to us from the point of view of understanding the spectra of substituted n-paraffins, ethers, or thioethers, and the effect of substitution of a chlorine for hydrogen. One of the important regions in infrared spectra of these molecules is the range from 1500 to 500 cm^{-1} where absorption due to CH2 vibrational motions occur. Hence, it is interesting to study the effect of chlorine substitution on the spectrum in this region. The possibility of transferring force constants from smaller model compounds (such as chloroethanethiol) to a larger molecule such as mustard gas seems to be more likely to succeed than for some other spectrum since the heavy S atom is located in the center of the large molecule which tends to isolate the vibrations for the two halves of molecule corresponding to the $ClCH_2CH_2S$- groups.

Experimental results from studies of Raman spectra of 2,2'-dichlorodiethyl sulfide (mustard) ($ClCH_2CH_2SCH_2CH_2Cl$), 2-chlorodiethyl sulfide ($ClCH_2CH_2SCH_2CH_3$), and diethyl sulfide

($CH_3CH_2SCH_2CH_3$) have recently been reported by Christesen (17). These results have been analyzed and compared with theoretical Raman intensities (18, 19). The *ab initio* calculations for this system at the 3-21G level have been published recently (14). The interpretation of the experimental spectrum is complicated by a lack of detailed knowledge of the structure of these three large molecules as well as by the lack of knowledge of characteristic frequency values for the many different possible vibrational modes. Of these three molecules, the infrared spectrum only of diethyl sulfide has been reported in the literature by Shimanouchi et al. (20). A partial spectrum (in vapor and solution) for mustard has been given by Hoffland, Piffath, and Bouck (21).

Since diethyl sulfide has two C-S axes associated with rotational isomerism, there are four possible rotamers, TT, TG, GG, and GG' (22). Their examinations (20) of the experimental and calculated results led to the following conclusion :

1- Only the all-trans rotameric forms exist in the crystalline state.
2- Many forms coexist in the liquid state. Most of them persist in the glassy state even at the liquid nitrogen temperature.
3- In the liquid state, the forms which are gauche about the C-S axis are more stable than those which are trans about the C-S axis.

4- The gauche conformation about the C-C axis directly adjoining the S-C axis is also quite stable and is only slightly less stable than the corresponding trans conformation.

A large number of experimental studies have been published (23-32) for chloroethanethiol ($ClCH_2CH_2SH$ or ClEtSH) and ethanethiol (CH_3CH_2SH or EtSH) which are closely related to the three larger molecules.

The rotational isomerism for ClEtSH was previously analyzed by Hayashi et al. (23) based on infrared spectroscopic studies, and they proposed that the trans and gauche rotamers about the C-C bond as well as those about the C-S bonds coexist in the gaseous and liquid states. They also concluded that the rotamer that is trans around the C-C bond has about 0.5 (± 0.3) kcal/mol lower energy than does the gauche form. From microwave spectroscopic studies, however, this molecule is believed to exist in only one form (24). Examination of the rotation about the C-S bond by Ohsaku (31) in a theoretical calculation made with 3-21G basis set shows that there are two minima corresponding to the gauche and trans forms about the C-S bond. They concluded that there is a very small energy difference (0.63 kcal/mol favoring the gauche form) between the gauche and trans forms around this bond and the barrier height from the gauche to the trans forms around the C-S bond is also very low (about 1.3 kcal/mol). The barrier for rotation around the C-C bond of ClEtSH from the gauche to the trans forms was estimated to be about 2.9 kcal/mol.

For EtSH, two molecular conformations are possible for the rotamers about the C-S bond (trans and gauche). In principle, the trans and gauche forms have different molecular frequencies and intensities, and bands of both forms might be expected in the molecular spectra. However, the spectrum of EtSH at room temperature corresponds very closely (32) to that of ethyl chloride, which has only one conformation, except for extra bands where the S-H stretching, C-S-H bending, and S-H torsional modes are expected to appear. At the beginning (32) the possibility of two spectroscopically distinct conformations did not seem very likely since the heavy sulphur atom prevented significant interaction between the vibrations of the thiol group and those for the rest of the molecule, so that the differences in the spectra of the two rotamers would not be detectable especially for studies at low resolution. The investigation of the IR spectrum by Smith, Devlin, and Scott (28), together with their normal coordinate calculations, suggested that both rotamers coexist in the spectra of vapor, liquid, and glassy states while only one conformer is believed to exist in the crystalline state. The most significant observation in their experiment for EtSH is the disappearance of the 783 cm^{-1} band of a glassy EtSH sample upon crystallization. This band is observed also in the spectrum of the liquid at room temperature. The persistence in the glass at liquid nitrogen temperature eliminates the possibility that it is a difference combination, and therefore it must be attributed to a second conformation present in the liquid and glass and not the crystal. Their normal coordinate calculations favor assigning the 783 cm^{-1} band to the CH_2 rocking mode of the trans conformation. Using the spectroscopic evidence that the gauche conformation is more stable and that the barrier height for thiol rotation is 1.42 kcal/mol, the energy difference (trans-gauche) is then predicted to be 0.3 kcal/mol.

1.3 Theoretical Determination of Vibrational Frequencies

The vibrational frequencies are determined from the force constants obtained from ab initio theoretical calculations at the harmonic approximation. The force constants are determined in turn by calculating numerical or analytical gradients of the potential energy (13, 33). Pople et al. (13) carried out Hartree-Fock self-consistent field (HF SCF) calculations with 3-21G and 6-31G* basis sets on 37 small to medium size molecules. They concluded that the 3-21G basis set performs comparably well with the 6-31G* basis in reproducing experimental vibrational frequencies which are found to be consistently larger than experimental values by 10-15%. It is to be expected, however, that problems may arise for molecules whose structures are not well described at the 3-21G level. In particular, frequencies calculated for molecules not adequately represented in terms of normal-valence structures are likely to be affected greatly by the addition of d functions to the basis; 3-21G* and 6-31G* calculations should provide a better description for these molecules than those at the 3-21G level (11). Consistent with the performance of the theory for normal-valent species, 3-21G* and 6-31G* calculations give frequencies that are uniformly higher than the measured values. It would appear that the harmonic frequencies calculated for hypervalent compounds are closer to experimental values than was found for the normal-valent systems. Frequencies calculated using the 3-21G basis set are closer to directly measured values (mean absolute error of 13.6%) than they are to corrected (harmonic) frequencies (error of 16.7%). At this 3-21G level, calculated frequencies are not always larger than the corresponding measured quantities (as are 3-21G* and 6-31G* frequencies), and comparison with harmonic frequencies (which are larger than measured values) does not necessarily lead to improved agreement. Their comparison (11) of calculated frequencies for sulphur-containing compounds with experimental harmonic values shows that the scatter for the calculations at the 3-21G level is much greater than that resulting from 3-21G* calculations. This parallels the well known inability of the 3-21G basis set to account properly for the equilibrium structures of hypervalent compounds (11).

According to Fogarasi and Pulay (12), the diagonal harmonic force constants in terms of internal coordinates are obtained within the reasonable accuracy of 10-30%; more importantly, the deviations are very systematic in a semi-quantitative sense, in that the errors occur consistently as an overestimation; for similar bonds in similar systems, this overestimation is also quantitatively systematic, i.e., well transferable. The off-diagonal terms are of comparable accuracy, and, considering that experimental values for these exhibit larger relative errors, the theoretical results are often competitive or superior to all but the most precise experimental data. Improvements in ab initio procedures by extending the basis set and introducing electron correlation are possible, but at present such an extension is economically feasible only for small molecules. Based on the observation that the remaining errors are mainly systematic, it is an obvious idea to introduce a few empirical parameters as scale factors (12) for the direct calculated force constants, and fit the parameters to the observed vibrational frequencies. We shall investigate this idea further in Chapter 5.

1.4 Theoretical Determination of Vibrational Intensities

Predicted IR spectra should include the intensities of the bands as well as the frequencies of the normal modes. As discussed in Chapter 2, the intensities are proportional to the square of the derivatives of the molecular dipole moment with respect to the normal coordinates. These dipole derivatives, like the force constants, reflect the chemical bonding characteristics of the molecule. One of the goals of infrared intensity theory is to study how the dipole derivatives change from one molecule to another and interpret these changes in terms of the types of atoms and bond present. Dipole derivatives can also be expressed in terms of other forms of the vibrational coordinates which are more useful for interpretation than the normal coordinates.

The space-fixed cartesian representation for the dipole derivatives has proven particularly advantageous for understanding the chemical factors that determine the intensities. These dipole derivatives are composed of a set of atomic polar tensors (APTs), one for each atom in the molecule (2). Studies have indicated that the values of the APT elements for a given atom tend to be relatively independent of which molecule the atom is in (2, 9, 34). Remarkable success has been achieved in predicting intensities for one molecule by transferring APTs from other chemically related molecules, and then transforming these APTs to dipole derivatives with respect to the normal coordinates of the first molecule (35-39). These result suggest that the APTs are fundamental indicators of the chemical properties of atoms in molecules.

1.5 Preview of the Present Study

A summary of the calculational procedure developed in this work, together with a brief review of both the normal coordinate analysis and the infrared intensity analysis, is given in Chapter 2. The results from these calculations (predicted geometries, frequencies, and intensities) are presented in Chapter 3 where the techniques of analyzing the intensity contributions are utilized to examine the different intensity patterns predicted from the calculations using the two different basis sets (3-21G and $6\text{-}31G^{**}$). The transferability of molecular parameters (force constants and polar tensors) is tested in Chapter 4. In this discussion the predicted spectra from transferring parameters are compared with those predicted from direct *ab initio* calculation. A discussion of choice of a transferable set of scaling factors to be applied to the force constants from the *ab initio* calculations is given in Chapter 5 along with our proposed choice of scaling factors for the calculated force constants for these molecules. The results of applying this set of scaling factors to the force constants from our best calculation (at $6\text{-}31G^{**}$ level) and then investigating their transferability are presented in Chapter 6. The comparison with experimental results also is given in that chapter in order to test the performance of these techniques. In Chapter 7, the 3 X 3 atomic polar tensor is represented by five invariants ($\bar{P}$, β, X, $\sqrt[3]{D}$, $\sqrt{C}$ defined in Chapter 7) and then reduced further to just two dimensional space by principal component analysis (PCA). The disagreement found for the total intensity sums obtained in Chapter 4 is explained by differences in the values of some of invariants of the two molecules (ex. EtSH versus diethyl sulfide) due to the chemical differences. Chapter 8 summarize the work presented in this dissertation.

CHAPTER 2
TECHNIQUES

In this chapter we shall outline the methods of calculation used for the prediction and interpretation of IR spectra. Our purpose in this chapter is to include enough details about our calculations so that the reader can reproduce our results or obtain analogous results, using a different force field or theoretical atomic polar tensors (APTs) calculated with a different basis set.

In order to do this, we shall first describe briefly the *ab initio* molecular orbital calculations that were used to obtain the harmonic force constants and atomic polar tensors (APTs) and then follow by a description of the calculations involved in interpreting the vibrational spectra. Since these theoretical techniques have been discussed in detail elsewhere (explicit references are given later in this chapter) our presentation will emphasize only those considerations that apply to the present work. We have developed new techniques (34, 40) in interpreting the intensity contributions using the theoretical APTs. This method will be used in interpreting the intensity contribution from each atom or from each internal coordinate to the normal mode.

2.1 Ab Initio Calculations

The theoretical harmonic force constants and atomic polar tensor data used in this study were calculated by C. Sosa of the Quantum Theory Project (QTP), Department of Chemistry (University of Florida).

The molecules under consideration were ethanethiol (CH_3CH_2SH or EtSH), 2-chloroethanethiol ($ClCH_2CH_2SH$ or ClEtSH), diethyl sulfide ($(CH_3CH_2)_2S$), 2-chlorodiethyl sulfide ($CH_3CH_2SCH_2CH_2Cl$) and 2,2'-dichlorodiethyl sulfide ($(ClCH_2CH_2)_2S$ or sulfur mustard). All the calculations were done by the restricted Hartree-Fock self-consistent field method (RHF SCF) (11,41) with a split valence 3-21G basis set (42). For the smaller model compounds, EtSH and ClEtSH, additional calculations were performed with a $6\text{-}31G^{**}$ basis set (43) which includes polarization functions on all atoms.

2.1.1 Geometry Optimizations

Application of molecular orbital theory requires a specification of molecular geometry. A complete theoretical treatment of equilibrium structure implies minimization of the energy with respect to each independent geometrical parameter, yielding a structure that is termed as the "optimized structure." The equilibrium geometries for the molecules used were optimized by using the GAUSSIAN 82 system of programs (44) with a split-valence 3-21G and $6\text{-}31G^{**}$ basis sets.

The optimization gave the all-trans, C_{2v}, structures for sulfur mustard and diethyl sulfide shown in Figure 2-1. For 2-chlorodiethyl sulfide, trans-EtSH and ClEtSH (Figures 2-1 and 2-2) the all-trans geometries have C_s symmetry. For gauche-EtSH, the symmetry is C_1. Other local minima are expected to be on the potential energy surface. It should be noted that the minimum energy does not necessarily imply the best "global minimum" geometry for the molecule.

2.1.2 Calculation of Harmonic Force Constants

The total energy of a molecule comprising N atoms near its equilibrium structure may be written (11) as

$$E = T + V = 0.5 \sum_{i=1}^{3N} \dot{q}_i^2 + V_{eq} + 0.5 \sum_{i=1}^{3N} \sum_{j=1}^{3N} \left(\frac{\partial^2 V}{\partial q_i \, \partial q_j} \right)_{eq} q_i q_j \qquad (2\text{-}1)$$

Here, the mass-weighted cartesian displacements, q_i, are defined in terms of the locations X_i of the nuclei relative to their equilibrium positions $X_{i,eq}$ and their masses M_i,

$$q_i = M_i^{½} \, (X_i - X_{i,eq}) \qquad (2\text{-}2)$$

V_{eq} is the potential energy at the equilibrium nuclear configuration, and the expansion (2-1) of the vibrational energy in terms of a power series is truncated at second order (45). For such a system, the classical-mechanical equations of motion takes the form

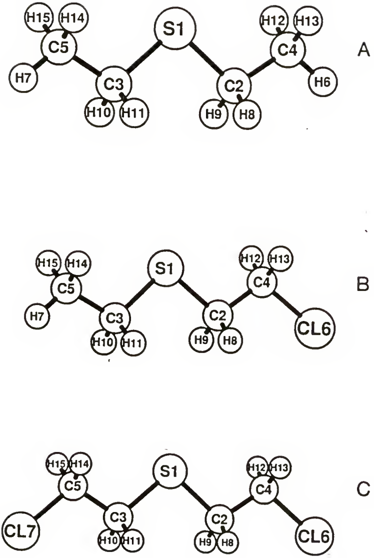

Figure 2-1. Structure and atom numbering for (A) diethyl sulfide; (B) 2-chlorodiethyl sulfide; and (C) mustard gas (2,2'-dichlorodiethyl sulfide).

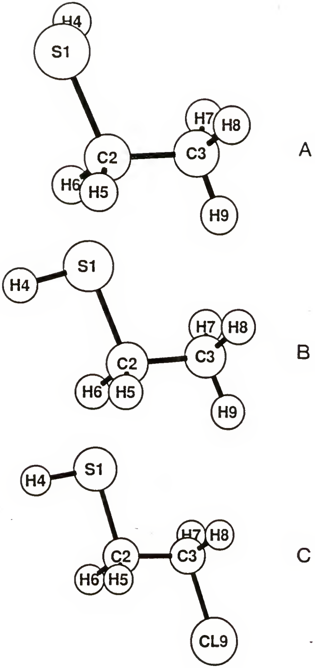

Figure 2-2. Structure and atom numbering for (A) gauche-ethanethiol; (B) trans-ethanethiol; and (C) all-trans-2-chloroethanethiol.

$$\ddot{q}_j = - \sum_{i=1}^{3N} f_{ij}q_i \qquad j = 1, 2, \ldots., 3N \tag{2-3}$$

The f_{ij}, termed "quadratic force constants", are the second derivatives of the potential energy with respect to mass-weighted cartesian displacements, evaluated at the equilibrium nuclear configuration, that is,

$$f_{ij} = \left(\frac{\partial^2 V}{\partial q_i \, \partial q_j} \right)_{eq} \tag{2-4}$$

The f_{ij}, may be evaluated by numerical second differentiation,

$$\frac{\partial^2 V}{\partial q_i \, \partial q_j} = \frac{\Delta(\Delta V)}{\Delta q_i \, \Delta q_j} \tag{2-5}$$

by numerical first differentiation of analytical first derivatives,

$$\frac{\partial^2 V}{\partial q_i \, \partial q_j} = \frac{\Delta(\partial V/ \partial q_j)}{\Delta q_i} \tag{2-6}$$

or by direct analytical second differentiation, Eq. (2-4). The choice of procedure depends on the quantum mechanical model employed, that is, single-determinant or post-Hartree-Fock, and on practical matters such as the size of system.

Equation (2-3) may be solved by standard methods (45) to yield a set of 3N normal-mode vibrational frequencies. Six of these (five for linear molecules) will be zero since they correspond to translational and rotational motions (rather than to vibrational degrees of freedom).

In this work, harmonic vibrational frequencies were computed with the ACES system of programs (46) and with GAUSSIAN 82 (44) using analytical second derivatives at the Hartree-Fock level with the 3-21G and 6-31G** basis set.

2.1.3. Calculation of Polar Tensors

In theoretical calculations, the atomic polar tensors or dipole moment derivatives can be calculated by numerical differentiation, using the dipole moment computed at the equilibrium geometry and other values computed for small displacements of each atom along the coordinate axes. The dipole moment derivatives can also be calculated numerically by determining the change in the analytical energy gradient (with respect to the atom positions) under the influence of a finite external electric field (47). Alternatively, the dipole moment derivatives can be calculated analytically (48 - 50) as were used by ACES program used in this work.

At the SCF level, the derivatives of the dipole moment with respect to the cartesian displacement coordinates (51) of each nucleus can be computed analytically :

$$\partial P_\alpha / \partial B_A = \sum_{\mu v} \left[(\partial P_{\mu v} / \partial B_A) <v|\alpha|\mu> + P_{\mu v} \, \partial <v|\alpha|\mu> / \partial B_A \right] + \sum_{A} \alpha_A Z_A \qquad (2\text{-}7)$$

where μ, v are the atomic orbitals from the basis set, $P_{\mu v}$ are the density matrix elements, $<v|\alpha|\mu>$ are the dipole moment integrals, α_A are the coordinates of nucleus A, and α, β are the cartesian directions x, y, and z ; subscript A indicates the cartesian coordinates locating center A. The derivatives of $P_{\mu v}$ are obtained by solving the coupled perturbed Hartree-Fock equations (CPHF) (41, 48).

2.2 Determination of Vibrational Frequencies

After the force constants have been evaluated, the next step is to calculate the vibrational frequencies and potential energy distributions. For a harmonic oscillator the solution of Newton's equations of motion (i.e. Eq. 2-3) gives the secular equation (52).

$$|\underline{G}\ \underline{F} - \underline{E}\ \underline{\Lambda}| = 0 \quad \text{or} \quad \underline{G}\ \underline{F}\ \underline{L} = \underline{L}\ \underline{\Lambda} \tag{2-8}$$

Here $\underline{F}$ is the (3N-6) X (3N-6) potential energy or force constant matrix, $\underline{G}$ is the corresponding inverse kinetic energy matrix, $\underline{E}$ is the identity matrix, $\underline{\Lambda}$ is the eigenvalue matrix and $\underline{L}$ is the matrix of the eigenvectors of $\underline{H} = \underline{G}\ \underline{F}$. The solution to this system gives the eigenvalues, or normal frequency parameters, $\underline{\Lambda}$, and the eigenvectors, or column vector representations of the normal coordinates, also known as the normal coordinate transformation matrix, $\underline{L}$.

The solution of the above secular equation (2-8) to obtain $\underline{L}$ and $\underline{\Lambda}$ is the central problem in vibrational spectroscopy. It can be solved by one of the several methods available in numerical calculus for the diagonalization of non-symmetric matrices or it can be reduced to symmetric form and then diagonalized.

2.2.1 Using Mass-Weighted Cartesian Coordinates.

If the potential energy matrix is represented in mass-weighted cartesian coordinates, then the inverse kinetic energy $\underline{G}$ matrix is the identity matrix (52). Equation (2-8) can then be rewritten as

$$|\underline{K} - \underline{E}\,\underline{\Lambda}| = 0 \quad \text{or} \quad \underline{K}\,\underline{\ell} = \underline{\ell}\,\underline{\Lambda} \tag{2-9}$$

where $\underline{K}$ represents the matrix of force constants in mass-weighted cartesian coordinates, $\underline{\ell}$ is the eigenvector matrix in these coordinates, and $\underline{\Lambda}$ is the diagonal eigenvalue matrix. The values of $\underline{\Lambda}$ are related to the vibrational frequencies by (53)

$$\nu_i\ (\mathrm{cm}^{-1}) = \lambda^{½}\ (\mathrm{md/u^{-1}A}) * (1/2\pi c) \quad \text{or} \quad \nu_i = 1303.1 * \lambda_i^{½} \tag{2-10}$$

The $\underline{\ell}$ matrix is the orthogonal normal coordinate transformation which transforms from the 3N-6 column vector of normal coordinates $\underline{Q}$ to the 3N column vector of mass-weighted cartesian coordinates, q

$$\underline{q} = \underline{\ell}\,\underline{Q} \tag{2-11}$$

Thus in mass-weighted cartesian coordinates, solving the secular equation reduces to finding the orthogonal matrix which diagonalizes the symmetric potential energy matrix, $\underline{K}$.

$$\underline{\ell}^{+} \, \underline{K} \, \underline{\ell} = \underline{\Lambda} \qquad (2\text{-}12)$$

where $\underline{\ell}^{+}$ is the transpose of $\underline{\ell}$.

2.2.2 Using Symmetrized-Internal Coordinates

The secular equation (2-8) set up in terms of internal coordinates is most conveniently solved by first reducing the H matrix to a symmetric form using a method introduced by Miyazawa (54). The geometrical basis for this method was discussed by Person and Crawford (55). For a nonlinear polyatomic molecule with N atoms there are 3N-6 normal modes of vibration (or 3N-5 if the molecule is linear). By using the molecular symmetry, it is possible to identify and classify these modes of vibration into their symmetry group species (45) and then to convert the H matrix to block diagonal form. Each block matrix can be solved separately, thus reducing the size of the secular equation. Since this method has been detailed by Califano (52), Chin (53), and Scott-Lebron (37) only a brief discussion will be given here.

The internal displacement coordinates are changes in bond lengths and bond angles of a molecule. For most applications five coordinates--bond stretching, angle bending, torsional motion, out-of-plane bending (wagging), and linear bending--

are sufficient to describe completely all of the vibrational motions (45, 52).

The internal coordinates are related to the cartesian coordinates by

$$R_k = (\partial R_k/\partial x_i)\ x_i \quad \text{where} \quad \begin{array}{l} k = 1, 2, \ldots, (3N - 6) \\ i = 1, 2, \ldots, (3N) \end{array} \tag{2-13}$$

or in matrix notation

$$\underline{R} = \underline{B}\ \underline{X} \tag{2-14}$$

where $\underline{B}$ is a (3N-6) X 3N matrix of the $\partial R_k/\partial x_i$ terms and $\underline{R}$ is the column vector representation of the 3N-6 non-redundant internal coordinates. The transformation from the internal coordinates $\underline{R}$ to the symmetry coordinates $\underline{S}$ is then expressed as

$$\underline{S} = \underline{U}\ \underline{R} \tag{2-15}$$

where $\underline{U}$ is a (3N-6) X (3N-6) orthogonal matrix, when existing redundancies have been eliminated. Two other important relations in the normal coordinate transformation are the $\underline{A}$ and $\underline{L}$ matrices. The $\underline{A}$ matrix, of dimension 3N by (3N-6), expresses the transformation from the internal coordinates back to cartesian coordinates

$$\underline{X} = \underline{A}\ \underline{R} \tag{2-16}$$

where the 3N X 3N-6 $\underline{A}$ matrix is effectively the inverse transformation from $\underline{B}$ matrix, that represented by the 3N-6 X 3N. The 3N-6 symmetry coordinates $\underline{S}$ are transformed to normal coordinates $\underline{Q}$ by $\underline{L}^{-1}$, which is the inverse of the normal (3N-6) X (3N-6) coordinate transformation matrix $\underline{L}$.

$$\underline{Q} = \underline{L}^{-1}\ \underline{S} \tag{2-17}$$

The construction of the $\underline{G}$-matrix is obviously the preliminary step in setting up the vibrational problem in internal coordinates. In accordance with Wilson et al. (45), the $\underline{G}$-matrix is defined as

$$\underline{G} = \underline{B}\ \underline{M}^{-1}\ \underline{B}^{+} \tag{2-18}$$

where $\underline{B}$ is the transformation matrix given by Eq. (2-14), $\underline{B}^{+}$ is its transpose and $\underline{M}^{-1}$ is a (3N X 3N) diagonal matrix of the reciprocal masses. The inverse of the $\underline{G}$ matrix then later is used to evaluate the "inverse" of $\underline{B}$ matrix, or namely the $\underline{A}$ matrix,

$$\underline{A} = \underline{M}^{-1}\ \underline{B}^{+}\ \underline{G}^{-1} \tag{2-19}$$

At this point it is appropriate to mention that the $\underline{A}$ matrix can be calculated by Eq. 2-19 only if the $\underline{G}$ matrix is a square non-singular matrix. This in turn means that there cannot be any redundant internal coordinates or that the redundancies must be expressed explicitly and the 3N-6 coordinates used in defining $\underline{R}$ must be defined orthogonal to the redundancy conditions. This problem can be solved if the symmetric $\underline{B}$ matrix is used to evaluate the $\underline{G}$ matrix in Eq. 2-18, and if the $\underline{S}$ coordinates are non-redundant.

$$\underline{B} = \underline{U}\ \underline{B}_i \tag{2-20}$$

where $\underline{U}$ is the transformation matrix defined in Eq. (2-15).

Consider the equation

$$\underline{G}\ \underline{A} = \underline{A}\ \underline{T} \tag{2-21}$$

where $\underline{A}$ is the matrix of the eigenvectors and $\underline{T}$ is the matrix (diagonal) of the eigenvalues of $\underline{G}$. Since $\underline{G}$ is real symmetric, $\underline{A}$ is orthogonal and thus

$$\underline{G} = \underline{A}\ \underline{T}\ \underline{A}^{+} = \underline{A}\ \underline{T}^{1/2}\ \underline{T}^{1/2}\ \underline{A}^{+} = \underline{W}\ \underline{W}^{+} \tag{2-22}$$

where $\underline{W} = \underline{A}\ \underline{T}^{1/2}$. Using Equation (2-22), the secular equation (2-8) can be written in the form

$$\underline{W}^{+}\ \underline{F}\ \underline{W}\ (\underline{W}^{-1}\ \underline{L}) = (\underline{W}^{-1}\ \underline{L}) \tag{2-23}$$

or

$$\underline{W}^{+}\ \underline{F}\ \underline{W}\ \underline{C} = \underline{C}\ \underline{\Lambda} \tag{2-24}$$

Comparison of Eq. (2-24) with Eq. (2-8) shows that the real symmetric matrix

$$\underline{H} = \underline{W}^{+}\ \underline{F}\ \underline{W} \tag{2-25}$$

has the same eigenvalues as the unsymmetrical $\underline{G}\ \underline{F}$ matrix and also the same eigenvectors

$$\underline{C} = \underline{W}^{-1}\ \underline{L} \tag{2-26}$$

Once the secular equation (2-24) has been solved for $\underline{C}$, the $\underline{L}$-matrix can be obtained from Eq. (2-26)

$$\underline{L} = \underline{W}\ \underline{C} \tag{2-27}$$

The solution of the secular equation (2-24) corresponds to finding a matrix $\underline{C}$ which diagonalizes the $\underline{H}$ - matrix since from (2-24) it follows that

$$\underline{C}^{+}\ \underline{H}\ \underline{C} = \underline{\Lambda} \tag{2-28}$$

Diagonalization methods for symmetrical matrices, based on iterative procedures, are very suited for computer program.

In this work, the iterative method of Jacobi (56) is employed. Once $\underline{\Lambda}$ is obtained, the vibrational frequencies can be evaluated using Eq. (2-10).

2.3 Determination of Vibrational Intensities

The concept of the atomic polar tensor (APTs) was introduced by Biarge, Herranz and Morcillo (8) and was later rediscovered and reformulated by Person and Newton (9). A complete discussion on the properties of APTs has already been given by Person (2). Briefly, the APT, $\underline{P}_x^\alpha$ is just the tensor representing the dipole derivatives

$$\underline{P}^x\alpha = \begin{pmatrix} \partial Px/\partial x_\alpha & \partial Px/\partial y_\alpha & \partial Px/\partial z_\alpha \\ \partial Py/\partial x_\alpha & \partial Py/\partial y_\alpha & \partial Py/\partial z_\alpha \\ \partial Pz/\partial x_\alpha & \partial Pz/\partial y_\alpha & \partial Pz/\partial z_\alpha \end{pmatrix} \tag{2-29}$$

Here (x_α, y_α, and z_α) are the coordinates, with respect to the space-fixed cartesian axes, of the α^{th} atom in the molecule and (Px, Py, and Pz) are the components of the total dipole moment vector expressed in the same axis system. This concept has been an extremely useful one in the interpretation of measurements of infrared intensities of fundamental vibrations of molecules (14, 57 - 61).

2.3.1 Using Mass-Weighted Cartesian Coordinates

The matrix $\underline{P}_q$ consists of the dipole moment derivatives in mass-weighted cartesian coordinate space and it is evaluated by

$$\underline{P}_q = \underline{P}_x \, \underline{M}^{-1/2} \tag{2-30}$$

where $\underline{P}_x$ is the 3 X 3N matrix composed of the juxtaposition of the APTs for the N atoms in the molecule, and $\underline{M}^{-1/2}$ is a diagonal matrix represented by the triplet sets of the reciprocal of the square root of the masses of the atoms in the molecule.

The transformation from $\underline{P}_q$ to $\underline{P}_Q$, can be accomplished with the $\underline{\ell}$ matrix (Eq. 2-11)

$$\underline{P}_Q = \underline{P}_q \, \underline{\ell} = \underline{P}_x \, \underline{M}^{-1/2} \, \underline{\ell} \tag{2-31}$$

where $\underline{P}_Q$ is the 3 X (3N-6) matrix of dipole moment derivatives in normal coordinate space.

The absolute integrated intensity for the ith mode is proportional to the sum of the squares of the vector components of the dipole moment derivatives for the ith column of $\underline{P}_Q$.

$$|\partial P/\partial Q_i|^2 = (\partial Px/\partial Q_i)^2 + (\partial Py/\partial Q_i)^2 + (\partial Pz/\partial Q_i)^2 \tag{2-32}$$

The actual value of the absolute intensity A_i in km/mole is then evaluated using the relation (34)

$$A_i \text{ (km/mol)} = \frac{N\pi}{(4\pi\epsilon_0)3000c} |\partial P/\partial Q_i|^2 \tag{2-33}$$

where N is the Avogadro's number, ϵ_0 is the permittivity of free space, and c is the speed of light. It should be noted that the $|\partial P/\partial Qi|$ is in $eu^{-\frac{1}{2}}$. If the proper constants are substituted into Eq. (2-33), than that equation can be simplified (53) to

$$A_i \text{ (km/mol)} = 974.9 * |\partial P/\partial Q_i|^2 \tag{2-34}$$

If Qi and Qk corresponds to the same frequency ($\lambda_i = \lambda_k$), then coordinates are said to be degenerate, and the total intensity at $\nu_i = \nu_k$ is $A_i + A_k = 2 * A_i$. In these equations the "absolute intensity" Ai is the value of the "integrated molar absorption coefficient" defined experimentally by

$$A_i = \frac{1}{C\ell} \ln (I_0/I)\, d\bar{\nu} \tag{2-35}$$

or

$$A_i \text{ (km/mol)} = \frac{1}{C * \ell * 100} \ln (I_0/I)\, d\bar{\nu} \tag{2-36}$$

where C is the concentration in moles/liter (moles/1000 cm^3), ℓ is the pathlength in cm, and $\bar{\nu}$ is in cm^{-1}.

2.3.2 Using Symmetrized-Internal Coordinates

In internal coordinate space, the polar tensor is the 3 X (3N-6) P_R tensor. Its relation with $\underline{P}_Q$ and $\underline{P}x$ is given by (2)

$$\underline{P}_Q = \underline{P}x\ \underline{A}\ \underline{L} = \underline{P}_R\ \underline{L} \tag{2-37}$$

where the $\underline{A}$ and $\underline{L}$ matrices are obtained while carrying out the normal coordinate analysis (Eq. 2-19 and 2-27). The absolute integrated intensity for ith normal mode is then evaluated using Eq. (2-32) through (2-34).

2.4 Potential Energy Distribution Analysis

After having carried out the Normal Coordinate Analysis, it is useful to calculate what percentage of the potential energy associated with a given normal coordinate is contributed by each symmetry coordinate (62).

The vibrational potential energy, V, can be given in terms of the normal coordinates, Q, by the following expression :

$$V = 0.5 \sum_k Q_k^2 \sum_i \sum_j L_{jk}\ L_{ik}\ F_{ij} \tag{2-38}$$

where F_{ij} denotes the potential energy matrix element (Eq. 2-8) and L_{jk} is the element of $\underline{L}$,transformation matrix

(Eq. 2-7) between the internal (or symmetry) coordinates and normal coordinates.

We see in Eq. 2-38 that the contribution from the jth symmetry coordinate to the potential energy contribution from the kth normal coordinate is measured by an element from the potential energy distribution matrix, PED (62), namely the kj element given by

$$[\mathrm{PED}]_{kj} = \Sigma_i L_{jk} L_{ik} F_{ij} \tag{2-39}$$

Because the potential energy expressed in terms of normal coordinates is just

$$2V = \sum_k \lambda_k Q_k^2 \tag{2-40}$$

$$k = \sum_j [\mathrm{PED}]_{jk} \tag{2-41}$$

or that $[\mathrm{PED}]_{jk}/\lambda_k$ is just the fraction contributed to the potential energy for the kth normal mode from the jth internal (symmetry) coordinates. Hence the percentage energy contribution, or "PED" is just

$$[\mathrm{PED}]_{kj} = 100 * \Sigma_i L_{jk} L_{ik} F_{ij} / \lambda_k \tag{2-42}$$

With the aid of Eq. (2-42), we can determine whether all the symmetry coordinates contribute equally to the total potential energy of a given normal coordinate or whether just a few predominate. It is a valuable guide to the interpretation of results from the normal coordinate analysis.

2.5 Contribution to Intensities

The detailed appearance of the APTs for each atom depends upon the choice of cartesian coordinates used to describe the positions for the atoms in the molecule. However, there are some properties of the APTs that are invariant to rotations of these cartesian axes with respect to the molecule (2, 63). These invariants properties have been defined by several authors (3-6, 64). We shall give further details in this dissertation in Chapter 7. Here we want to examine just one of these invariants; namely the square of the "effective charge of the α^{th} atom"

$$X_\alpha^2 = (1/3)\ \mathrm{Tr}[Px^\alpha\ (Px^\alpha)^+] \tag{2-43}$$

This invariant has been used by Person and KuBulat (34) to interpret the atomic contribution to the sum of all vibrational and rotational infrared intensities for the molecules.

The reason that this particular invariant property of the APT is important is because of the intensity sum rule (3) which can be expressed as

$$\sum_{s=1}^{3N-6} A_s + \Omega = 974.9 * \sum_{\alpha}^{N} 3X_\alpha^2/m_\alpha \tag{2-44}$$

where Ω is the "rotational correction" defined as the sum of the intensities calculated for the pure rotation of the molecule and m_α is the mass for the α^{th} atom.

From Eq. (2-44) we see that the contribution from the α^{th} atom to total intensity sum $(\Sigma A_i + \Omega)$,is just $3X_\alpha^2/m_\alpha$. It is worth noting that Ω is small relative to the vibrational intensity sum ΣA_s for the large molecules considered here, so that it can often be ignored.

It is also possible to calculate the contribution of each atom to the intensity of each normal mode, Q_s (34). This relationship may be seen by re-writing Eq. (2-31) to examine just one term in the $\underline{P}_Q$ tensor ; for example :

$$\partial Px/\partial Q_s = \sum_{x_\alpha=1}^{3N} (1/\surd m_\alpha)(\partial Px/\partial x_\alpha)\, \ell_{x_{\alpha s}} \tag{2-45}$$

Hence the contribution from the α^{th} atom to this component of the dipole derivative $(\partial Px/\partial Q_s)$ is just

$$(1/\surd m_\alpha)[(\partial Px/\partial x_\alpha)\, \ell_{x_{\alpha s}} + (\partial Px/\partial y_\alpha)\, \ell_{y_{\alpha s}} + (\partial Px/\partial z_\alpha)\, \ell_{z_{\alpha s}}] \tag{2-46}$$

By re-writing Eq. (2-37), the relationship in internal coordinate may also be seen

$$\partial Px/\partial Q_s = \Sigma\ (\partial Px/\partial R_i)\ L_{is} \qquad (2\text{-}47)$$

Hence the contribution to the x component of the dipole derivative, hence intensity, of the sth normal mode from each atom can be evaluated by Eq. 2-46, or the contribution to the intensity from each internal coordinate can be evaluated by Eq. 2-47 (the ith internal coordinate contribution $(\partial Px/\partial R_i) L_{is}$ to that intensity).

CHAPTER 3
SYSTEMATIC SUMMARY OF RESULTS

As mentioned in Chapter 2 the optimized geometries, harmonic force constants, and atomic polar tensors were calculated for the $XCH_2CH_2SCH_2CH_2X$ and XCH_2CH_2SH series of molecules using _ab initio_ molecular orbital methods. Calculations were carried out by Carlos Sosa using two split-valence basis sets: 3-21G and 6-31G**. Vibrational frequencies, infrared intensities, and potential energy distribution (PEDs) were then computed (or recomputed) by us from his calculated force constants and polar tensors using normal coordinate programs (65a) which are an extension of the Schachtschneider programs (65b).

Some discussion of the calculational procedures, the performance of the 3-21G basis set in comparison with experimental results, and the conformational stability for this series of molecules have already been discussed by Sosa et al. (14). The purpose of the present work is to discuss them in more detail and to include some issues that are not covered in the paper. In this chapter, we shall discuss the performance of the 3-21G basis set in predicting the geometries, force constants, and atomic polar tensors in comparison with the larger 6-31G** basis set and the including polarization functions on all atoms.

In order partially to determine the effect of conformational changes, calculations were carried out for the gauche and trans conformers of ethanethiol (CH_3CH_2SH or EtSH) with the two different basis sets: 3-21G and 6-31G**. Since detailed experimental studies have been reported for EtSH (28), here we shall be able to examine some details of the comparison between the predicted spectrum and the experimental spectrum. For the larger molecules, results from experimental studies are much less available. In order to try to compare our results with experimental values, the program package (MVIB), developed by Shimanouchi and co-workers (66) which includes the data file of the geometric structures and the transferable set of force constants that they have developed for these molecules (66a), was used to calculate values for the "experimental" vibrational frequencies for diethyl sulfide, 2-chlorodiethyl sulfide, and 2,2'-dichlorodiethyl sulfide.

It is worth noting that the wavenumbers we refer to throughout discussion in this dissertation (until Chapter 4) are the calculated wavenumbers that have been scaled by a single scaling factor of 0.89 (13). In order to get a better agreement with experimental values (say within ± 0.5%), the method of scaling each diagonal force constant by a different scaling factor suggested by Fogarasi and Pulay (12) can be used. The description and the application of this method to our system will be discussed in the Chapter 5.

Some new techniques have been developed here in order to try to understand the complex problem of explaining why some normal modes have high intensities and others have low intensities. These methods could be used either in cartesian or in non-redundant internal coordinate systems. The most valuable features of the methods are that they could explain the drastic changes in the intensity predicted for some normal modes when calculations are made with different basis sets, even though their intensity sum (over all modes) may be approximately the same. We hope in the future that these methods may be useful for understanding disagreements between predicted and observed infrared spectra.

In this chapter we shall divide the discussion into two major parts: a review of predicted geometries and a discussion and interpretation of the calculated vibrational spectra. Comparison with experimental values is given whenever possible.

3.1 Geometries

The optimized geometries of trans- and gauche-EtSH calculated with two different basis sets, 3-21G and 6-31G**, are presented in Table 3-1 along with the experimental parameters (25-27). (For convenience of the reader, all tables and figures are presented at the ends of the appropriate chapters.) In Table 3-2, the optimized geometries of all-trans ClEtSH calculated with these two basis sets are listed along with the incomplete experimental geometries (24). For ease of comparison the optimized geometries at the 3-21G level of all-trans diethyl sulfide, 2-chlorodiethyl sulfide, and 2,2'-dichlorodiethyl sulfide are reported for each of the two fragments (ethyl and chloroethyl) in Table 3-3, together with the optimized geometries of trans-EtSH and trans-ClEtSH calculated with the same basis set.

The optimization was for the local minimum all-trans C_{2v} structures for the symmetrical molecules, mustard gas and diethyl sulfide. For trans-EtSH, ClEtSH, and 2-chlorodiethyl sulfide, the all-trans geometries have C_s symmetry. For gauche-EtSH, the symmetry is C_1.

The total energies and dipole moments computed for the optimized geometries are collected in Table 3-4. It seems that both basis sets correctly predict that the gauche form of EtSH is more stable than the trans structure which is consistent with experimental observation (28). The energy differences (E_{gauche} - E_{trans}) are -0.26 and -0.17 kcal/mol, respectively, for

3-21G and 6-31G** calculations. These numbers are in remarkably excellent agreement with experimental value of -0.3 kcal/mol (28).

The total dipole moment predicted using a 3-21G basis set always has a higher value than measured experimentally. Enlarging the basis set from 3-21G to 6-31G** to include the polarization functions on all atoms decreases the predicted dipole moment by 0.34, 0.41, and 0.47 D for trans and gauche conformers of EtSH, and for trans-ClEtSH. These predicted dipole moments from the 6-31G** basis are still about 0.30 D higher than the experimental values (27). For EtSH, the 6-31G** calculation predicts that the total dipole moment of the two conformers differs by only 0.05 D. This number is very close to the experimental observation (27) of 0.03 D (1.58 D for trans and 1.61 for gauche).

As expected, the 3-21G basis set predicts bond lengths for bonds to the S and Cl atoms that are somewhat too long, while the 6-31G** set predicts more reasonable bond lengths. The C-S bond length predicted at the SCF level with the 3-21G basis set for trans- and gauche-EtSH overestimates the experimental value (25-27) by almost 0.09 A. The 3-21G basis set also overestimates the experimental value (24) of the C-Cl bond length in trans-ClEtSH by almost 0.11 A (Table 3-2). However, the C-S and C-Cl bond lengths calculated at the

$6\text{-}31G^{**}$ level are in excellent agreement with experimental values(within ±0.003 A). The predicted values for C-C, C-H, and S-H bond lengths agree with the reported experimental parameters within ±0.010 and ±0.005 A, for 3-21G and $6\text{-}31G^{**}$ calculations, respectively.

The largest change in a geometrical parameter from trans (C_s) to gauche (C_1) EtSH (except for the HSCC and SCCH torsional angles) is for the SCC angle which is predicted to be 109.7° (108.3°) for the trans isomer compared to 114.2° (112.4°) for the gauche structure. (Please note that the parameter obtained from 3-21G is given in the parentheses right after the value from $6\text{-}31G^{**}$ basis). Therefore, the predicted SCC angle of gauche conformer is about 4.5° (4.1°) larger than it is for the trans conformer, and this is in excellent agreement with the experimental (27) result of 113.3 -108.6 = 4.7°. Another significant change from the trans to gauche conformer is the S-C-H5 angle. [Notice that H5 is the methylene hydrogen that is nearly trans (see Table 3-1) with respect to the thiol hydrogen.] Both basis sets predict that the S-C-H5 angle for the gauche conformer is smaller than in the trans by about 2°. This result is in excellent agreement with the experimental observation (25-27) of change of about 4°. However, these significant changes in the SCC and SCH angles might also affect the frequencies and intensities of some of the bending modes for CH2 group. It is possible that these changes could be used as a key in the experimental infrared spectrum to distinguish these two conformers.

For both geometries, the largest discrepancy in the calculation for gauche-EtSH is in the prediction of the SCH angles. Both calculations predict that both the S-C-H5 and S-C-H6 angles have the same value of 106.7° (105.8°), but it has been observed in the experiments (26, 27) that the angles differ by as much as 4°, where of course the S-C-H6 angle has the larger value. It is well known that polarization functions and correlation corrections may be required to predict accurate geometries (10), and the few discrepancies observed here in Tables 3-1 and 3-2 are much smaller than expected.

Comparing EtSH with ClEtSH, the change from hydrogen (H9) to chlorine appears to have little effect on the C-H bond lengths of $HSCH_2$- fragment, or on the C-S and S-H bond lengths; the difference between the calculated values (3-21G and 6-31G**) of these bond lengths in ClEtSH compared to EtSH appears to be only on the order of 0.001 A (0.001 A). However, the C-H bond lengths of the $ClCH_2$-fragment and the C-C bond length of ClEtSH are calculated to be about 0.006 A (0.014 A) shorter than those of the C-H bonds in the CH_3- group and in the C-C bond of EtSH. The strengthening of these bonds is called the α-effect of chlorine substitution (67). The results from both 3-21G and 6-31G** calculations appear to predict the experimental values of the bond angles within 0.8° and 0.5°, respectively.

Similar trends can be expected for prediction of the geometries of the $XCH_2CH_2SCH_2CH_2X$ series of molecules (Table 3-3). The C-S distance is predicted to change by some amount as hydrogen thiol is substituted by XCH_2CH_2- group to form a larger compounds. In order to make the comparison easier, the geometries for these larger molecules are listed in Table 3-3 for each of the two fragments, CH_3CH_2S- and $ClCH_2CH_2S$-. For the CH_3CH_2S- fragments, the C-S distance predicted at the SCF level with the 3-21G basis set for EtSH, diethyl sulfide, and 2-chlorodiethyl sulfide are 1.901, 1.891, and 1.895 A, respectively. However, for the ClCH2CH2S- fragments, the C-S distance is predicted to be 1.902, 1.896, and 1.894 A for ClEtSH, mustard gas, and 2-chlorodiethyl sulfide, respectively. It seems that the trend for both type of fragments is that the larger molecule always has a shorter C-S bond length, or more stronger bond, compared to its smaller model compounds. All the other bonds, (C-C, C-H, and C-Cl) are not affected (only by ±0.001 A) by this structural change to form a larger molecule. For example, at the 3-21G level, the C-Cl bond length in both ClEtSH and mustard gas is predicted to have the same value of 1.895 A. This value is of course about 0.11 A larger than the experimental value (4) of 1.789 A as previously discussed for the ClEtSH compound. Enlarging the basis set by including polarization functions on all atoms, (6-31G**), is expected to improve the agreement between the predicted values of all bond lengths and the reported experimental parameters to within ±0.005 A.

3.2 Effect of Basis Set on the Prediction of Vibrational Spectra of Molecules in the XCH2CH2SH Series

In this section, we shall discuss the effect of using different basis sets on the prediction of vibrational frequencies, infrared intensities, and potential energy distribution. Trans-EtSH and trans-ClEtSH, which were calculated at both the 3-21G and 6-31G** levels, will be used as examples for this discussion. In order to discuss and compare results of the two calculations, we have partitioned the spectrum into the four regions which contain the fundamental modes of vibration: the 3000-2800 cm^{-1} region, the 2600-2500 cm^{-1} region, the 1500-500 cm^{-1} region, and the region below 300 cm^{-1}.

3.2.1 trans-Ethanethiol

The harmonic vibrational frequencies, infrared intensities and potential energy distribution analysis(PEDs) for this molecule calculated at two different SCF levels, 3-21G and 6-31G**, are presented in Table 3-5 and 3-6, respectively. The predicted IR spectrum calculated at 3-21G level is given in Fig. 3-1 while for 6-31G**, the spectrum is given in Fig. 3-2. By looking at the intensity pattern predicted for the first five modes in Table 3-5 compared with Table 3-6 (in order of decreasing frequency) 14.7, 10.3, 35.8, 0.2, and 19.4 km/mol for the 3-21G calculation in Table 3-5 and 41.4, 42.0, 5.3, 24.7, and 28.1 km/mol for the 6-31G** calculation in Table 3-6 we see that the intensity distribution is predicted to be really different from these two calculations.

3.2.1.1 C-H stretching (3000 - 2800 cm^{-1})

A normal mode mixing between the CH2 s-str and CH3 ipl a-str coordinates is predicted by the 3-21G calculation but not by 6-31G** calculation. In the 3-21G calculation the normal mode dominated by the CH2 s-str (64%) is predicted at a higher frequency, 2916 cm^{-1}, compared to the one dominated by the CH3 ipl a-str, 2903 cm^{-1}. However for the 6-31G** calculation the CH2 s-str frequency is predicted to be only 2872 cm^{-1} while the CH3 ipl a-str is predicted to stay the same at 2903 cm^{-1}.

The intensity for the CH3 ipl a-str is predicted to decrease drastically from 42.0 km/mole in the 6-31G** calculation to 0.2 km/mol in the 3-21G calculation. This effect could be explained by looking at the PEDs and also the sign of the $\underline{L}^{-1}$ elements for each coordinate printed right after the PED values. As mentioned above, there are two coordinates mixing for the mode at 2903 cm^{-1} (3-21G): 62% of the CH3 ipl a-str coordinate with a minus sign and 36% of the CH2 s-str with a plus sign. This phenomenon is called "out-of-phase mixing" and may cancel the intensity contributions from each coordinate to the normal mode at 2903 cm^{-1}.

The corresponding enhancement of intensity due to the "in-phase mixing" of these two coordinates is observed at 2916 cm^{-1} for the CH2 s-str and CH3 ipl a-str for the 3-21G calculation. The intensity of pure CH2 s-str is predicted to be only 24.7 km/mol in the 6-31G** calculation where there is no coordinate mixing, but it is predicted to increase to 35.8 km/mol for the in-phase combination of the CH2 s-str (64%) and CH3 ipl a-str (35%) in the 3-21G calculation.

Of course, it is not true to say that the relative signs of the $\underline{L}^{-1}$ elements is the only factor that causes the intensity of a particular mode to be higher or lower in one calculation than in the other. Since the element of $\underline{P}_Q$ is evaluated by multiplying the elements of $\underline{P}_R$ and $\underline{L}$ altogether (see definition in Chapter 2), then the value of the $\underline{P}_Q$ element is determined by the signs of both $\underline{L}$ and $\underline{P}_R$ elements. In order to do this analysis efficiently, the computer programs named "intensity contribution analysis" or ICA have been developed here and are diagrammed in Appendix A for ICA1 and in Appendix B for ICA2. For a given set of force constants and polar tensors, the program will print the contribution from the change of each symmetry coordinate, or from the displacement of each atom to the normal mode intensity. Parts of the printed output of the ICA programs for trans EtSH in symmetry coordinates and for the atom contribution from displacement of its cartesian coordinates are shown in Tables 3-7 and 3-8. Here we are going to use these outputs to explain the decrease or increase in intensities of normal modes due to the mixing of coordinates.

Table 3-7 shows the intensity analysis in symmetry coordinates for a normal mode (#3 in Table 3-5) predicted at 2916 cm^{-1} in trans EtSH for the calculation at the 3-21G level. For each normal mode, the contributions to $\underline{P}_Q$ form three columns (for the x, y, and z components) and 3N-6 (or 3N-5) rows (for the symmetry coordinates). The star at the beginning of a value in this table designates a contribution larger than 0.01 $eu^{-½}$. As previously mentioned, this band is one illustrating enhancement in intensity due to the in-phase mixing of the vibrational modes. By looking at the values of the contributions to $\underline{P}_Q$ that are marked by the stars, we see that the larger contributions to the intensity of this band are from symmetry coordinates 1 and 10 (the CH2 s-str and CH3 ipl a-str, respectively), plus a smaller contribution from the C-S str (#16). The enhancement of the intensity vectors because the contributions are summed with the same signs. For example in this case both terms contributing to P_{Qx} are positive (0.0729 and 0.0208 $eu^{-½}$) and both values are negative (-0.0964 and -0.0792 $eu^{-½}$) under P_{Qz}.

In order to know the contributions from the motion of each atom to the intensity of this normal mode, the intensity analysis in cartesian coordinate is needed. Table 3-8 shows the intensity for the 3-21G calculation of the same band at 2916 cm^{-1}. The contributions to $\underline{P}_Q$ are still shown in three columns for x, y, and z components, but now there are 3N rows instead of 3N-6 (or 3N-5), with three rows for each atom for its displacement in the x, y, or z direction. The first, second, and the third row for each atom set in the first column represents the P_x values when an atom is displaced in the x, y, and z direction, respectively. From Table 3-8, it could be concluded that the intensity contributions are from the motion of the out-of-plane hydrogen atoms (H5 - H8) of the -CH2- and CH3- groups plus a smaller contribution from the motion of the carbon atom of -CH2- (C3). Contributions from these four out-of-plane hydrogens add up together because they all have the same sign (-) under each $\underline{P}_Q$, but not the in-plane hydrogen (H9) whose contribution has the opposite sign. It is worthwhile to note that the direction of the transition dipole moment of any mode is given by the components of the total $\underline{P}_Q$

values. For this normal mode, the direction of the transition dipole moment is directed at an angle of about 30° counter-clockwise from the S-C bond (or z-axis).

The effect of out-of-phase mixing is seen in the normal mode at 2903 cm^{-1} for the 3-21G calculation (Table 3-5). The total intensity predicted for this mode is very low, only 0.2 km/mol. In Table 3-7 we see that this is because the contribution from the CH2 s-str (S1) is cancelled out by the contribution from CH3 ipl a-str (S10) which has the opposite sign. From the intensity analysis in cartesian coordinates, Table 3-8, it is very clear that this very low intensity is due to the cancellation of the contribution from methylene hydrogens (H5, H6) contribution by that from methyl hydrogens (H7, H8) or vice versa.

The effect of mixing is seen once more here (Tables 3-5 and 3-6) where the intensity is predicted to increase from 14.7 km/mol for the pure CH2 a-str at 2967 cm^{-1} for the 3-21G calculation to 41.4 km/mol at 2925 cm^{-1} for the 6-31G** calculation. The latter, with its high intensity, is due to the in-phase mixing of CH2 a-str (74%) and CH3 opl a-str (26%). The out-of-phase mixing of these two vibrational modes, as expected, lowers the intensity of CH3 opl a-str from 10.3 km/mol at 2918 cm^{-1} (3-21G) to 5.3 km/mol at 2902 cm^{-1} the in 6-31G** calculation.

However, it was observed in both calculations that the CH3 s-str doesn't mix with any other vibrational mode. This mode is predicted at 2855 cm^{-1} (19.4 km/mol) in the 3-21G calculation just a few wavenumbers higher than in 6-31G** calculation, which is at 2841 cm^{-1} (28.1 km/mol). (Please note that the wavenumbers used in the discussion are the wavenumbers that have been scaled by a constant factor of 0.89). Therefore, these small differences in frequencies and intensities predicted for this mode are due only to basis set effects, and indicate the magnitude that may be expected for these effects.

Another significant difference between these two calculations due to the basis set effects is the difference in the intensity sum of the C-H stretching modes. The total intensity is predicted to be only 80.4 km/mol in 3-21G while it is 141.5 km/mol in 6-31G**, indicating that the predicted APTs differ significantly in these two calculations.

3.2.1.2 S-H Stretching (2600 - 2500 cm^{-1})

The effect on the calculation from adding of polarization functions on the sulfur atom can be seen clearly in the predictions for the S-H stretching vibration. With the 3-21G basis set, the S-H str frequency is predicted to be at 2335 cm^{-1}, which is about 236 cm^{-1} lower than the experimental value (28) of 2571 cm^{-1}. For the calculation with the 6-31G** basis set the scaled frequency, 2571 cm^{-1}, calculated for this mode is exactly the same as found in experiment. It has been shown (11) that calculations with d functions (3-21G*, 6-31G*, or 6-31G**) accurately predict the equilibrium geometries and the vibrational frequencies of compounds containing hypervalent atoms such as S. The IR intensities calculated at this level also are expected to be in better agreement with experimental values.

It is well known (11) that compounds involving first-row atoms generally obey the classical octet rule. In contrast, the classical octet rule is frequently violated in compounds incorporating second-row elements (eg. S, Cl, P, ..). The existence of such compounds, often with high thermochemical stability, is due to additional bonding involving low-lying d-type atomic orbitals on the second-row element (68).

The simplest basis sets for second-row atoms--STO-3G and 3-21G basis sets for example--do not incorporate functions of d-type symmetry. These models are unlikely to prove satisfactory in describing bonding in hypervalent compounds. As previously mentioned, calculations at the 3-21G level consistently predict bond lengths to the second-row element that are longer than the corresponding experimental quantities. However, the S-H bond length predicted with the 6-31G** basis set (1.328 A, see Table 3-1) agrees quite well with the experimental values (1.322 A (25) and 1.328 A (27)), and the corresponding prediction for the S-H str frequency (Table 3-6) is also in excellent agreement with experiment.

3.2.1.3 1500 - 500 cm^{-1} region

This large region contains all the normal modes connected with bending motions and heavy atom stretching. In this region, only the CH2 wagging mode appears to have a very high intensity, 53 km/mol (1274 cm^{-1}) with the 3-21G basis and 48 km/mol (1281 cm^{-1}) for the 6-31G** basis. All other modes in this region are predicted to have very low intensities, i.e. less than 10 km/mol. Here again the frequency from 3-21G calculation underestimates the C-S str frequency by 72 cm^{-1} compared to the experimental value, while the predicted wavenumber is in excellent agreement for the 6-31G** calculation (refer to Table 3-5 and 3-6).

3.2.1.4 300 - 0 cm^{-1} region

Only three vibrational modes of trans-EtSH are predicted to appear in this region: the SCC bend, and the CC and S-H torsions. For the SCC bend, both basis sets predict the same value for the frequency at 292 cm^{-1}, about 17 cm^{-1} lower than experimental value (28). The two low frequency torsion modes are predicted to be mixed together with force constants from the 6-31G** calculation but not with the 3-21G basis.

The highest intensity mode in this region is expected to be the S-H torsion (32.2 km/mol with the 3-21G and 21.4 km/mol with the 6-31G** basis set). The S-H torsion frequency predicted at the 3-21G level is exactly the same as experimental value which has been assigned (30) at 158 cm^{-1}, while the calculation with the 6-31G** basis set overestimates it by about 20 cm^{-1}. It is worthwhile to note that calculations with both basis sets predict the intensity of the S-H torsion to be nearly equal to the intensity of S-H stretching mode.

It is very interesting to see that the total of the vibrational intensities predicted for both basis sets differ only by 2.0 km/mol (265.8 km/mol for the 3-21G calculation compared with 263.9 km/mol for the 6-31G** calculation) even though the two calculations differ significantly in the predicted distribution of intensities.

3.2.2 trans-Chloroethanethiol

The differences in frequencies and intensities predicted from calculation at different SCF levels are also observed for this molecule. The comparison for this molecule should be very useful since it contains two second-row atoms, S and Cl. The harmonic vibrational frequencies, infrared intensities and potential energy distribution analysis (PEDs) for this molecule calculated at 3-21G and 6-31G** levels are presented in Table 3-9 and 3-10, respectively. The predicted IR spectrum calculated at 3-21G is shown in Fig. 3-3 while the spectrum calculated with the of 6-31G** basis is shown in Fig. 3-4.

3.2.2.1 C-H stretching (3000 - 2800 cm^{-1})

The four highest frequency bands for this molecule are calculated to be CH2 a-str and CH2 s-str modes where both basis sets predict that the CH2 a-str modes have higher frequencies than the CH2 s-str vibrations. The difference in frequencies between these two CH2(Cl) str modes is predicted to be 71 cm^{-1} for the 3-21G and 62 cm^{-1} for the 6-31G** calculations. For CH2(S) str modes, the separation between the asym and sym modes is smaller (58 cm^{-1} for the 3-21G and only 52 cm^{-1} for the 6-31G** calculation). However, the intensities for these four bands are all predicted to be very low compared to the intensities predicted for the corresponding CH2 str modes in EtSH. The intensity pattern in decreasing order of frequency for the first four bands, is predicted to be 0.3, 0.7, 4.4, and 3.6 km/mol for the 3-21G calculation and 8.6, 2.8, 18.3, and 11.6 km/mol for the 6-31G** calculation. From these predicted intensities, it seems likely that only the symmetric stretching modes will be observed in the experiment.

The substituent effect on the vibrational spectrum when a Cl atom is substituted for an H atom in the CH3 group is pronounced and may be seen by comparing the spectrum predicted for the all-trans conformer of ClEtSH in Table 3-10 with the spectrum predicted for the trans conformer of EtSH in Table 3-6. This comparison is made using the result from the 6-31G** calculation since the predicted scaled harmonic vibrational frequencies are expected to agree very well with the experimental values. The CH2 stretching modes in ClEtSH are predicted to be slightly, but significantly, higher in frequency and decidedly lower in intensity than through in EtSH. The intensity sum of the four CH stretching modes in ClEtSH is only 41.3 km/mol (6-31G**) compared with an intensity sum of 141.5 km/mol predicted for the five CH stretching modes in EtSH at the same level of calculation.

3.2.2.2 S-H stretching (2600 - 2500 cm^{-1})

As previously mentioned in the EtSH, this vibrational frequency, which involved the S atom, is affected very much by the inclusion of polarization functions in 6-31G** calculation. At the 6-31G** level, this mode is predicted (scaled by 0.89) to appear at 2581 cm^{-1} (about 238 cm^{-1} higher than predicted in the 3-21G calculation). As expected, this calculated scaled frequency from the 6-31G** calculation is in excellent agreement with the experimental value of 2571 cm^{-1} (23). The intensity predicted at the 6-31G** level, 9.6 km/mol, is only one-half of that calculated at the 3-21G level (20.2 km/mol). From the experimental spectrum (23), the intensities of the S-H str relative to those for the CH2 s-str, may be estimated. The agreement of the 6-31G** calculating with the observed relative intensities appears to be superior to that for the relative intensities from the 3-21G prediction.

At both levels of calculation, the effect of chlorine substitution is to increase this stretching frequency by about 10 cm^{-1}. However, this predicted increase is not detected in the experimental spectra, where the same value (2570 cm^{-1}) was reported (23, 28) for the SH str in EtSH and for the ClEtSH.

3.2.2.3 1500 - 500 cm^{-1} region

This very large region is belong to all type of bending and heavy atom stretching. In this region, only two very strong bands are predicted to appear in the IR spectrum: the CH2 wagging at 1229 cm^{-1} and the C-Cl stretching mode (with some C-S stretching) at 614 cm^{-1}.

The CH2 wagging (predicted at 1230 cm^{-1} in both calculations) has equal contributions to the PED from the in-phase combination of CH2(S) and CH2(Cl) wagging motions. Furthermore, both basis sets predict that the absolute intensity for this mode is around 62 km/mol.

The second strong band in this region is predicted at 614 cm^{-1} (3-21G basis) or at 693 cm^{-1} for the 6-31G** calculation. This band is predicted to be an out-of-phase combination of C-Cl and C-S stretching motions. At the 3-21G level, the intensity of this band is predicted to be 96.9 km/mol, about 30 km/mol greater than that predicted at the 6-31G** level. The frequency of this mode, which involves both the second-row atoms, S and Cl, is expected to be underestimated by the 3-21G calculation. The predicted frequency at the 6-31G** level, 693 cm^{-1}, is in excellent agreement with the reported (23) experimental value of 695 cm^{-1}.

One question that might arise is why the intensity is predicted to be enhanced for this out-of-phase mixing of the C-Cl and C-S stretching motions, while in the previous case discussed above for EtSH, the intensity for an out-of-phase combination of the CH str modes is predicted to drop nearly to zero (refer to Figure 3-1). In order to investigate this complex problem, the output from the intensity analysis program is really a must. Part of the output from this analysis obtained from the 6-31G** calculation is shown in Table 3-11, which gives the individual contributions from each of symmetry coordinate to this normal mode intensity. Again the stars indicate contributions to the transition moment that are of greater or equal to 0.01 eu$^{-½}$ in magnitude. It is very clear from this figure that the largest contributions are from symmetry coordinates 15 and 16, the C-Cl str and C-S str, respectively. All $\underline{P}_Q$ elements involving these two symmetry coordinates have the same positive sign even though the corresponding $\underline{L}^{-1}$ elements have the opposite signs (negative for the C-Cl str and positive for the C-S str). This perhaps surprising result is easily explained by looking at the $\underline{P}_R$ values given for ClEtSH in Appendix C. Since the components of $\underline{P}_R$ (P_{Rx} and P_{Rz}) from the C-Cl str are both negative and the components of $\underline{P}_R$ for the C-S str are both positive, the product of $\underline{P}_R\underline{L}$ shown in Table 3-11 will all be positive. As previously mentioned, such a combination of intensity contributions with the same sign will add up to give a large intensity for this mode. Of course, in this particular case, Table 3-11 shows clearly that most of the intensity of this mode come from the C-Cl stretch alone, with only a small additional increase from the C-S stretch.

In order to determine which atom really contributes to the intensity of this normal mode, we may examine the output of the intensity analysis for cartesian coordinates. Table 3-12 presents part of the output of the program which shows the individual atomic contributions to this mode calculated at 6-31G** level. The output clearly shows that the intensity of this mode is primarily contributed by the P_x and P_z components of the dipole moments derivatives from the displacement of the C3 and Cl atoms in the z-direction. A smaller contribution from the C-S bond displacements as seen in Table 3-12 for displacement of the C2 and S atoms in the z-direction (along the C-S bond). The angle made by the transition dipole moment for this normal mode is predicted to be 11.3° clockwise from the z-axis (or S-C bond).

3.2.2.4 300 - 0 cm^{-1} region

There are four IR bands predicted for ClEtSH to appear in this region where the heavy atom bending modes and the torsions are expected to appear. The torsion predicted to appear at around 82-90 cm^{-1} is expected to have the highest intensity in this region (Figure 3-3 and 3-4).

It is somewhat surprising to find that inclusion of polarization functions in the calculation result in an exchange in the frequency and intensity predicted for the C-C torsion and the H-S torsion. In the 3-21G calculation, the vibrational frequency of C-C torsion is predicted to be higher than that for the H-S torsion by about 24 cm^{-1}. However, the case is reversed in the 6-31G** calculation where the C-C torsion is predicted to be lower than H-S torsion by about 36 cm^{-1}. Some kind of switching is also predicted for the relative intensities. In the 3-21G calculation, the intensity of H-S torsion is predicted to be higher than that for the C-C torsion but the case is reversed in the 6-31G** calculation. Both calculations predict considerable normal mode mixing for these two motions and a slight error in the predicted force constant (involving the S atom, for example) in the 3-21G basis could lead to this effect due to the inclusion of polarization functions in 6-31G** basis set, but this effect is not observed in calculations for trans EtSH.

Another important bit of information obtained from the comparison of the predicted spectra of ClEtSH and EtSH is that the predicted total intensity sum for all the vibrational modes for these two molecules are not very much different for the higher level calculation. In the 6-31G** calculation (Tables 3-6 and 3-10), the intensity sum for ClEtSH is predicted to be 257.1 km/mol which is only 6.8 km/mol lower than that for EtSH. However, the case is reversed in the 3-21G calculation where the intensity sum for ClEtSH is predicted to be higher than that for EtSH by as much as 25 km/mol. (In the 3-21G calculation the intensity sum for ClEtSH is 290.8 km/mol compared to 265.8 km/mol for EtSH.)

3.3 Comparison of Vibrational Spectra Predicted for trans-Ethanethiol with that for gauche-Ethanethiol

The vibrational frequencies, infrared intensities, and potential energy distributions (PEDs) for gauche-EtSH are summarized in Table 3-13 (3-21G) and 3-14 (6-31G**) and the predicted IR spectra are shown in Fig. 3-5 and 3-6, respectively. It should be noted that the results from 3-21G and 6-31G** calculations for trans-EtSH (discussed previously) are shown in Table 3-5 (Fig. 3-1) and in Table 3-6 (Figure 3-2), respectively.

The most important feature of these tables is the comparison between the predicted spectra for the two conformers. Since the comparison at 3-21G level has already been discussed (14), here more attention will be given to the values predicted at the 6-31G** level. The result of from the 3-21G calculation will be discussed only if there is sum disagreement with the 6-31G** results. Values from the 3-21G calculation are presented in this discussion in parentheses just following the 6-31G** values.

3.3.1 C-H Stretching (3000 - 2800 cm^{-1})

In this region, calculation with both basis sets predict no significant differences between the conformers for the frequencies of the corresponding C-H stretching modes. Therefore, we could expect that the spectral bands for the two conformers would overlap in the experimental spectrum. The distribution of intensities seems to be more sensitive to the conformational changes around the C-S bond. The intensity pattern for the first five C-H stretching modes in order of decreasing frequency for trans conformer is 41.4, 42.0, 5.3, 24.7, and 28.1 km/mol, while for the gauche conformer the corresponding pattern is predicted to be 37.3, 13.8, 42.8, 15.3, and 32.7 km/mol. One might wonder why the intensities of the second and the third band are interchanged from the trans to the gauche conformer. From the PED analyses given in Table 3-6 and 3-14, it is clearly seen that the switching in intensity for these two modes corresponds to the switching in the predicted frequency for the CH3 opl a-str and CH3 ipl a-str. However, the predicted wavenumbers of these two bands are very nearly the same; only 1 cm^{-1} different for the trans conformer and about 8 cm^{-1} different for the gauche conformer. In the 3-21G calculation, a similar switching of assignment and intensity is also predicted for the second and third bands. However, in that case the PED analysis shows that the switching is between the CH3 opl a-str and CH2 s-str instead of CH3 ipl a-str. These predictions are a first example of the phenomenon of "nearly degenerate" normal modes and the confusion in interpreting such intensity and PED patterns for these "nearly degenerate" normal modes. This problem is discussed in more detail in the next chapter.

Even though the intensity patterns are predicted to be slightly different, both basis sets predict that the intensity sum in this region for each conformer is exactly the same (80 km/mol in the 3-21G and 142 km/mol in 6-31G** calculation).

3.3.2 S-H Stretching (2600 - 2500 cm^{-1})

For this stretching mode, both basis sets predict no significant difference either in frequency or in intensity between the two conformers.

3.3.3 1500 - 500 cm^{-1} Region

Because bending and heavy atom stretching modes appear in this region, it is probably the most interesting region for comparison between the predicted spectra of the trans and gauche conformers. In this region the calculation at the 6-31G** level predicts that there is only one mode which is dominated by the CH2 rocking motion, that is different for the two conformers. The PED analysis of this band, which is predicted to appear at 758 cm^{-1} in the trans conformer shows in-phase mixing of CH2 rocking (61%) and CH3 out-of-plane rocking (33%), whereas for the gauche conformer, the band is predicted to appear at 708 cm^{-1} and to consist of a similar mixing of CH2 rocking (61%) and CH3 out-of-plane rocking (17%) motions with the HSC bending (13%) motion. It is worth noting that in the trans (C_s) conformation, the CH2 rocking motion and HSC bending motion belong to different symmetry species and cannot interact, whereas in the gauche (C_1) conformations both are in the same species.

This prediction agree very well with the experimental observations and interpretation reported by Smith, Devlin, and Scott (28). In their experiment, the band at 783 cm^{-1} (corresponding to our predicted value at 758 cm^{-1}) observed in the "glass state" disappeared upon crystallization. They assigned this band to the CH2 rocking mode of the trans conformer, while the band at 737 cm^{-1} (corresponding to our predicted value at 708 cm^{-1}) observed in the spectra of both the "glass" and the "crystal" is assigned to the coupled CH2 rocking and HSC bending mode of the gauche conformer. However, this weak band observed at 783 cm^{-1} is the only manifestation in their spectra of the existence of trans conformer, in agreement with our calculation (Tables 3-6 and 3-14) that there are no other changes expected in the spectra for the two conformers.

It should be noted that the difference between the observed wavenumbers of the CH2 rocking between trans and gauche conformers is about 46 cm^{-1} (783 - 737 cm^{-1}), and is in excellent agreement with the predicted difference of 50 cm^{-1} (6-31G**) and 58 cm^{-1} (3-21G). It is worthwhile to mention that the calculated wavenumbers for the CH2 rocking modes would be in better agreement with experimental values if a scaling factor of $(0.90)^2$ is used for the force constants instead of $(0.89)^2$. This larger scaling factor will bring up the predicted wavenumber for this mode in the trans conformer to

767 cm^{-1} and that for the gauche conformer to 716 cm^{-1} in much better agreement with the experimental values of 783 cm^{-1} and 737 cm^{-1}, respectively.

Another interesting feature about the predicted spectra in this region for this conformers is that, even though the predicted frequencies for the two conformers are very much the same (except for the CH2 rocking discussed above) the predicted intensities do seem to be very sensitive to the conformational changes. For example the intensity of the CH2 wagging mode at 1282 cm^{-1} (1274 cm^{-1}) is predicted to decrease from 48.4 (53.0) km/mol in the trans conformer to 28.3 (31.1) km/mol for the gauche conformer. (Please note that the values in parentheses are from the 3-21G calculation). The predicted decrease in the intensity of the CH2 wagging mode for the gauche conformer, however, compensated by the predicted increases in the intensities of the other bands in this region since the total intensity for this entire region is exactly the same for both conformers, i.e. 78 km/mol (6-31G**) and 114 km/mol (3-21G).

3.3.4 300 - 0 cm^{-1} Region

Only three bands are predicted to appear in this region: the SCC bending mode and the C-C and H-S torsions. At the 3-21G level, the H-S torsion is predicted to be displaced upward by as much as 31 cm^{-1} from 158 to 189 cm^{-1} from trans to gauche conformers, while at the 6-31G** level, this band is predicted to be displaced in the same direction but only about 14 cm^{-1} (from 178 to 192 cm^{-1}). The differences in the experimental values for the H-S torsion frequencies between these two conformers has been reported by Inagaki, Harada, and Shimanouchi (30) in their far-infrared study of this molecule. The observed values for this torsion mode for trans and gauche conformers are 158 and 190 cm^{-1}, respectively, (with 32 cm^{-1} different) and are in very good agreement with the predicted values calculated at both levels.

If the intensity parameters (atomic polar tensors) do not change at all from one conformer to the other, then the sum of the intensities calculated at the same level should be exactly the same (ignoring the intensity sum, Ω, for the pure rotation) (2). Therefore, the intensity sum for the trans conformer in Table 3-5 is expected to be exactly the same as that for the gauche conformer in Table 3-13, and that for Table 3-6 is also expected to be exactly the same as that for Table 3-14. As seen in those tables, the intensity sum for trans EtSH is 263.9 (265.8) km/mol and it is 259.3 (259.7) km/mol for the gauche form. This result suggest that the changes in the APTs, or rather those in the total of mass-weighted squared effective charges (34, 63) are indeed very minor for the change from the trans to the gauche conformer.

Nevertheless, the small change in this sum calculated for the two conformers (from 264 to 259 km/mol) indicates that the APTs are not exactly identical.

3.4 Prediction of Infrared Spectra of Molecules in the $XCH_2CH_2SCH_2CH_2X$ Series

The vibrational frequencies, infrared intensities, and potential energy distribution analyses from the calculation at the 3-21G level for the all-trans conformers (trans along C-S and C-C bonds) of diethyl sulfide ($CH_3CH_2SCH_2CH_3$), mustard gas ($ClCH_2CH_2SCH_2CH_2Cl$), and 2-chlorodiethyl sulfide ($CH_3CH_2SCH_2CH_2Cl$) calculated at 3-21G level are summarized in Tables 3-15, 3-16, and 3-17, and the "stick" simulation of the corresponding infrared spectra are given in Figures 3-7, 3-8, and 3-9, respectively. We should notice that these larger molecules are formed by just combining the two smaller model compounds. Combination of two CH_3CH_2S- groups (less one S atom) gives diethyl sulfide and combining two $ClCH_2CH_2S$- group gives mustard. The combination of CH_3CH_2S- with the $ClCH_2CH_2S$- group gives the unsymmetrical molecule chlorodiethyl sulfide.

For the two symmetrical molecules we may expect (14) that their predicted spectra will be, to some extent, just "doubled" versions of the spectra of their model compound. Thus, each CH stretching mode predicted for EtSH is predicted to be doubled in the diethyl sulfide molecule; for example, the out-of-plane asymmetric stretching mode of the CH3 group predicted at 2918 cm^{-1} for trans-EtSH (Table 3-5) is coupled in the diethyl sulfide to give in-phase and out-of-phase combinations of this motion (Table 3-15) both at 2913 cm^{-1}. Because of the symmetry, the out-of-phase combination has zero intensity. These two modes are predicted to have the same frequency since the coupling is very weak between the two CH3 groups at each end of the molecule.

The replacement of the H(S) atom in EtSH by the CH_3CH_2- group to form the diethyl sulfide is predicted to affect the PEDs, frequency, and the intensity distribution of several modes in the spectrum especially in the low-frequency region ("fingerprint region") from 1500 to 300 cm^{-1}. The vibrations of the CH_3CH_2- groups are no longer coupled with the S-H vibrations (HSC bending), but with CSC bending instead. However, it is quite easy to see the pairs of bands in the larger molecule that correspond to single modes in the model compounds.

The C-S stretching vibration is predicted to be the most affected by the structural changes from model compounds to the larger molecules. First of all the larger molecules of course have two C-S stretching modes (a weak in-phase at 620 cm^{-1} and a stronger out-of-phase mode at 609 cm^{-1} for diethyl sulfide). Here the frequency of this mode is predicted to increase from the corresponding predicted value for EtSH (586 cm^{-1}). This predicted shift is in excellent agreement with experimental observations, since this symmetric stretching frequency for all-trans diethyl sulfide is assign by Shimanouchi et al. (20) about 36 cm^{-1} higher than the C-S stretching mode for trans-EtSH assigned by Smith, Devlin, and Scott (28). (The experimental C-S stretching frequency of diethyl sulfide was assigned at 693 cm^{-1} (20) while it is only 657 cm^{-1} in EtSH (28)).

Identical comments can be made about the relationship between the spectrum of mustard gas (Table 3-16) and its model compound, ClEtSH (Table 3-9).

For the unsymmetrical molecule $CH_3CH_2SCH_2CH_2Cl$, the calculated spectrum (Table 3-17) may be more correctly described as a superposition of the spectrum from the CH_3CH_2S-group onto that from $ClCH_2CH_2S$- group. However, this assumption is not always correct; for example see the CH_2 wagging mode predicted at 1294 cm^{-1} in Table 3-17. In this region the coupling between the CH_2 group bending modes become more complex due to the existence of three chemically different CH_2 groups: one from CH_3-$\underline{CH_2}$-S and two from Cl-$\underline{CH_2}$-$\underline{CH_2}$-S. Thus, the CH_2 wagging of ClCH2-$\underline{CH_2}$- is coupled not only with the CH_2 wagging of Cl-$\underline{CH_2}$-CH_2- but also with the wagging from the CH_2 of CH_3-$\underline{CH_2}$- group. The total intensity for all the wagging modes in this molecule, 101 km/mol, as expected, is approximately equal to the intensity sum of wagging CH_2 modes in EtSH and ClEtSH, i.e. 53.0 + 63.7 = 116.7 km/mol. This small difference of about 15 km/mol might be due to the changes in the charge distribution when H(S) atom is replaced by the larger fragment, ethyl or chloroethyl, to form this molecule.

It is of some interest here to compare our calculated spectra for diethyl sulfide (Table 3-15), mustard gas (Table 3-16), and 2-chlorodiethyl sulfide (Table 3-17), with that calculated by using force constants recommended by Shimanouchi et al. (66) as transferable force constants for molecules of this type.

Shimanouchi and co-workers have compared the calculated spectra (wavenumbers and PEDs) for diethyl sulfide (66) with their experimental studies (20) of the spectra for this molecule. The agreement was very good (within 10 cm^{-1}) with their experimental spectra. Their assignment of the experimental spectrum is based upon their calculated PEDs, so the agreement is force to some extent. However, since their force field was chosen to be transferable among a large number of these kinds of molecules, it is believed to be a reasonable representation of a "true experimental force field". Hence, their calculated frequencies and PEDs may be taken as the best "experimental" values available.

A more complete discussion of the PEDs for these molecules has already been given in our paper (14). Hence, only a brief discussion will be presented here. The calculated vibrational frequencies, infrared intensities and potential energy analyses (PEDs) for diethyl sulfide are listed in Table 3-15, together with the experimental frequencies obtained from the infrared experiment (20) except that the experimental frequencies listed in Table 3-15 in the CH stretching region are those predicted using Shimanouchi's transferable set of force constants (66).

Comparing the calculated frequencies (scaled by 0.89), with the experimental frequencies (Table 3-15), we see that the general agreement is actually very good. As can be expected for calculations made with this small basis set (3-21G) without polarization functions for the second-row atoms, there are, however, a number of differences. The major discrepancy between the two calculations for the CH stretching region (3000 - 2800 cm^{-1}) is that our calculation predicts that both in-phase and out-of-phase CH_2 asymmetric stretching modes have a higher frequencies than any of the CH3 stretching modes. For the CH_2 and CH_3 bending modes (1500 - 1200 cm^{-1}) the agreement is quite acceptable. The CC stretching force constants are predicted to be considerably smaller than the experimental values so that the predicted scaled wavenumbers

(918 and 911 cm^{-1}) for these modes are lower than the experimental values (at 986 and 973 cm^{-1}). However, if a larger scaling factor is used for this force constant (for example $(0.95)^2$ instead of $(0.89)^2$) the calculated scaled frequencies for these CC stretching modes are 984 and 976 cm^{-1}, values which are in excellent agreement with the experimental values. As expected, the predicted wavenumbers for the CS stretching modes (620 and 609 cm^{-1}) are considerably lower than the experimental modes at 693 and 683 cm^{-1}. For these force constants, the scaling factor of 1.0 (as previously suggested (14) for the EtSH frequencies calculated at the 3-21G level) will bring up the predicted frequencies to 697 and 684 cm^{-1}, in excellent agreement with experimental values. An excellent review on the use of different scaling factors for the force constants is already given by Fogarasi and Pulay (12) in 1985 and will be discussed later. However, the agreement between our predicted values and the "experimental values" from Shimanouchi et al. for the PEDs of the remaining modes of diethyl sulfide is remarkably good.

An examination of the comparison between our calculated values and the "experimental" wavenumbers (66) for mustard gas and 2-chlorodiethyl sulfide is presented in Table 3-16 and 3-17, respectively, indicates the same general agreement for these more complicated molecules. As previously mentioned, the agreement with experimental values for the stretching vibrations of S-C, C-Cl, and C-C would be better if different scaling factors are used. A discussion of the use of this method together with its application to these molecules in this series will be presented in the latter section.

In spite of the problems mentioned here, the general agreement between the calculated spectrum and the experimental spectrum, even for these very complicated molecules, is promising.

Table 3-1: Optimized Geometries[a] for trans- and gauche-EtSH Calculated with Two Different Basis Sets, 3-21G and 6-31G**.

	trans				gauche			
	3-21G	6-31G**	obs.		3-21G	6-31G**	obs.	
H-S	1.353	1.328	1.322[b]	1.328[c]	1.353	1.328	1.336[d]	1.328[c]
C2-S	1.901	1.828	1.820	1.829	1.899	1.826	1.814	1.829
C2-C3	1.532	1.525	1.529	1.530	1.530	1.524	1.528	1.530
H5/6-C2	1.078	1.082	1.090	1.088	1.079	1.083	1.089	1.088
H7/8-C3	1.083	1.085	1.092	1.093	1.083	1.085	1.091	1.093
H9-C3	1.084	1.085	1.095	1.093	1.086	1.086	1.091	1.093
C2-S-H	98.2	98.1	96.2	95.2	97.0	97.3	96.0	95.2
S-C2-C3	108.3	109.7	108.6	108.6	112.4	114.2	113.6	113.3
S-C2-H5	107.8	109.0	109.4	110.9	105.8	106.7	104.9	106.1
S-C2-H6	107.8	109.0	109.4	110.9	105.8	106.7	109.3	110.8
C3-C2-H5	111.3	110.3	110.2	109.6	111.8	110.8	110.7	109.6
C3-C2-H6	111.3	110.3	110.2	109.6	111.8	110.8	111.3	109.6
H5-C2-H6	110.0	108.4	108.9	107.2	108.9	107.1	106.6	107.3
C2-C3-H7/8	110.7	111.2	110.6	109.7	110.8	111.1	110.6	109.7
C2-C3-H9	109.7	109.8	109.7	109.7	109.9	110.1	110.5	109.7
H7-C3-H8	108.7	108.3	108.1	109.2	108.5	108.1	106.9	109.2
H7-C3-H9	108.5	108.1	108.6	109.2	108.1	107.9	109.0	109.2
H8-C3-H9	108.5	108.1	108.6	109.2	108.8	108.5	109.0	109.2
H-S-C2-C3	180.0	180.0	180.0	180.0	63.2	63.1	61.8	60.0
S-C2-C3-H9	180.0	180.0	180.0	180.0	180.0	180.0	180.0	180.0
H-S-C2-H5	59.4	59.1			174.6	174.0		
S-C2-C3-H7	60.3	60.4			60.6	60.6		
H5-C2-C3-H7	178.7	179.5			179.5	178.8		

[a] Bond lengths are in A and angles in degrees. [bcd] From ref. 25, 27, and 26, respectively.

Table 3-2: Optimized Geometries[a] for all-trans ClEtSH Calculated with Two Different Basis Sets, 3-21G and 6-31G**.

	3-21G	6-31G**	obs[b]
H-S	1.352	1.326	
C2-S	1.902	1.829	
C2-C3	1.513	1.519	1.519
H5/6-C2	1.076	1.081	
H7/8-C3	1.074	1.079	1.082
Cl-C3	1.895	1.793	1.789
C2-S-H	97.3	97.2	
S-C2-C3	106.9	108.3	
S-C2-H5/6	108.6	109.7	
C3-C2-H5/6	111.0	110.0	
H5-C2-H6	110.6	109.1	
C2-C3-H7/8	113.0	111.6	
C2-C3-Cl	108.2	110.4	110.1
H7-C3-H8	111.7	109.4	
H7/8-C3-Cl	105.1	106.8	
H-S-C2-C3	180.0	180.0	58.4
S-C2-C3-Cl	180.0	180.0	63.3
H-S-C2-H5	60.2	59.9	
S-C2-C3-H7	64.1	61.4	
H5-C2-C3-H7	177.6	178.7	

[a]Bond lengths are in A and angles in degrees. [b]From ref. 24.

Table 3-3: Optimized Geometries[a] at 3-21G Level for trans-EtSH, all-trans Diethyl Sulfide (DS), all-trans Chlorodiethyl Sulfide (Cl-DS), trans-ClEtSH, and Mustard Gas (MU), Listed for Each of the Two Fragments, CH_3CH_2S- and $ClCH_2CH_2S$-.

	CH3CH2S- fragment			ClCH2CH2S- fragment		
	EtSH	DS	Cl-DS	ClEtSH	MU	Cl-DS
H-S	1.353			1.352		
C2-S	1.901	1.891	1.895	1.902	1.896	1.894
C2-C3	1.532	1.533	1.532	1.513	1.513	1.513
H5-C2	1.078	1.080	1.079	1.076	1.077	1.078
H7-C3	1.083	1.083	1.083	1.074	1.074	1.074
H9-C3	1.084	1.085	1.084			
Cl-C3				1.895	1.895	1.899
C2-S-H	98.2			97.3		
C2-S-C3		100.1	99.4		98.7	99.4
S-C2-C3	108.3	109.1	108.8	106.9	107.4	107.6
S-C2-H5	107.8	107.9	107.6	108.6	108.5	108.6
C3-C2-H5	111.3	111.1	111.4	111.0	111.0	110.9
H5-C2-H6	110.0	109.6	109.9	110.6	110.5	110.2
C2-C3-H7	110.7	110.6	110.7	113.0	113.0	113.1
C2-C3-H9	109.7	110.0	109.7			
C2-C3-Cl				108.2	108.3	108.5
H7-C3-H8	108.7	108.6	108.7	111.7	111.7	111.7
H7-C3-H9	108.5	108.5	108.5			
H7-C3-Cl				105.1	105.0	104.9

---

[a] Bond lengths are in A and angles in degrees.

Table 3-4: Total Energies and Dipole Moments Calculated at the SCF Level with the 3-21G Basis Set for all Compounds and with 6-31G** Basis Set for trans- and gauche-EtSH, and also for trans-ClEtSH.

		SCF energy E, au	calculated dipole moments (Debye)				experimental total dipole moments (Debye)
			μ_x	μ_y	μ_z	μ_T	μ_T
EtSH							
trans	3-21G	-474.34725	0.0794	2.1917	0.0000	2.1931	
	6-31G**	-476.74740	0.0322	1.8516	0.0000	1.8519	1.56[a] 1.58[b]
gauche	3-21G	-474.34766	2.0583	0.0643	1.0600	2.3161	
	6-31G**	-476.74767	1.6960	0.1091	0.8628	1.9060	1.61[b]
ClEtSH							
trans	3-21G	-931.06371	0.7464	1.7127	0.0000	1.8683	
	6-31G**	-935.64558	0.4104	1.3331	0.0000	1.3948	
DS							
all-trans	3-21G	-551.98973	0.0000	0.0000	1.9905	1.9905	
ChloroDS							
all-trans	3-21G	-1008.70761	2.2937	-2.0260	0.0000	3.0603	
Mustard gas							
all-trans	3-21G	-1465.42361	0.0000	0.0000	1.3049	1.3049	

[a,b] From ref. 1 and 2, respectively.

Table 3-5: Harmonic Vibrational Frequencies, Infrared Intensities and the Potential Energy Distribution Analysis (PED) Predicted for trans-EtSH Using the 3-21G Basis Set.

normal coord	wavenumbers, cm^{-1} exptl[d]	scl[a]	A, km/mol	PED[b,c]
1	2988	2967	14.7	CH2 a-str(95+)
2	2967	2918	10.3	CH3 opl a-str(95-)
3	2932	2916	35.8	CH2 s-str(64+) CH3 ipl a-str(35+)
4	2902	2903	0.2	CH3 ipl a-str(62-) CH2 s-str(36+)
5	2875	2855	19.4	CH3 s-str(97-)
6	2571	2335	34.0	S-H str(100+)
7	1460	1488	4.3	CH3 ipl a-def(92+)
8	1450	1484	9.4	CH3 opl a-def(91+)
9	1434	1465	6.5	CH2 sciss(98+)
10	1376	1408	7.7	CH3 s-def(101-)
11	1273	1274	53.0	CH2 wag(89+)
12	1251	1252	0.6	CH2 twist(57+) CH3 opl rock(30+)
13	1094	1072	4.2	CH3 ipl rock(59+) HSC bend(13+) C-C str(10-)
14	1052	1023	0.1	CH2 twist(41+) CH3 opl rock(35-) CH2 rock(19+)
15	970	924	8.1	C-C str(69+) CH3 ipl rock(14+)
16	869	807	6.0	HSC bend(74+) C-C str(19+)

---

continued

Table 3-5 -- continued

normal coord	wavenumbers, cm^{-1} exptl[d]	scl[a]	A, km/mol	PED[b,c]
17	783	769	5.6	CH2 rock(71+) CH3 opl rock(25+)
18	658	586	7.9	C-S str(89+)
19	318	292	4.8	SCC def(86+)
20	241	232	1.1	C-C tors(90-)
21	191	158	32.2	H-S tors(93+)
		ΣA_i	265.8	

Average Deviation[e] = 2.83%

---

[a] Scale factor is 0.89 for all modes.

[b] Percentage contributions greater than or equal to 10% are given in parentheses.

[c] Definitions of symmetry coordinates are the same as given by Shimanouchi et al. (66). The + and - signs give the relative phases of each symmetry coordinate in the normal coordinate (see ref 66). str = stretch; def = deformation; tors = torsion; scis = scissors; ipl = in plane; opl = out of plane.

[d] From ref 28.

[e] Average Deviation = $(100/n) \sum_{i=1}^{n} \mathrm{abs}\ (\bar{\nu}_{scl} - \bar{\nu}_{exptl}) / \bar{\nu}_{exptl}$; the summation is carried out for all modes, n, with wavenumber greater than 500 cm^{-1}.

Table 3-6: Harmonic Vibrational Frequencies, Infrared Intensities and the Potential Energy Distribution Analysis (PED) Predicted for trans-EtSH Using the 6-31G** Basis Set.

normal coord	wavenumbers, cm^{-1} exptl^{d}	scl^{a}	A, km/mol	PED^{b,c}
1	2988	2925	41.4	CH2 a-str(74+) CH3 opl a-str(26+)
2	2967	2903	42.0	CH3 ipl a-str(96+)
3	2932	2902	5.3	CH3 opl a-str(74-) CH2 a-str(26+)
4	2902	2872	24.7	CH2 s-str(96+)
5	2875	2841	28.1	CH3 s-str(100-)
6	2571	2571	17.5	S-H str(100+)
7	1460	1452	1.2	CH3 ipl a-def(70+) CH2 sciss(24-)
8	1450	1446	3.8	CH2 sciss(73+) CH3 ipl a-def(22+)
9	1434	1444	6.3	CH3 opl a-def(92+)
10	1376	1380	2.3	CH3 s-def(95+)
11	1273	1281	48.4	CH2 wag(86-)
12	1251	1231	0.3	CH2 twist(60+) CH3 opl rock(29+)
13	1094	1078	3.3	CH3 ipl rock(46+) HSC bend(22+) C-C str(17-) SCC def(10+)
14	1052	1021	0.3	CH2 twist(37+) CH2 rock(30+) CH3 opl rock(30-)

----

continued

Table 3-6 -- continued

normal coord	wavenumbers, cm^{-1} exptl[d]	scl[a]	A, km/mol	PED[b,c]
15	970	945	3.0	C-C str(60-) CH3 ipl rock(19-) CH2 wag(10+)
16	869	846	3.9	HSC bend(71-) C-C str(13-) CH3 ipl rock(13+)
17	783	758	2.5	CH2 rock(61+) CH3 opl rock(33+)
18	658	648	3.3	C-S str(86+)
19	319	292	2.7	SCC def(86+)
20	241	241	2.1	C-C tors(80-) H-S tors(16+)
21	191	178	21.4	H-S tors(84+) C-C tors(17+)
		ΣA_i	263.9	

Average Deviation[e] = 1.44%

[a-e]As in Table 3-5.

Table 3-7: Part of the Intensity Analysis in Symmetry Coordinates for trans-EtSH Calculated at the 3-21G Level.

scaled freqs(cm^{-1})		2916		2903	
major PEDs(%)		$S1(64+) + S10(35+)^a$		$S10(62-) + S1(36+)^a$	
intensity(km/mol)		35.8		0.2	
		P_{Qx}^b	P_{Qz}^b	P_{Qx}^b	P_{Qz}^b
CH2 s-str	1	* 0.0729	* -0.0964	* 0.0542	* -0.0717
CH2 sciss	2	-0.0020	-0.0019	-0.0006	-0.0005
CH2 a-str	3	0.0000	0.0000	0.0000	0.0000
CH2 rock	4	0.0000	0.0000	0.0000	0.0000
CH2 wag	5	-0.0002	0.0036	0.0001	-0.0012
CH2 twist	6	0.0000	0.0000	0.0000	0.0000
CH2 def	7	0.0009	0.0027	0.0050	* 0.0145
CH3 s-str	8	0.0087	0.0058	* -0.0165	* -0.0110
CH3 s-def	9	-0.0003	0.0000	0.0008	0.0000
CH3 ipl a-str	10	* 0.0208	* -0.0792	* -0.0277	* 0.1055
CH3 ipl a-def	11	-0.0003	0.0048	0.0004	-0.0059
CH3 ipl rock	12	0.0006	0.0030	-0.0022	* -0.0115
CH3 opl a-str	13	0.0000	0.0000	0.0000	0.0000
CH3 opl a-def	14	0.0000	0.0000	0.0000	0.0000
CH3 opl rock	15	0.0000	0.0000	0.0000	0.0000

----

continued

Table 3-7 -- continued

scaled freqs(cm^{-1}) major PEDs(%) intensity(km/mol)		2916 S1(64+) + S10(35+)[a] 35.8		2903 S10(62−) + S1(36+)[a] 0.2	
		P_{Qx}[b]	P_{Qz}[b]	P_{Qx}[b]	P_{Qz}[b]
C-S str	16	-0.0022	* -0.0107	-0.0015	-0.0072
C-C str	17	-0.0015	0.0012	-0.0017	0.0014
H-S tors	18	0.0000	0.0000	0.0000	0.0000
C-C tors	19	0.0000	0.0000	0.0000	0.0000
HSC bend	20	-0.0031	0.0006	-0.0025	0.0005
H-S str	21	0.0013	0.0005	0.0008	0.0003
		0.0957	-0.1660	0.0086	0.0131

[a] S1 = CH2 s-str, S10 = HSC bend.

[b] The numbers in this column (in $eu^{-\frac{1}{2}}$) give the contribution from each coordinate to the trasition dipole. (Refer to Eq. 2-47). Note that $P_{Qy}=0$, since these are in-plane vibrational modes.

Table 3-8: Part of the Intensity Analysis in Atomic Cartesian Coordinates for trans-EtSH Calculated at the 3-21G Level.

scaled freqs(cm^{-1})		2916		2903	
major PEDs		S1(64+) + S10(35+)^{a}		S10(62-) + S1(36+)^{a}	
intensity(km/mol)		35.8		0.2	
		P_{Qx}^{b}	P_{Qz}^{b}	P_{Qx}^{b}	P_{Qz}^{b}
S-1	x	0.0000	0.0000	0.0000	0.0000
	y	0.0000	0.0000	0.0000	0.0000
	z	0.0000	0.0001	0.0000	0.0000
C-2	x	0.0014	-0.0075	-0.0010	0.0056
	y	0.0000	0.0000	0.0000	0.0000
	z	0.0013	* 0.0177	-0.0009	*-0.0120
C-3	x	-0.0007	-0.0009	-0.0011	-0.0013
	y	0.0000	0.0000	0.0000	0.0000
	z	-0.0033	-0.0022	-0.0043	-0.0028
H-4	x	-0.0013	-0.0004	0.0008	0.0002
	y	0.0000	0.0000	0.0000	0.0000
	z	0.0003	-0.0001	-0.0003	0.0001
H-5	x	0.0020	0.0047	-0.0014	-0.0035
	y	*-0.0358	* 0.0212	* 0.0268	*-0.0159
	z	-0.0008	* 0.0187	0.0006	*-0.0140
H-6	x	0.0020	0.0047	-0.0014	-0.0035
	y	*-0.0358	* 0.0213	* 0.0268	*-0.0159
	z	-0.0008	* 0.0187	0.0006	*-0.0140
H-7	x	0.0023	0.0001	0.0033	0.0002
	y	*-0.0195	0.0096	*-0.0278	* 0.0137
	z	-0.0035	-0.0059	-0.0051	-0.0085

continued

Table 3-8 -- continued

scaled freqs(cm^{-1}) major PEDs intensity(km/mol)		2916 S1(64+) + S10(35+)[a] 35.8		2903 S10(62-) + S1(36+)[a] 0.2	
		P_{Qx}[b]	P_{Qz}[b]	P_{Qx}[b]	P_{Qz}[b]
H-8	x	0.0023	0.0001	0.0033	0.0002
	y	*-0.0195	0.0096	*-0.0278	* 0.0137
	z	-0.0035	-0.0059	-0.0051	-0.0085
H-9	x	-0.0006	0.0006	-0.0006	0.0006
	y	0.0000	0.0000	0.0000	0.0000
	z	* 0.0181	* 0.0617	* 0.0231	* 0.0786
		-0.0957	0.1660	0.0086	0.0131

[a] As in Table 3-7.

[b] Refer to Eq. 2-45.

Table 3-9: Harmonic Vibrational Frequencies, Infrared Intensities and the Potential Energy Distribution Analysis (PED) Predicted for trans-ClEtSH Using 3-21G basis set.

normal coord	wavenumbers, cm^{-1} exptl[d]	scl[a]	A, km/mol	PED[b,c]
1	2995	3026	0.3	Cl(CH2) a-str(92-)
2	2950	2988	0.7	S(CH2) a-str(92-)
3	-	2955	4.4	Cl(CH2) s-str(98-)
4	-	2930	3.6	S(CH2) s-str(98-)
5	2570	2343	20.2	S-H str(100+)
6	1445	1466	5.8	S(CH2) sciss(91-)
7	1423	1461	10.9	Cl(CH2) sciss(91-)
8	1310	1289	0.6	S(CH2) wag(48+) Cl(CH2) wag(47-)
9	1268	1280	0.0	S(CH2) twist(45+) Cl(CH2) twist(37+) S(CH2) rock(10-)
10	1227	1229	63.1	Cl(CH2) wag(50+) S(CH2) wag(47+)
11	1143	1110	0.6	Cl(CH2) twist(54-) S(CH2) twist(41+)
12	1045	1009	6.2	C-C str(72-) HSC bend(20+)
13	1021	926	0.1	Cl(CH2) rock(43+) S(CH2) rock(39-) S(CH2) twist(12-)
14	860	816	6.1	HSC bend(69+) C-C str(24+)
15	754	753	4.9	S(CH2) rock(47+) Cl(CH2) rock(43+)

---

continued

Table 3-9 -- continued

normal coord	wavenumbers, cm^{-1} exptl[d]	scl[a]	A, km/mol	PED[b,c]
16	724	668	2.4	C-S str(48-) CCCl def(21+) SCC def(14+) C-Cl str(10-)
17	699	614	96.9	C-Cl str(68-) C-S str(31+)
18	300	264	1.4	CCCl def(33+) C-Cl str(22+) C-S str(22+) SCC def(19+)
19	255	193	11.4	SCC def(57+) CCCl def(42-)
20	220	106	0.7	C-C tors(60-) H-S tors(32+)
21	-	82	50.6	H-S tors(68+) C-C tors(32+)
		ΣA_i	290.8	

Average Deviation[e] = 3.91%

[a-c,e] As in Table 3-5.

[d] From ref 23.

Table 3-10: Harmonic Vibrational Frequencies, Infrared Intensities and the Potential Energy Distribution Analysis (PED) Predicted for trans-ClEtSH Using the 6-31G** Basis Set.

normal coord	wavenumbers, cm^{-1} exptl^{d}	scl^{a}	A, km/mol	PED^{b,c}
1	2995	2973	8.6	Cl(CH2) a-str(89-) S(CH2) a-str(11-)
2	2950	2943	2.8	S(CH2) a-str(89-) Cl(CH2) a-str(11+)
3	-	2911	18.3	Cl(CH2) s-str(98-)
4	_	2891	11.6	S(CH2) s-str(98+)
5	2570	2581	9.6	S-H str(100+)
6	1445	1449	1.4	S(CH2) sciss(72-) Cl(CH2) sciss(23-)
7	1423	1447	6.6	Cl(CH2) sciss(75+) S(CH2) sciss(25-)
8	1310	1321	2.4	Cl(CH2) wag(58-) S(CH2) wag(36+)
9	1268	1262	0.0	Cl(CH2) twist(46+) S(CH2) twist(39+)
10	1227	1231	61.2	S(CH2) wag(56+) Cl(CH2) wag(41+)
11	1143	1115	1.8	Cl(CH2) twist(46-) S(CH2) twist(43+)
12	1045	1035	4.8	C-C str(63+) HSC bend(22-)
13	1021	964	0.3	S(CH2) rock(43-) Cl(CH2) rock(40+) S(CH2) twist(14-)
14	860	864	7.2	HSC bend(58-) C-C str(26-)

----

continued

Table 3-10 -- continued

normal coord	wavenumbers, cm^{-1} exptl[d]	scl[a]	A, km/mol	PED[b,c]
15	754	745	2.0	S(CH2) rock(45+) Cl(CH2) rock(43+)
16	724	729	6.0	C-S str(37+) CCCl def(17-) C-Cl str(17+) HSC bend(15+) SCC def(11-)
17	699	693	68.4	C-Cl str(62-) C-S str(39+)
18	300	281	1.1	CCCl def(39-) C-S str(19-) SCC def(18-) C-Cl str(17-)
19	255	201	8.5	SCC def(61+) CCCl def(37-)
20	220	126	6.2	H-S tors(66+) C-C tors(28-)
21	_	90	28.2	C-C tors(65+) H-S tors(34+)
		ΣA_i	257.1	

Average Deviation[e] = 1.14%

[a-e] As in Table 3-5.

Table 3-11: Part of the Intensity Analysis in Symmetry Coordinates for all-trans-ClEtSH Calculated at 6-31G** Level.

scaled freqs(cm^{-1})		693	
major PEDs(%)		S15(62-)[a] + S16(39+)[a]	
intensity(km/mol)		68.4	
		P_{Qx}[b]	P_{Qz}[b]
S(CH2) s-str	1	0.0001	-0.0001
S(CH2) sciss	2	0.0006	0.0004
S(CH2) a-str	3	0.0000	0.0000
S(CH2) rock	4	0.0000	0.0000
S(CH2) wag	5	-0.0016	0.0070
S(CH2) twist	6	0.0000	0.0000
SCC bend	7	* 0.0132	0.0090
Cl(CH2) s-str	8	-0.0001	0.0001
Cl(CH2) sciss	9	0.0017	0.0006
Cl(CH2) a-str	10	0.0000	0.0000
Cl(CH2) rock	11	0.0000	0.0000
Cl(CH2) wag	12	-0.0032	0.0083
Cl(CH2) twist	13	0.0000	0.0000
C-C-Cl bend	14	* -0.0142	-0.0061
C-Cl str	15	* 0.0454	* 0.1977
C-S str	16	0.0045	* 0.0458
C-C str	17	-0.0002	-0.0001
H-S tors	18	0.0000	0.0000
C-C tors	19	0.0000	0.0000
HSC bend	20	0.0057	-0.0028
H-S tors	21	0.0001	0.0001
		0.0520	0.2598

[a] S15 = C-Cl str, S16 = C-S str.

[b] As in Table 3-7.

Table 3-12. Part of the Intensity Analysis in Atomic Cartesian Coordinate for all-trans-ClEtSH Calculated at the 6-31G** Level.

scaled freqs(cm^{-1})		693	
major PEDs(%)		S15(62-)[a] + S16(39+)[a]	
intensity(km/mol)		68.4	
		P_{Qx}[b]	P_{Qz}[b]
S-1	x	0.0000	-0.0001
	y	0.0000	0.0000
	z	-0.0067	-0.0098
C-2	x	-0.0004	-0.0027
	y	0.0000	0.0000
	z	-0.0011	* -0.0597
C-3	x	0.0010	0.0007
	y	0.0000	0.0000
	z	* -0.0240	* -0.1802
H-4	x	-0.0011	-0.0005
	y	0.0000	0.0000
	z	-0.0011	0.0007
H-5	x	0.0001	0.0000
	y	-0.0002	0.0001
	z	-0.0015	* 0.0116
H-6	x	0.0001	0.0000
	y	-0.0002	0.0001
	z	-0.0015	* 0.0116
H-7	x	0.0004	-0.0001
	y	-0.0007	0.0005
	z	-0.0017	* 0.0114
H-8	x	0.0004	-0.0001
	y	-0.0007	0.0005
	z	-0.0017	* 0.0114
Cl-9	x	-0.0003	-0.0001
	y	0.0000	0.0000
	z	* -0.0110	* -0.0551
		-0.0520	-0.2598

[a] As in Table 3-11.

[b] As in Table 3-8.

Table 3-13: Harmonic Vibrational Frequencies, Infrared Intensities and the Potential Energy Distribution Analysis (PED) Predicted for gauche-EtSH Using the 3-21G Basis Set.

normal coord	wavenumbers, cm^{-1}		A, km/mol	PED[b,c]
	exptl[d]	scl[a]		
1	2988	2966	9.2	CH2 a-str(94-)
2	2967	2917	25.9	CH2 s-str(55+) CH3 opl a-str(30-) CH3 ipl a-str(14+)
3	2932	2912	16.7	CH3 opl a-str(62+) CH2 s-str(32+)
4	2902	2897	6.5	CH3 ipl a-str(80+) CH2 s-str(12-)
5	2875	2847	22.2	CH3 s-str(94-)
6	2571	2333	28.7	S-H str(100-)
7	1460	1485	3.7	CH3 ipl a-def(87+)
8	1450	1483	11.7	CH3 opl a-def(86+)
9	1434	1461	6.6	CH2 sciss(97-)
10	1376	1408	6.6	CH3 s-def(100+)
11	1273	1273	31.1	CH2 wag(84-)
12	1251	1256	0.7	CH2 twist(61+) CH3 opl rock(25+)
13	1094	1083	10.6	CH3 opl rock(24+) HSC bend(21-) CH2 rock(20-) CH2 twist(19-)
14	1052	1041	4.0	CH3 ipl rock(59+)
15	970	913	8.2	C-C str(86+)
16	869	846	16.1	HSC bend(52+) CH3 opl rock(24+) CH2 twist(10-)

---

continued

Table 3-13 -- continued

normal coord	wavenumbers, cm^{-1} exptl[d]	scl[a]	A, km/mol	PED[b,c]
17	737	711	2.0	CH2 rock(60+) HSC bend(24-) CH3 opl rock(10+)
18	658	580	14.1	C-S str(87-)
19	319	311	1.1	SCC def(86+)
20	241	241	2.5	C-C tors(91+)
21	191	189	31.5	H-S tors(94-)
		ΣA_i	259.7	

Average Deviation[e] = 2.07%

[a-e] As in Table 3-5.

Table 3-14: Harmonic Vibrational Frequencies, Infrared Intensities and the Potential Energy Distribution Analysis (PED) Pedicted for gauche-EtSH Using the 6-31G** Basis Set.

normal coord	wavenumbers, cm^{-1} exptl^{d}	wavenumbers, cm^{-1} scl^{a}	A, km/mol	PED^{b,c}
1	2988	2925	37.3	CH2 a-str(74-) CH3 opl a-str(25-)
2	2967	2902	13.8	CH3 opl a-str(59-) CH2 a-str(20+) CH3 ipl a-str(17+)
3	2932	2894	42.8	CH3 ipl a-str(74-) CH3 opl a-str(15-)
4	2902	2872	15.3	CH2 s-str(91+)
5	2875	2835	32.7	CH3 s-str(97-)
6	2571	2569	14.6	S-H str(100+)
7	1460	1447	2.0	CH3 ipl a-def(87-)
8	1450	1442	6.9	CH3 opl a-def(92-)
9	1434	1433	1.5	CH2 sciss(90-)
10	1376	1379	1.9	CH3 s-def(95-)
11	1273	1283	28.3	CH2 wag(86-)
12	1251	1242	1.3	CH2 twist(69-) CH3 opl rock(23-)
13	1094	1094	12.9	HSC bend(28+) CH2 rock(24+) CH3 opl rock(22-) CH2 twist(11+)
14	1052	1032	0.6	CH3 ipl rock(49+) C-C str(21-)
15	970	940	5.5	C-C str(65-) CH3 ipl rock(16-)

----
continued

Table 3-14 -- continued

normal coord	wavenumbers, cm^{-1} exptl[d]	scl[a]	A, km/mol	PED[b,c]
16	869	849	9.7	HSC bend(53-) CH3 opl rock(24-) CH2 twist(14+)
17	737	708	1.1	CH2 rock(61+) CH3 opl rock(17+) HSC bend(13-)
18	658	638	6.6	C-S str(82+)
19	319	314	1.6	SCC def(85+)
20	241	245	2.2	C-C tors(88-)
21	191	192	20.6	H-S tors(90-)
		ΣA_i	259.3	

Average Deviation[e] = 1.42%

[a-e] As in Table 3-5.

Table 3-15: Harmonic Vibrational Frequencies, Infrared Intensities and the Potential Energy Distribution Analysis (PED) Predicted for all-trans Diethyl Sulfide Using 3-21G Basis Set.

normal coord	wavenumbers, cm^{-1} exptl[d]	scl[a]	A, km/mol	PED[b,c]
1	2963	2948	0.0	CH2 a-str(44-) CH2 a-str(44+)
2	2963	2947	47.4	CH2 a-str(44-) CH2 a-str(44-)
3	2962	2913	14.5	CH3 opl a-str(46-) CH3 opl a-str(42-)
4	2962	2913	0.0	CH3 opl a-str(46+) CH3 opl a-str(42-)
5	2943	2908	56.0	CH3 ipl a-str(45+) CH3 ipl a-str(34+) CH2 s-str(11+)
6	2943	2908	13.0	CH3 ipl a-str(46-) CH3 ipl a-str(35+) CH2 s-str(10-)
7	2907	2891	12.4	CH2 s-str(40+) CH2 s-str(39+)
8	2905	2891	1.0	CH2 s-str(42+) CH2 s-str(41-)
9	2880	2853	1.7	CH3 s-str(49+) CH3 s-str(48+)
10	2880	2852	50.5	CH3 s-str(49-) CH3 s-str(48+)
11	1478	1489	6.6	CH3 ipl a-def(46+) CH3 ipl a-def(46+)
12	1458	1489	1.4	CH3 ipl a-def(46-) CH3 ipl a-def(46+)

----

continued

Table 3-15 -- continued

normal coord	wavenumbers, cm^{-1} exptl[d]	scl[a]	A, km/mol	PED[b,c]
13	1454	1485	0.0	CH3 opl a-def(46+) CH3 opl a-def(45-)
14	1450	1484	17.8	CH3 opl a-def(46-) CH3 opl a-def(45-)
15	1444	1468	1.0	CH2 sciss(49-) CH2 sciss(49-)
16	1438	1461	14.0	CH2 sciss(49+) CH2 sciss(49-)
17	1380	1406	7.9	CH3 s-def(51-) CH3 s-def(50-)
18	1375	1406	5.2	CH3 s-def(51-) CH3 s-def(50+)
19	1299	1290	15.7	CH2 wag(45-) CH2 wag(45-)
20	1264	1254	0.1	CH2 twist(29+) CH2 twist(29+) CH3 opl rock(15+) CH3 opl rock(15+)
21	1286	1251	63.1	CH2 wag(43+) CH2 wag(43-)
22	1256	1247	0.0	CH2 twist(28+) CH2 twist(28-) CH3 opl rock(15+) CH3 opl rock(15-)
23	1042	1065	0.3	CH3 ipl rock(33+) CH3 ipl rock(33+)
24	1032	1028	0.9	CH2 twist(20+) CH2 twist(20+) CH3 opl rock(17-) CH3 opl rock(17-) CH2 rock(11+) CH2 rock(11+)

continued

Table 3-15 -- continued

normal coord	wavenumbers, cm^{-1} exptl[d]	scl[a]	A, km/mol	PED[b,c]
25	1028	1027	10.5	CH3 ipl rock(35-) CH3 ipl rock(35+)
26	1014	1015	0.0	CH2 twist(21+) CH2 twist(21-) CH3 opl rock(18-) CH3 opl rock(18+)
27	986	918	6.6	C2-C4 str(42+) C3-C5 str(42+)
28	973	911	4.2	C3-C5 str(46-) C2-C4 str(46+)
29	798	779	11.5	CH2 rock(34+) CH2 rock(34+) CH3 opl rock(14+) CH3 opl rock(14+)
30	784	761	0.0	CH2 rock(36-) CH2 rock(36+) CH3 opl rock(12-) CH3 opl rock(12+)
31	693	620	0.6	C2-S str(34+) C3-S str(34+)
32	683	609	9.3	C3-S str(48+) C2-S str(48-)
33	348	324	1.5	SCC def(46+) SCC def(46-)
34	332	300	1.5	CSC bend(23-) SCC def(21-) SCC def(21-) C3-S str(14-) C2-S str(14-)
35	273	227	0.0	C3-C5 tors(47-) C2-C4 tors(47-)
36	262	226	0.3	C3-C5 tors(49-) C2-C4 tors(49+)

---

continued

Table 3-15 -- continued

normal coord	wavenumbers, cm^{-1} exptl[d]	scl[a]	A, km/mol	PED[b,c]
37	187	127	0.4	CSC bend(66-) SCC def(16+) SCC def(16+)
38	72	70	0.0	C2-S tors(49-) C3-S tors(49-)
39	55	47	1.3	C3-S tors(50-) C2-S tors(50+)
			ΣA_i 378.2	

[a,b,c] As in Table 3-5.

[d] From ref 20 and 66.

Table 3-16: Harmonic Vibrational Frequencies, Infrared Intensities and the Potential Energy Distribution Analysis (PED) Predicted for all-trans-2,2'-Dichlorodiethyl Sulfide Using the 3-21G Basis Set.

normal coord	wavenumbers, cm^{-1} exptl[d]	scl[a]	A, km/mol	PED[b,c]
1	3005	3024	0.0	Cl(CH2) a-str(48+) Cl(CH2) a-str(46-)
2	3005	3023	0.5	Cl(CH2) a-str(49-) Cl(CH2) a-str(46-)
3	2944	2978	0.0	S(CH2) a-str(47+) S(CH2) a-str(47-)
4	2944	2977	2.5	S(CH2) a-str(48-) S(CH2) a-str(48-)
5	2956	2954	2.2	Cl(CH2) s-str(49-) Cl(CH2) s-str(49+)
6	2956	2953	6.3	Cl(CH2) s-str(50-) Cl(CH2) s-str(49-)
7	2906	2920	1.0	S(CH2) s-str(49-) S(CH2) s-str(49+)
8	2904	2920	6.0	S(CH2) s-str(50-) S(CH2) s-str(49-)
9	1439	1466	2.4	S(CH2) sciss(44+) S(CH2) sciss(44+)
10	1434	1461	10.1	Cl(CH2) sciss(45+) Cl(CH2) sciss(44+)
11	1428	1461	4.3	Cl(CH2) sciss(47+) Cl(CH2) sciss(46-)
12	1410	1459	21.7	S(CH2) sciss(47-) S(CH2) sciss(47+)
13	1306	1299	2.5	S(CH2) wag(30-) S(CH2) wag(30-) Cl(CH2) wag(18+) Cl(CH2) wag(18+)

---

continued

Table 3-16 -- continued

normal coord	wavenumbers, cm^{-1} exptl[d]	scl[a]	A, km/mol	PED[b,c]
14	1282	1281	1.4	S(CH2) twist(23+) S(CH2) twist(23+) Cl(CH2) twist(19+) Cl(CH2) twist(19+)
15	1305	1279	6.3	Cl(CH2) wag(33+) Cl(CH2) wag(33-) S(CH2) wag(15+) S(CH2) wag(15-)
16	1281	1276	0.0	S(CH2) twist(21-) S(CH2) twist(21+) Cl(CH2) twist(20+) Cl(CH2) twist(20-)
17	1218	1235	45.5	Cl(CH2) wag(31+) Cl(CH2) wag(31+) S(CH2) wag(18+) S(CH2) wag(18+)
18	1218	1211	53.0	S(CH2) wag(34+) S(CH2) wag(34-) Cl(CH2) wag(15+) Cl(CH2) wag(15-)
19	1149	1112	0.2	Cl(CH2) twist(27-) Cl(CH2) twist(27-) S(CH2) twist(21+) S(CH2) twist(21+)
20	1145	1108	0.0	Cl(CH2) twist(26+) Cl(CH2) twist(26-) S(CH2) twist(21-) S(CH2) twist(21+)
21	1043	992	2.4	C3-C5 str(44+) C2-C4 str(44+)
22	1014	964	15.9	C2-C4 str(48+) C3-C5 str(48-)

---

continued

Table 3-16 -- continued

normal coord	wavenumbers, cm^{-1} exptl[d]	scl[a]	A, km/mol	PED[b,c]
23	988	935	0.0	S(CH2) rock(21-) S(CH2) rock(21-) Cl(CH2) rock(20+) Cl(CH2) rock(20+)
24	980	919	0.0	Cl(CH2) rock(23+) Cl(CH2) rock(23-) S(CH2) rock(18+) S(CH2) rock(18-)
25	756	759	10.2	Cl(CH2) rock(23-) Cl(CH2) rock(23-) S(CH2) rock(22-) S(CH2) rock(22-)
26	756	748	0.0	S(CH2) rock(25+) S(CH2) rock(25-) Cl(CH2) rock(20+) Cl(CH2) rock(20-)
27	791	708	4.3	C3-S str(20-) C2-S str(20-) SCC def(12+) SCC def(12+)
28	751	674	1.5	C2-S str(28-) C3-S str(27+) CCCl def(11+) CCCl def(11-)
29	723	625	163.9	C5-Cl str(32-) C4-Cl str(32+) C3-S str(16+) C2-S str(16-)
30	696	607	44.4	C4-Cl str(36+) C5-Cl str(35+) C2-S str(16-) C3-S str(15-)

----

continued

Table 3-16 -- continued

normal coord	wavenumbers, cm^{-1} exptl[d]	scl[a]	A, km/mol	PED[b,c]
31	348	305	6.2	SCC def(17-) SCC def(17+) C4-Cl str(14-) C5-Cl str(14+) CCCl def(10-) CCCl def(10+)
32	361	294	1.5	CSC bend(39+) CCCl def(26-) CCCl def(26-)
33	218	195	0.3	C3-S str(15-) C2-S str(15-) SCC def(13-) SCC def(13-) C5-Cl str(10-) C4-Cl str(10-)
34	198	188	11.3	CCCl def(27-) CCCl def(27+) SCC def(22-) SCC def(22+)
35	130	104	18.8	C2-C4 tors(46-) C3-C5 tors(46+)
36	117	97	0.0	C3-C5 tors(40+) C2-C4 tors(40+)
37	60	54	2.1	CSC bend(49+) SCC def(18-) SCC def(18-)
38	75	43	0.0	C3-S tors(44+) C2-S tors(44+)
39	43	26	0.0	C3-S tors(49+) C2-S tors(49-)
		ΣA_i	449.0	

[a,b,c] As in Table 3-5.

[d] From ref 66.

Table 3-17: Harmonic Vibrational Frequencies, Infrared Intensities and the Potential Energy Distribution Analysis (PED) Predicted for all-trans- 2-Chlorodiethyl Sulfide Using the 3-21G Basis Set.

normal coord	wavenumbers, cm^{-1} exptl[d]	scl[a]	A, km/mol	PED[b,c]
1	3005	3025	0.5	C4(CH2) a-str(96+)
2	2944	2971	2.0	C2(CH2) a-str(96+)
3	2943	2956	17.2	C3(CH2) a-str(91-)
4	2956	2955	4.6	C4(CH2) s-str(99-)
5	2963	2917	8.2	CH3 opl a-str(92+)
6	2904	2916	5.5	C2(CH2) s-str(99-)
7	2962	2911	28.9	CH3 ipl a-str(74-) C3(CH2) s-str(25-)
8	2907	2897	3.9	C3(CH2) s-str(75-) CH3 ipl a-str(24+)
9	2880	2855	22.6	CH3 s-str(98+)
10	1464	1488	4.3	CH3 ipl a-def(92-)
11	1463	1484	10.1	CH3 opl a-def(91+)
12	1419	1467	2.6	C2(CH2) sciss(68+) C3(CH2) sciss(28+)
13	1434	1461	8.6	C4(CH2) sciss(94-)
14	1441	1460	15.6	C3(CH2) sciss(70-) C2(CH2) sciss(27+)
15	1382	1407	6.8	CH3 s-def(101-)
16	1305	1294	18.2	C2(CH2) wag(39+) C3(CH2) wag(30+) C4(CH2) wag(26-)

----

continued

Table 3-17 -- continued

normal coord	wavenumbers, cm^{-1} exptl[d]	scl[a]	A, km/mol	PED[b,c]
17	1282	1278	0.5	C2(CH2) twist(44+) C4(CH2) twist(37+) C2(CH2) rock(10-)
18	1272	1266	26.4	C3(CH2) wag(52+) C4(CH2) wag(35+)
19	1257	1250	0.0	C3(CH2) twist(57-) CH3 opl rock(30-)
20	1217	1218	56.4	C2(CH2) wag(53-) C4(CH2) wag(37-)
21	1147	1107	0.1	C4(CH2) twist(54-) C2(CH2) twist(41+)
22	1066	1050	5.6	CH3 ipl rock(65+)
23	1037	1024	0.7	C3(CH2) twist(40+) CH3 opl rock(35-) C3(CH2) rock(20+)
24	1024	975	12.3	C2-C4 str(88-)
25	984	924	0.1	C4(CH2) rock(42+) C2(CH2) rock(39-) C2(CH2) twist(13-)
26	982	913	5.5	C3-C5 str(88+)
27	783	773	8.9	C3(CH2) rock(62+) CH3 opl rock(23+)
28	753	750	1.8	C2(CH2) rock(43+) C4(CH2) rock(37+)
29	776	697	7.9	C2-S str(49+) CCCl def(18-) C2(SCC) def(18-)
30	715	620	93.6	C4-Cl str(43-) C2-S str(28+) C3-S str(25-)

---

continued

Table 3-17 -- continued

normal coord	wavenumbers, cm^{-1} exptl[d]	scl[a]	A, km/mol	PED[b,c]
31	676	596	19.1	C3-S str(57+) C4-Cl str(27-)
32	387	339	1.6	C3(SCC) def(50+) CCCl def(15-) CSC bend(12+)
33	289	246	2.5	C2(SCC) def(41-) CSC bend(29-) CCCl def(10+)
34	254	226	0.1	C3-C5 tors(96-)
35	245	226	5.6	CCCl def(39+) C3(SCC) def(21+) C2-S str(19+) C4-Cl str(12+)
36	123	105	8.4	C2-C4 tors(77+) C3-S tors(16-)
37	97	85	1.9	CSC bend(51+) C2(SCC) def(27-) CCCl def(12+)
38	81	55	2.9	C3-S tors(64+) C2-S tors(18+) C2-C4 tors(16+)
39	47	32	0.5	C2-S tors(81-) C3-S tors(19+)
		ΣA_i	422.3	

[a,b,c] As in Table 3-5.

[d] From ref 66.

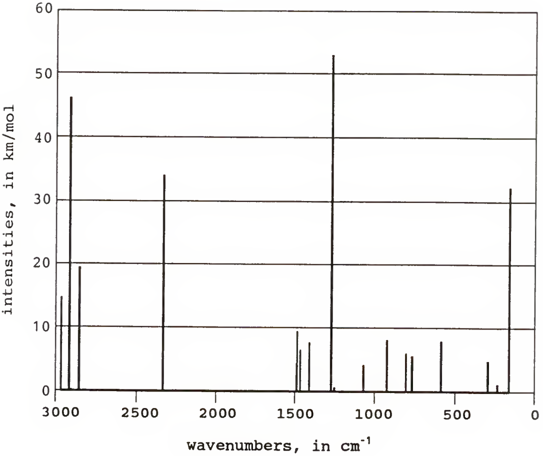

Figure 3-1. Infrared spectrum of trans-EtSH predicted at the 3-21G level. The height of each bar is equal to the intensity in Table 3-5, while the wavenumber is the scaled value listed in the same table.

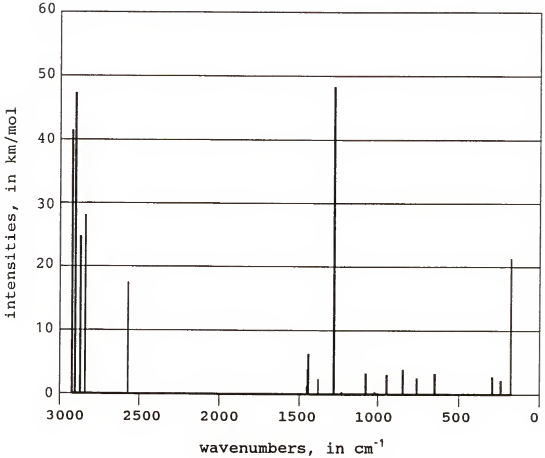

Figure 3-2. Infrared spectrum of trans EtSH predicted at the 6-31G** level. (See caption to Fig 3-1).

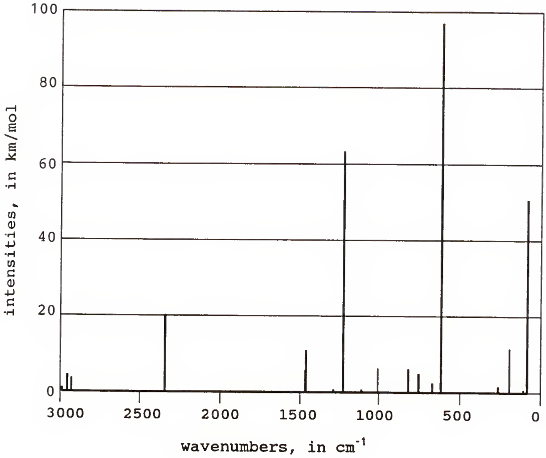

Figure 3-3. Infrared spectrum of trans-ClEtSH predicted at the 3-21G level. (See caption to Fig 3-1).

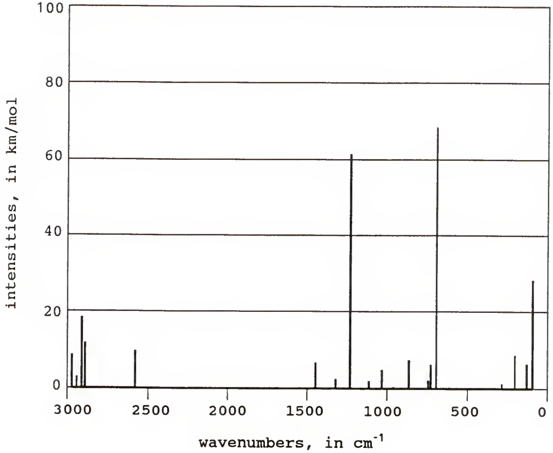

Figure 3-4. Infrared spectrum of trans-ClEtSH predicted at the 6-31G** level. (See caption to Fig 3-1).

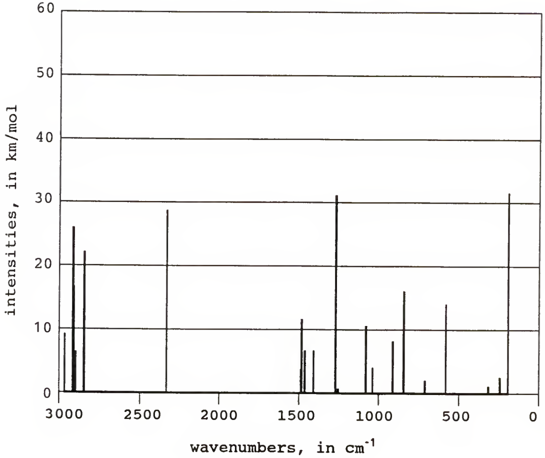

Figure 3-5. Infrared spectrum of gauche-EtSH predicted at the 3-21G level. (See caption to Fig 3-1).

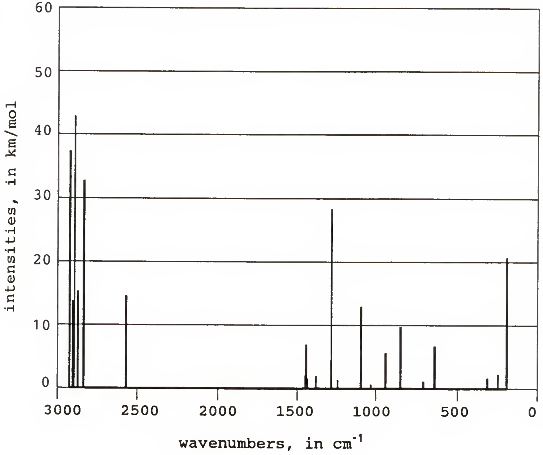

Figure 3-6. Infrared spectrum of gauche-EtSH predicted at the 6-31G** level. (See caption to Fig 3-1).

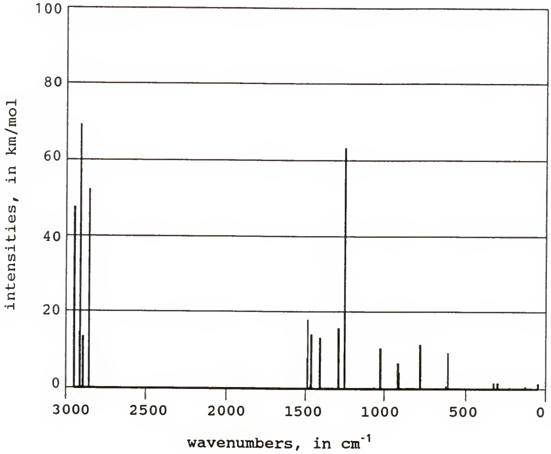

Figure 3-7. Infrared spectrum of all-trans diethyl sulfide predicted at the 3-21G level. (See caption to Fig 3-1).

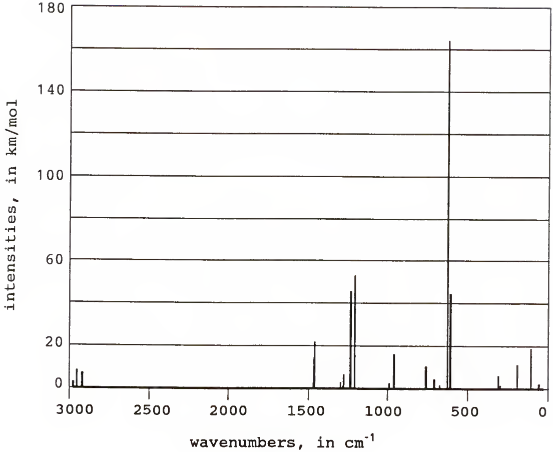

Figure 3-8. Infrared spectrum of all-trans-2,2'-dichlorodiethyl sulfide predicted at 3-21G level. (See caption to Fig 3-1).

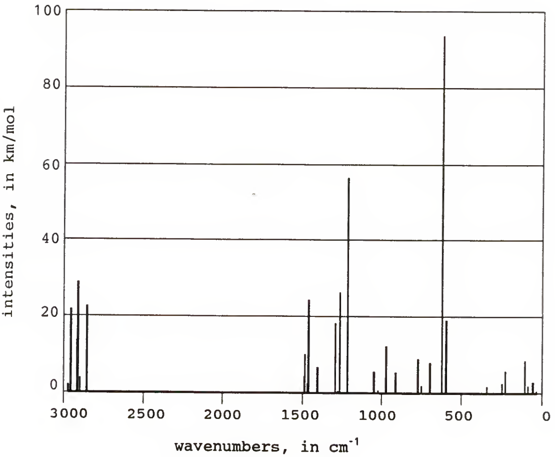

Figure 3-9. Infrared spectrum of all-trans-2-chlorodiethyl sulfide calculated at the 3-21G level. (See caption to Fig 3-1).

CHAPTER 4
DIRECT TRANSFER OF VIBRATIONAL PARAMETERS

The transference of localized parameters (35 - 39) is a common technique used by chemists in attempting to estimate molecular properties when direct experimental observation is difficult. Several examples easily come to mind: standard bond distances and angles are transferred to predict geometries of molecules for which structural data are incomplete; molecular dipole moments are estimated from bond dipole moment, force constants of molecules with completely analyzed spectra are frequently transferred to molecules for which experimental observations are difficult or band assignments are uncertain; atomic polar tensors are often transferred from one molecule to another to calculate the IR intensities of the latter. In all such cases it is assumed that the parameters to be transferred are constants and insensitive to the differences between the electronic environments of the original molecules and those of the molecules to which the parameters are transferred. Eventual discrepancies are then explained on the basis of chemist's knowledge of the differences in the electronic structures of the molecules involved.

As discussed earlier in Chapter 3, the spectrum of diethyl sulfide (and also mustard gas) is approximately just a "doubled version" of the spectrum of its smaller model compound, EtSH (and ClEtSH for mustard). If so, then it might be expected that the force constants for diethyl sulfide expressed in internal symmetry coordinates would be quite similar to these for EtSH expressed in its internal symmetry coordinates. The force field in internal symmetry coordinates calculated at the 3-21G level for trans-EtSH and all-trans-diethyl sulfide (given in the parentheses) are listed in Table 4-1. In order to save some space, only the lower triangle of the force constants matrix is presented. From this comparison, it seems that the force constants of the two molecules are indeed quite similar (within ±0.90%). A similar comparison of force constants is given also for ClEtSH and mustard gas (Table 4-2). For this pair of molecules, the deviation from one molecule to another seems to be smaller (within ±0.61%).

Although the intensities of the individual bands do not show any obvious relationships between one molecule and another, there is some reason to expect that the intensity sums are related (34). Thus we expect that the intensity sum for $CH_3CH_2SCH_2CH_3$ will be just twice the sum for the CH_3CH_2S- group. We can estimate the latter sum by subtracting the intensity contributions due to the S-H group from the total intensity sum for trans-EtSH (265.8 km/mol, Table 3-5). We subtract the intensity of the SH stretch, of the HSC bend, and of the SH torsion to obtain $265.8 - 35.3 - 7.7 - 32.9 = 189.9$ km/mol as the intensity sum for the CH_3CH_2S- group. Hence the intensity sum for $CH_3CH_2SCH_2CH_3$ is predicted to be $2*189.9 =$

379.8 km/mol plus the intensity of the CSC bend and of the CS torsion to become 379.8 + 0.4 + 1.3 = 381.5 km/mol, in excellent agreement with the actual sum, 378.2 km/mol (Table 3-15).

Similarly, we calculate the intensity sum for the $ClCH_2CH_2S$- group to be 290.8 - 22.5 - 10.4 - 38.4 = 219.5 km/mol (Table 3-9). Thus the intensity sum for $CH_3CH_2SCH_2CH_2Cl$ is predicted to be 193.6 + 219.5 plus the intensity of the CSC bend (1.9 km/mol) and for the CS torsion (3.4 km/mol) = 418.4 km/mol, compared with 422.3 km/mol in Table 3-17. That for $ClCH_2CH_2SCH_2CH_2Cl$ is predicted to be 2 * 219.5 + 3.6 + 0.0 = 442.6 km/mol, compared with 449.0 km/mol found in Table 3-16. It is worth noting that the intensity sum rule is rigorously correct, if the APTs (effective charges, X^2) really are the same for the two molecules.

Comparing all these results from frequencies and from the vibrational total intensities calculation, lead us to believe that the transferability of force constants and polar tensors from one molecule to another may really be feasible.

4.1 Choosing the Vibrational Coordinates for Force Constants

There are two basically equivalent, but from the practical point of view very different, choices for the description of distortions from a reference geometry: cartesian displacement coordinates versus internal valence displacement coordinates (bond lengths, angles, dihedral angles). Cartesian coordinates are easiest to use, while the construction of internal coordinates requires some additional human effort. The purpose of this section is to illustrate that the advantages of using internal coordinates outweigh the inconvenience (12).

The direct results of a quantum mechanical gradient calculation are the energy derivatives with respect to cartesian coordinates. These are calculated for appropriately distorted geometries and the second derivatives (or force constants) have been obtained by finite difference. As an important new development, programs emerged recently which evaluate also the second derivatives analytically in an efficient way (12, 41). In any case, the easiest method is to use directly the cartesian force constants in the (harmonic) vibrational analysis.

If it is only the frequencies which are of interest in a study, the use of cartesian force constants is perfectly adequate. Note, however, that even in this case the data can only be used for one molecule (and its isotopomers) and cannot be transferred to larger, similar systems because of changes in the orientation of the new molecule (and hence in the force constants) in the cartesian coordinate system. It seems to us that the use of internal coordinates is inevitable in any detailed vibrational study.

There are at least three important requirements (12) which should be met by the selection of a coordinate system, and these are discussed briefly in the following.

1- The coordinates should make it easy to compare and transfer force constants between related molecules.

If one wants to develop a method applicable to larger systems of chemical interest, the direct quantum mechanical approach becomes prohibitively expensive. Thus, the transferability of the results, by building up the force field from smaller segments, is a crucial requirement. As has been practiced by spectroscopists for many years, this can be done easily only in terms of internal coordinates. Also, internal force constants give a very useful insight into the dynamical structure of a molecule.

2- Systematic errors in the calculations should be easily detectable.

When using cartesian coordinates, the theoretical results can be compared with experiment only in the final stage, at the level of the frequencies. This is, however, much less informative than the analysis of force constants in internal coordinates. In cartesian coordinates the diagonal force constants are not necessarily dominant, and the useful concept of partitioning the potential into dominant diagonal versus less important coupling terms is lost.

In term of cartesian coordinates it is not possible to distinguished between different types of distortions which are, as experience has shown, differently affected by basis set truncation and correlation effects. For example, in Hartree-Fock calculations with double-zeta or split valence basis sets, the accuracy of calculated stretching force constants may be about 10 to 15%, while deformation force constants are often overestimated by 20 to 30% (12). All this information, which remains hidden in terms of the frequencies, can be very well utilized for systematic corrections of the force field.

3- When going beyond the harmonic approximation, the expansion of the potential in a power series should be rapidly convergent. Again, this can be achieved with internal coordinates only, and is not expected to be true for cartesian coordinates.

However, the use of internal coordinates leads to redundancy problems wherever the interbond angles around an atom exceed the number of independent deformations. There is then a set of relations among the angles in terms of which the precise redundant coordinates may be evaluated (66b).

4.2 Procedure for Transferring Force Constants and Atomic Polar Tensors

The procedure for transferring force constants and polar tensors employed in this work can be describe as follows.

1- The similarity in structure (at least for characteristic groups) between model compounds and the test molecules should be defined. The model compounds used in this work are

EtSH and ClEtSH, which consist of CH_3CH_2S- and $ClCH_2CH_2S$- groups that are similar to those in the test molecules: $CH_3CH_2SCH_2CH_3$ and $ClCH_2CH_2SCH_2CH_2Cl$.

2- The force constants and polar tensors for model compounds and test molecules must be computed using the same basis set. In this work, the 3-21G basis set is employed.

3- The force constants for a model compound must be transformed from cartesian coordinates to internal coordinates, which later can be transferred to the test molecule. The SH torsion and HSC bending force constants must be replaced by those for the CS torsion and CSC bend, respectively. These two values are taken directly from the test molecules. It is worth mentioning that the interaction force constants between the two $-SCH_2CH_2X$ groups are taken to be zero.

Polar tensors of model compounds, which depend on the orientation of each atom in the cartesian axes must be transformed so that they correspond to the axes for the test molecule. The CSC angle used for diethyl sulfide and for mustard gas is 100.1° and 98.7°, respectively. These values are taken from the optimized geometries of the test molecules from Table 3-3. After rotation of the axes for the transferred polar tensors, the atomic polar tensor matrix for the sulphur atom is evaluated using the null condition.

4- The vibrational frequencies, infrared intensities and potential energy distributions are evaluated using these transferred parameters and the result are then compared with those from the direct ab initio calculation for the test molecules.

4.3 Comparison of Vibrational Spectra Predicted by Transfer of Parameters with those Predicted from Ab Initio Calculations

The harmonic vibrational frequencies, infrared intensities, and potential energy distribution analysis for diethyl sulfide predicted using the transferred force constants and polar tensors from trans-EtSH evaluated at the 3-21G level are presented in Table 4-3 along with the results from direct calculation at the same level for diethyl sulfide. The result for mustard gas is given in Table 4-4.

4.3.1 Diethyl Sulfide

In Table 4-3, the result from transferred parameters (Set A) is compared to the result from direct ab initio calculation (Set B) using the same basis set, ie. 3-21G. Figures 4-1 to 4-4 and 4-5 to 4-8 show a bar representation of the predicted IR spectra from Set A and Set B, respectively, with an arbitrary bandwidth of 4 cm^{-1}.

Generally speaking, prediction for both Set A and Set B are very similar to each other with the average deviation in the predicted frequencies is only 0.38%. It should be noted that this percentage deviation does not include the deviation in the prediction of the lower frequency modes below 500 cm^{-1} in order to avoid misinterpretation of large deviations due to small errors divided by small frequencies. There might be several reasons for this deviation but two most important reasons are the differences in geometries for the two sets (bond lengths and bond angles) and the assumption that the intergroup interaction force constants from Set A are zero.

The total intensity of the vibrational modes predicted from Set A is 389.1 km/mol, only about 10.9 km/mol higher than the direct calculation in Set B (378.2 km/mol). This is not a big surprise since this value, 381.5 km/mol, is approximately predicted using the intensity sum rule. Hence X^2 transfers.

4.3.1.1 3050 - 2850 cm^{-1} region (Fig. 4-1 and 4-5)

In this CH stretching region, the percentage deviation of the predicted frequencies from transferred force constants (Set A) is only 0.35% compared to those from Set B. This deviation is all due to the higher values for the CH stretching force constants for EtSH than were found for diethyl sulfide. [For example, see elements (1,1), (3,3), (8,8) of the force constants matrix in Table 4-1].

It is hard to understand why the distribution of the CH stretching intensities for the two molecules (EtSH and diethyl sulfide) are so significantly different (Table 3-5 and Table 3-15). In Set A, the total intensity of the CH2 s-str is predicted to be greater than that for the CH2 a-str while the reverse case is observed for intensities predicted from Set B. Another significant difference is observed for the CH3 ipl a-str and the CH3 s-str where both intensities are underestimated from Set A compared with those from Set B. Therefore it is no surprise to discover that the total intensity in this CH stretching region is underestimated from Set A (160.1 compared with 196.5 km/mol).

4.3.1.2 1500 - 500 cm^{-1} region

This fingerprint region is actually includes all CH bending and C-C stretching modes as well as C-S and C-Cl stretches. The frequencies predicted for Set A seem to be in excellent agreement with those for Set B. The average deviation for the frequencies in this region is only 0.39%.

Comparing Figure 4-3 and 4-7 (in the region of 1100-500 cm^{-1}), the spectra predicted from both calculations are very similar except for the wagging modes. In the Set B, Fig 4-7, the two CH2 wagging bands are located 39 wavenumbers (1290-1251 cm^{-1}) apart, compared to only 8 wavenumbers (1282-1274 cm^{-1}) predicted by Set A in Fig. 4-3. Both sets predict that these modes will have the highest intensity in this region. The total intensity the CH2 wags mode is overestimated in Set A (105.4 compared with 78.8 km/mol from Set B). This result is actually a transferred characteristic the CH2 wagging mode in EtSH which has an intensity of 26.5 km/mol per C-H bond (see Table 3-5). Since the wagging modes for diethyl sulfide involve four C-H bonds, the total intensity of the wagging mode is expected to be around 4*26.5 = 106.0 km/mol, as obtained from Set A calculations. In this low intensity region (1100-500 cm^{-1}), the agreement for frequencies and intensities predicted from the two calculations seem to be excellent except for the intensity of the C-S stretching modes (at about 600 cm^{-1}) which are overestimated in Set A. (The total for both modes from Set A is 24.4 compared with 9.9 km/mol for Set B.)

Due to the overestimation of wagging and C-S stretching intensities when Set A is used, the total intensity in this region, of course is higher for Set A (193.7 km/mol) than for Set B (166.8 km/mol).

4.3.1.4 350 - 0 cm^{-1} region (Fig 4-4 and 4-8)

This low frequency region of the diethyl sulfide spectrum includes the heavy atom bending modes (SCC def, CSC bend) and also torsions of all kinds (CC and CS torsions). Generally speaking, the agreement in frequencies from the two sets seems to be very good. The difference of about 15 cm^{-1} for the SCC deformation is due to the assumption in Set A that the coupling force constant between the two C-S bonds is zero. The inclusion of this coupling force constant with a value of 0.06521 mdyn-A will bring down the predicted SCC def frequency in Set A to 329 cm^{-1} which in excellent agreement with the frequency obtained in Set B (324 cm^{-1}). However the intensity predicted for the SCC def mode in Set A is about four times higher than that from Set B; this comparison is probably not significant, since the intensity of this mode is itself very low (less than 10 km/mol).

4.3.2 2,2'-Dichlorodiethyl Sulfide

The comparison of harmonic vibrational frequencies, infrared intensities, and potential energy distributions calculated using the transferred parameters (Set A) with those from direct ab initio calculation (at the 3-21G level) are presented in Table 4-4. The average percentage deviation of 0.41% in frequencies shows that the agreement between the frequencies predicted from the two calculations is very good indeed.

The total intensity predicted for the vibrational modes from Set A is 446.1 km/mol, only 2.9 km/mol lower than from the direct calculation of Set B (449.0 km/mol). The total intensity from Set A is approximately the same number as was estimated above using the simple intensity sum rule (442.6 km/mol).

Since almost all the fundamental modes for this molecule have very low intensities (<10 km/mol), this discussion will focus only on bands which have predicted intensities of 15 km/mol or higher, and we shall not discuss the comparison region by region. If we examine Table 4-4 the first bands predicted with significant intensity (24.0 to 30 km/mol) are those associated with the CH2 scissors for the $ClCH_2$- and -CH_2S- groups at around 1460 cm^{-1}. In the region from 1240 to 1200 cm^{-1}, there are predicted to be two relatively strong from the CH2 wagging modes. The intensity for the CH2 wagging from the $-CH_2Cl$ group is overestimated by about 19.3 km/mol in Set A compared with Set B, while an excellent agreement is observed for the CH2 wagging mode from the $-CH_2S-$ group. Another significant difference in predicted intensities is observed for the CC stretching mode around 965 cm^{-1} even though the frequencies are predicted to be very much the same for both sets. The intensity of this mode is underestimated in Set A by about 12 km/mol compared to the value of 15.9 km/mol calculated for Set B.

The largest contribution to the infrared absorption intensity in this compound is predicted to be from the C-Cl stretching modes at around 630-600 cm^{-1}. It is really surprising that for these modes, the frequencies and intensities predicted from transferred parameters Set A are in excellent agreement with the direct calculations for Set B.

It is very encouraging to see that this method of transferring parameters (force constants and polar tensors) is feasible to reproduce an IR spectrum for a molecule with excellent agreement in both frequencies and intensities (within experimental error) with these values obtained from a direct ab initio calculation.

Table 4-1: Comparison of the Unscaled Force Constants[a,b] in Symmetry Coordinates[c] between trans-EtSH and all-trans-Diethyl Sulfide (in parentheses) Obtained from the 3-21G calculation.

		1	2	3	4	5
CH2 s-str	1	6.05(5.98)				
CH2 sciss	2	0.17(0.17)	0.69(0.70)			
CH2 a-str	3			5.94(5.86)		
CH2 rock	4			0.11(0.12)	0.83(0.85)	
CH2 wag	5	-0.05(-0.04)	-0.01(-0.01)			0.80(0.79)
CH2 twist	6			-0.07(-0.06)	-0.02(-0.02)	
SCC def	7	-0.08(-0.09)				0.02(0.03)
CH3 s-str	8	0.00(0.01)	-0.01(-0.01)			-0.02(-0.02)
CH3 s-def	9	-0.01(-0.01)	0.01(0.01)			0.03(0.03)
CH3 i.a-str	10	0.02(0.02)				0.02(0.02)
CH3 i.a-def	11					
CH3 i.rock	12	-0.02(-0.02)	0.03(0.03)			0.06(0.06)
CH3 o.a-str	13			0.03(0.03)	-0.03(-0.04)	
CH3 o.a-def	14				0.01(0.00)	
CH3 o.rock	15			-0.04(-0.04)	-0.11(-0.11)	
C-S str	16	0.06(0.08)	-0.16(-0.16)			0.43(0.41)
C-C str	17	0.10(0.10)	-0.14(-0.14)			-0.32(-0.32)
H-S tors	18			-0.01	0.02	
C-S tors	18			(0.01)	(-0.03)	
C-C tors	19				0.01(-0.01)	
HSC bend	20	0.00	0.03			-0.04
CSC bend	20	(-0.01)	(0.03)			(-0.06)

		6	7	8	9	10
CH2 twist	6	0.76(0.75)				
SCC def	7		1.07(1.04)			
CH3 s-str	8			5.96(5.95)		
CH3 s-def	9		-0.02(-0.02)	0.14(0.14)	0.73(0.73)	
CH3 i.a-str	10		0.06(0.06)	-0.03(-0.03)		5.76(5.74)
CH3 i.a-def	11		0.02(0.02)			-0.19(-0.19)
CH3 i.rock	12		0.14(0.13)		0.02(0.01)	0.16(0.16)
CH3 o.a-str	13	0.03(0.03)				

----

continued

Table 4-1 -- continued

		6	7	8	9	10
CH3 o.a-def	14					
CH3 o.rock	15	0.12(0.12)				
C-S str	16		0.22(0.21)		-0.01(-0.01)	-0.03(-0.03)
C-C str	17		0.22(0.21)	0.15(0.15)	-0.43(-0.42)	0.01(0.01)
H-S tors	18	-0.01				
C-S tors	18					
C-C tors	19					
HSC bend	20		0.23	0.01	-0.02	0.01
CSC bend	20		(0.25)	(0.01)	(-0.02)	(0.01)

		11	12	13	14	15
CH3 i.a-def	11	0.71(0.71)				
CH3 i.rock	12	-0.01(-0.01)	0.84(0.83)			
CH3 o.a-str	13			5.81(5.80)		
CH3 o.a-def	14			0.18(0.18)	0.70(0.70)	
CH3 o.rock	15			0.15(0.15)	0.01(0.01)	0.86(0.86)
C-S str	16	-0.01(0.00)	0.07(0.06)			
C-C str	17	0.01(0.01)	-0.05(-0.05)			
H-S tors	18			0.01	-0.01	
C-S tors	18			(-0.01)	(0.01)	(-0.01)
C-C tors	19				-0.01(0.01)	
HSC bend	20		0.05			
CSC bend	20	(0.01)	(0.05)			

		16	17	18	19	20
C-S str	16	2.88(2.94)				
C-C str	17	0.15(0.15)	4.61(4.59)			
H-S tors	18			0.03		
C-S tors	18			(0.04)		
C-C tors	19			-0.01(-0.01)	0.04(0.04)	
HSC bend	20	0.17	0.06			0.91
CSC bend	20	(0.10)	(0.07)			(1.01)

----

continued

Table 4-1 -- continued

---

[a] Only force constants of greater than 0.0005 are given in this table.

[b] Units are mdyn/A for the diagonal stretching and off-diagonal stretching-stretching constants, mdyn for the off-diagonal stretching-bending constants, and mdyn-A for the diagonal bending, off-diagonal bending-bending, and diagonal torsional constants.

[c] Definitions of symmetry coordinates are the same as given by Shomanouchi et al. (66). See footnote c in Table 3-5.

Table 4-2: Comparison of the Unscaled Force Constants^{a,b,d} in Symmetry Coordinates^{c} between trans-ClEtSH and all-trans 2,2'-Dichlorodiethyl Sulfide (in parentheses) Obtained from the 3-21G Calculation.

		1	2	3	4	5
CH2 s-str	1	6.13(6.09)				
CH2 sciss	2	0.15(0.16)	0.68(0.68)			
CH2 a-str	3			6.04(6.00)		
CH2 rock	4			0.12(0.12)	0.81(0.83)	
CH2 wag	5	-0.06(-0.06)	0.02(0.01)			0.82(0.81)
CH2 twist	6			-0.08(-0.08)	-0.06(-0.06)	
SCC def	7	-0.08(-0.09)				0.03(0.03)
CH2' s-str	8	-0.01(-0.01)				-0.02(-0.02)
CH2' sciss	9	-0.01(-0.01)	0.01(0.01)			0.02(0.02)
CH2' a-str	10			0.02(0.02)	-0.03(-0.03)	
CH2' rock	11			-0.04(-0.04)	-0.07(-0.07)	
CH2' wag	12	0.02(0.02)	-0.02(-0.02)			-0.04(-0.04)
CH2' twist	13			-0.02(-0.02)	-0.08(-0.07)	
CCCl def	14	-0.05(-0.05)	0.03(0.03)			0.04(0.04)
C-Cl str	15	0.02(0.02)				0.02(0.02)
C-S str	16	0.04(0.06)	-0.15(-0.16)			0.41(0.40)
C-C str	17	0.09(0.09)	-0.16(-0.16)			-0.38(-0.38)
H-S tors	18			-0.01	0.02	
C-S tors	18			(0.01)	(-0.03)	
C-C tors	19			-0.01(0.00)		
HSC bend	20		0.03			-0.04
CSC bend	20		(0.03)			(-0.06)

		6	7	8	9	10
CH2 twist	6	0.78(0.77)				
SCC def	7		1.04(1.01)			
CH2' s-str	8		-0.02(-0.02)	6.23(6.23)		
CH2' sciss	9		0.02(0.02)	0.15(0.15)	0.68(0.68)	
CH2' a-str	10	0.03(0.03)				6.15(6.15)
CH2' rock	11	0.08(0.08)				0.10(0.10)
CH2' wag	12		-0.03(-0.03)	0.06(0.05)	0.04(0.04)	
CH2' twist	13	0.07(0.07)				0.09(0.09)

----

continued

Table 4-2 -- continued

		6	7	8	9	10
CCCl def	14		0.13(0.13)	-0.06(-0.06)	-0.01(-0.01)	
C-Cl str	15		0.11(0.11)	0.03(0.03)	-0.21(-0.21)	
C-S str	16		0.27(0.25)	0.02(0.02)		
C-C str	17		0.14(0.13)	0.10(0.10)	-0.15(-0.15)	
H-S tors	18	-0.01				0.01
C-S tors	18					(-0.01)
C-C tors	19					0.01(-0.01)
HSC bend	20		0.22	0.01	0.01	
CSC bend	20		(0.23)		(0.01)	

		11	12	13	14	15
CH2' rock	11	0.84(0.84)				
CH2' wag	12		0.84(0.84)			
CH2' twist	13			0.76(0.76)		
CCCl def	14		-0.06(-0.06)		1.10(1.10)	
C-Cl str	15		-0.50(-0.50)		0.32(0.31)	2.85(2.84)
C-S str	16		-0.02(-0.02)		0.09(0.09)	-0.02(-0.03)
C-C str	17		0.31(0.31)		0.14(0.15)	0.17(0.17)
H-S tors	18			0.01		
C-S tors	18			(-0.01)		
C-C tors	19	0.01(-0.01)				
HSC bend	20				0.05	0.05
CSC bend	20				(0.04)	(0.04)

		16	17	18	19	20
C-S str	16	2.92(2.90)				
C-C str	17	0.14(0.14)	4.89(4.86)			
H-S tors	18			0.01		
C-S tors	18			(0.02)		
C-C tors	19			-0.01(-0.01)	0.05(0.05)	
HSC bend	20	0.19	0.02			0.90
CSC bend	20	(0.12)	(0.03)			(0.98)

[a,b,c] As in Table 4-1. [d] A prime symbol (CH2') refers to Cl$\underline{CH}_2$- groups.

Table 4-3: Calculated Harmonic Vibrational Frequencies, Infrared Intensities, and Potential Energy Distributions (PEDs) for all-trans-Diethyl Sulfide Calculated using the Transferred Force Constants and Polar Tensors from trans-EtSH(3-21G), Compared with the Direct Ab Initio Calculation at the Same Level.

set A transferred			set B direct *ab initio*		
wave-numbers^{a,b} cm^{-1}	A, km/mol	PED^{c,d}	wave-numbers^{a,b} cm^{-1}	A, km/mol	PED^{c,d}
2967[d]	29.2	CH2 a-str(94)	2948[d]	47.4	CH2 a-str(88)
2920[d]	70.5	CH2 s-str(76),	2913[d]	14.5	CH3 opl a-str(88)
2918[d]	20.8	CH3 opl a-str(95)	2908[d]	69.0	CH3 ipl a-str(79), CH2 s-str(11)
2904[d]	1.5	CH3 ipl a-str(75), CH2 s-str(13)	2891[d]	13.4	CH2 s-str(83)
2855[d]	38.0	CH3 s-str(97)	2853[d]	52.2	CH3 s-str(97)
1487[d]	8.3	CH3 ipl a-def(92)	1489[d]	8.0	CH3 ipl a-def(92)
1484[d]	18.2	CH3 opl a-def(91)	1485[d]	17.8	CH3 opl a-def(91)
1458[d]	13.1	CH2 sciss(98)	1461[d]	15.0	CH2 sciss(98)
1408[d]	15.5	CH3 s-def(100)	1406[d]	13.1	CH3 s-def(100)
1282	41.7	CH2 wag(89)	1290	15.7	CH2 wag(90)

----

continued

Table 4-3 -- continued

set A transferred			set B direct *ab initio*		
wave-numbers^{a,b} cm^{-1}	A, km/mol	PED^{c,d}	wave-numbers^{a,b} cm^{-1}	A, km/mol	PED^{c,d}
1274	63.6	CH2 wag(89)	1251	63.1	CH2 wag(86)
1254	1.2	CH2 twist(58), CH3 opl rock(29)	1247	0.1	CH2 twist(56), CH3 opl rock(30)
1062	0.4	CH3 ipl rock(67)	1065	0.3	CH3 ipl rock(66)
1038	3.4	CH3 ipl rock(71)	1028	0.9	CH2 twist(40), CH3 opl rock(34), CH2 rock(22)
1030	0.1	CH2 twist(31), CH3 opl rock(28), CH2 rock(18)	1027	10.5	CH3 ipl rock(70)
1021	0.1	CH2 twist(33), CH3 opl rock(30), CH2 rock(15)	1015	0.0	CH2 twist(42), CH3 opl rock(36)
916[d]	15.2	C-C str(84)	916[d]	10.8	C-C str(84)
778	12.7	CH2 rock(65), CH3 opl rock(26)	779	11.5	CH2 rock(68), CH3 opl rock(28)

----

continued

Table 4-3 -- continued

set A transferred			set B direct *ab initio*		
wave-numbers[a,b] cm^{-1}	A, km/mol	PED[c,d]	wave-numbers[a,b] cm^{-1}	A, km/mol	PED[c,d]
762	0.0	CH2 rock(70), CH3 opl rock(24)	761	0.0	CH2 rock(72), CH3 opl rock(24)
618	2.6	C-S str(78)	620	0.6	C-S str(68)
597	21.8	C-S str(97)	609	9.3	C-S str(96)
339	6.1	SCC def(92)	324	1.5	SCC def(92)
298	1.7	CSC bend(24), SCC def(40), C-S str(28)	300	1.5	CSC bend(23), SCC def(42), C-S str(28)
227	0.3	C-C tors(96)	227	0.3	C-C tors(98)
125	0.8	CSC bend(65), SCC def(34)	127	0.4	CSC bend(66), SCC def(32)
70	0.0	C-S tors(96)	70	0.0	C-S tors(98)
48	2.0	C-S tors(100)	47	1.3	C-S tors(100)
ΣA_i	389.1		ΣA_i	378.2	

----
continued

Table 4-3 -- continued

Average Deviation[e] = 0.38%

---

[a] Scale factor is 0.89 for all modes.

[b] [d] = "degenerate modes"; two modes are calculated to have this frequency.

[c] Percentage contributions greater than or equal to 10% are given in parentheses.

[d] Definitions of symmetry coordinates are the same as given by Shimanouchi et al. (66). See footnote c in Table 3-5.

[e] Average Deviation = $(100/n)\sum_{i=1}^{n} \mathrm{abs}(\bar{\nu}_{\mathrm{SetB}} - \bar{\nu}_{\mathrm{Set\ A}})/\bar{\nu}_{\mathrm{Set\ B}}$; the summation is carried out for all modes, n, with wavenumber greater than 500 cm^{-1}. See text.

Table 4-4: Calculated Harmonic Vibrational Frequencies, Infrared Intensities, and Potential Energy Distributions (PEDs) for all-trans-2,2-Dichlorodiethyl Sulfide Calculated Using the Force Constants and Polar Tensors from trans-ClEtSH(3-21G), Compared with the Direct *Ab Initio* Calculation.

set A transferred			set B direct *ab initio*		
wave-numbers[a,b] cm^{-1}	A, km/mol	PED[c,d,f]	wave-numbers[a,b] cm^{-1}	A, km/mol	PED[c,d,f]
3026[d]	0.5	CH2' a-str(92)	3024[d]	0.5	CH2' a-str(95)
2989[d]	1.3	CH2 a-str(93)	2978[d]	2.5	CH2 a-str(96)
2955[d]	8.8	CH2' s-str(94)	2954[d]	8.5	CH2' s-str(99)
2929[d]	6.8	CH2 s-str(97)	2920[d]	7.0	CH2 s-str(99)
1463[d]	3.7	CH2 sciss(73), CH2' sciss(20)	1466[d]	24.1	CH2 sciss(88)
1461[d]	29.5	CH2' sciss(75), CH2 sciss(22)	1461[d]	14.4	CH2' sciss(93)
1290	0.2	CH2 wag(50), CH2' wag(44)	1299	2.5	CH2 wag(60), CH2' wag(36)
1287	2.1	CH2' wag(52), CH2 wag(43)	1281[d]	1.4	CH2 twist(46), CH2' twist(38)
1282[d]	0.0	CH2 twist(46), CH2' twist(34)	1279	6.3	CH2' wag(66), CH2 wag(30)

continued

Table 4-4 -- continued

set A transferred			set B direct *ab initio*		
wave-numbers^{a,b} cm^{-1}	A, km/mol	PED^{c,d,f}	wave-numbers^{a,b} cm^{-1}	A, km/mol	PED^{c,d,f}
1231	64.8	CH2' wag(52), CH2 wag(44)	1235	45.5	CH2' wag(62), CH2 wag(36)
1223	56.6	CH2 wag(54), CH2' wag(44)	1211	53.0	CH2 wag(68), CH2' wag(30)
1124	0.9	CH2' twist(56), CH2 twist(35)	1110[d]	0.2	CH2' twist(54), CH2 twist(42)
1110	0.5	CH2' twist(54), CH2 twist(41)			
993	1.0	C-C str(89)	992	2.4	C-C str(88)
969	4.2	C-C str(95)	964	15.9	C-C str(96)
926[d]	0.3	CH2' rock(44), CH2 rock(28), CH2 twist(11)	935	0.0	CH2 rock(42), CH2' rock(40)
772	6.5	CH2 rock(48), CH2' rock(37)	919	0.0	CH2' rock(46), CH2 rock(36)

----

continued

Table 4-4 -- continued

set A transferred			set B direct *ab initio*		
wave-numbers^{a,b} cm^{-1}	A, km/mol	PED^{c,d,f}	wave-numbers^{a,b} cm^{-1}	A, km/mol	PED^{c,d,f}
750	4.8	CH2 rock(48), CH2' rock(42)	759	10.2	CH2' rock(46), CH2 rock(44)
			748	0.0	CH2 rock(50), CH2' rock(40)
712	2.9	C-S str(42), SCC def(24)	708	4.3	C-S str(40), SCC def(24)
670	5.3	C-S str(48), CCCl def(22)	674	1.5	C-S str(55), CCCl def(22)
630	151.4	C-Cl str(58), C-S str(40)	625	163.9	C-Cl str(64), C-S str(32)
605	53.0	C-Cl str(72), C-S str(30)	607	44.4	C-Cl str(71), C-S str(30)
315	1.6	SCC def(36), C-Cl str(30)	305	6.2	SCC def(34), C-Cl str(28), CCCl def(20)
294	1.6	CSC bend(38), CCCl def(52)	294	1.5	CSC bend(39), CCCl def(52)

----

continued

Table 4-4 -- continued

set A transferred			set B direct ab initio		
wave-numbers^{a,b} cm^{-1}	A, km/mol	PED^{c,d,f}	wave-numbers^{a,b} cm^{-1}	A, km/mol	PED^{c,d,f}
194	0.3	C-S str(30), SCC def(26), C-Cl str(10)	195	0.3	C-S str(30), SCC def(26), CCCl str(20)
190	15.1	CCCl def(56), SCC def(40)	188	11.3	CCCl def(54), SCC def(44)
103	18.5	C-C tors(90)	104	18.8	C-C tors(92)
96	1.9	C-C tors(77)	97	0.0	C-C tors(80)
54	2.0	CSC bend(49), SCC def(36)	54	2.1	CSC bend(49), SCC def(36)
45	0.0	C-S tors(86)	43	0.0	C-S tors(88)
26	0.0	C-S tors(100)	26	0.0	C-S tors(98)
	------			------	
ΣA_i	446.1		ΣA_i	449.0	
Average Deviation^e = 0.41%					

$^{a-e}$As in Table 4-3.

^{f}A prime symbol (CH2') refers to vibrations of $ClCH_2$- groups.

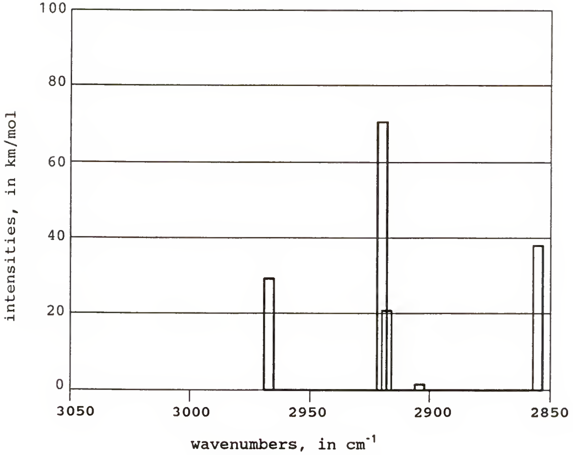

Figure 4-1. Simulated predicted bar IR spectrum (3050 - 2850 cm^{-1}) of diethyl sulfide (Set A) calculated using the transferred force constants and polar tensors from trans-EtSH (3-21G). The height of each bar is equal to the intensity in Table 4-3, while the wavenumber is the scaled value listed in the same table. This simulated spectrum is expected to predict the appearance of an experimental IR matrix isolation spectrum for a molecule with absorption bands having equal bandwidths.

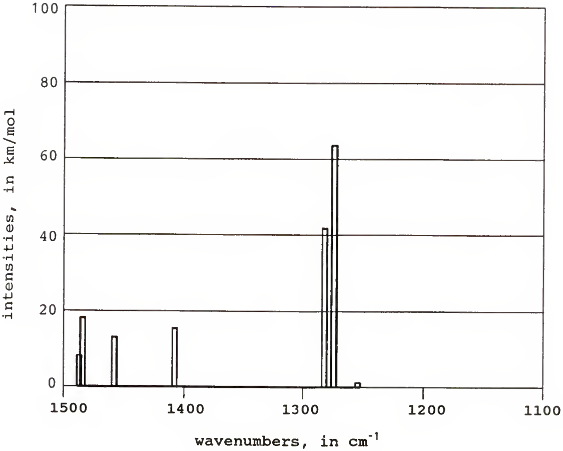

Figure 4-2. Simulated predicted bar IR spectrum (1500 - 1100 cm^{-1}) of diethyl sulfide (Set A) calculated using the transferred force constants and polar tensors from trans-EtSH (3-21G). (See caption to Fig. 4-1).

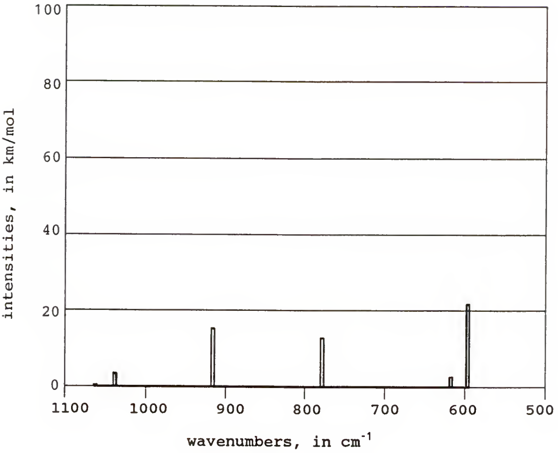

Figure 4-3. Simulated predicted bar IR spectrum (1100 - 500 cm^{-1}) of diethyl sulfide (Set A) calculated using the transferred force constants and polar tensors from trans-EtSH (3-21G). (See caption to Fig. 4-1).

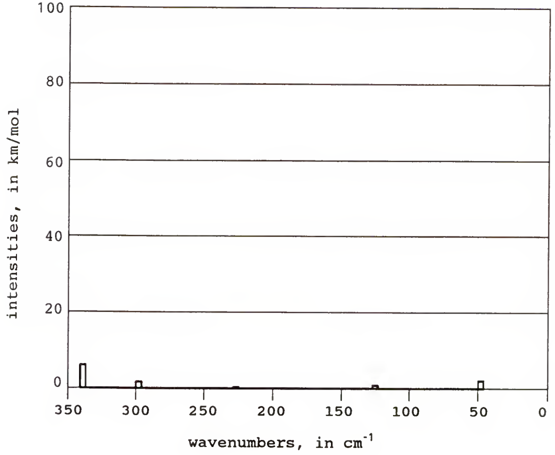

Figure 4-4. Simulated predicted bar IR spectrum (350-0 cm^{-1}) of diethyl sulfide (Set A) calculated using the force constants and polar tensors transferred from trans-EtSH (3-21G). (See caption to Fig. 4-1).

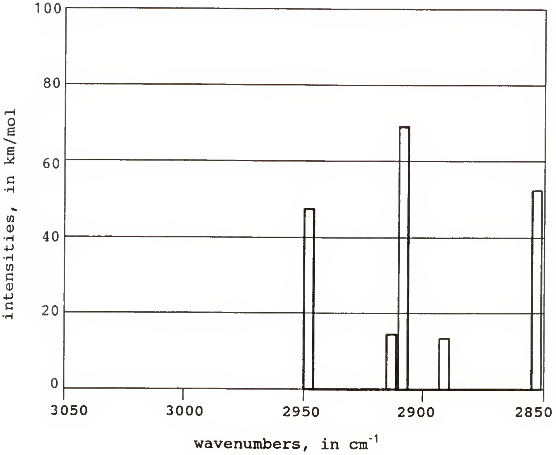

Figure 4-5. Calculated bar IR spectrum (3050 - 2850 cm^{-1}) of diethyl sulfide from direct calculation (Set B) at the 3-21G level. (See caption to Fig 4-1).

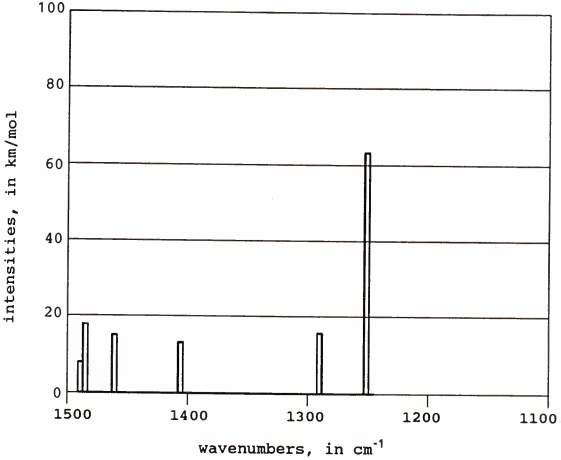

Figure 4-6. Calculated bar IR spectrum (1500 - 1100 cm^{-1}) of diethyl sulfide from direct calculation (Set B) at the 3-21G level. (See caption to Fig 4-1).

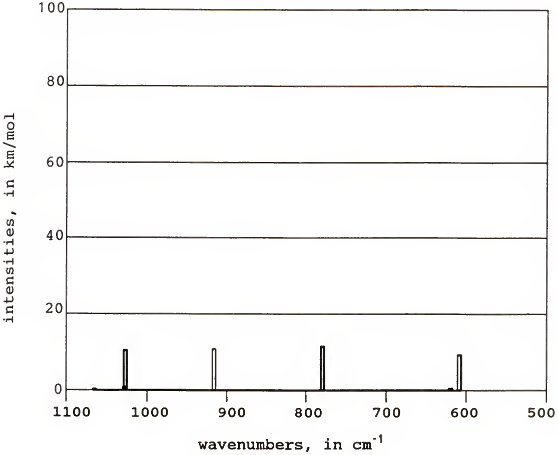

Figure 4-7. Calculated bar IR spectrum (1100 - 500 cm^{-1}) of diethyl sulfide from direct calculation (Set B) at the 3-21G level. (See caption to Fig 4-1).

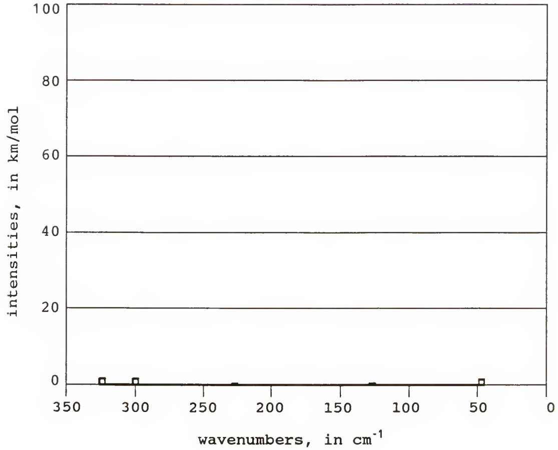

Figure 4-8. Calculated bar IR spectrum (<350 cm^{-1}) of diethyl sulfide from direct calculation (Set B) at the 3-21G level. (See caption to Fig 4-1).

CHAPTER 5

SCALING OF THE QUANTUM MECHANICAL FORCE FIELD

Reliable prediction of vibrational spectra would obviously greatly enhance the power of infrared and Raman spectroscopy as a structural tool. To this aim, knowledge of the force field is necessary at least in the harmonic approximation.

It has long been an important objective of vibrational spectroscopy to determine force fields for smaller molecules, which could then be transferred to larger systems, thus making predictions possible. It is well known, however, that for molecules larger than triatomics, tremendous efforts are needed to collect the necessary number of data points (isotope data, etc.) which would uniquely fix the force field. Even for simple polyatomic molecules, truly reliable experimental force fields are very rare. In addition, the transferability of force constants is limited.

It would thus be of great importance if force constants could be determined by theoretical methods with sufficient accuracy. To be of true practical value, however, this means that the prediction of frequencies should be accurate to better than 1% so that the force constants, at least the dominant diagonal terms, should be calculated within about 2%.

This requirement is a very serious challenge for the quantum chemical methods.

5.1 Scaling Procedure

Most quantum chemical force field calculations have been performed within the Hartree-Fock (H-F) Self-Consistent Field (SCF) method using moderate sized basis set (double zeta or split valence) (11). The accuracy of these calculations is limited, but the errors are fairly systematic: diagonal stretching force constants are overestimated by 10-15%; the overestimation of the diagonal bending force constants is usually 20-30% (12, 69).

While the accuracy of SCF results is not sufficient, they can be successfully used when combined with experimental data. The idea of combining theoretical and experimental information was suggested by Pulay et al. (70, 71), and several slightly different schemes have been used since. Scaling procedures were introduced by Blom and Altona (72) and also by Pulay and coworkers (73, 74). For a review, see ref. 12.

It is important to note that the scale factors are corrections for the use of a finite basis set and neglect of electron correlation in the computations. Basis set, reference geometry and internal coordinates are carefully selected in a uniform way. In the scaling procedure, the internal coordinates are separated into different groups according to their chemical type, and a scale factor C_i is assigned to group i. Then, if the diagonal terms F_{ii} and F_{jj} are scaled by

C_i and C_j, the geometric mean $(C_iC_j)^{1/2}$ is used for the off-diagonal F_{ij} elements. In matrix notation (12), the relationship between the theoretical force constant matrix F_{th} and the experimental F matrix becomes

$$F = C^{1/2} F_{th} C^{1/2} \tag{5-1}$$

where C is the diagonal matrix of the scale factors. Through optimization of the scale factors (the number of which is kept at a minimum) the complete force field is fitted to the experimental fundamentals.

5.2 Survey of Results

In calculating the scale factors of the force field, gauche-EtSH is chosen since the experimental assignment of its frequencies has already been published (28). The estimated scale factors for the force constants are evaluated by taking the squared ratio of experimental to theoretical harmonic frequencies calculated using two different basis sets (3-21G and 6-31G**). Using these estimated scale factors, approximate frequencies are calculated and the assignment of fundamentals is checked. Once a reliable assignment has been established, the scale factors are adjusted to give a force field F that better fits the experimental frequencies, thus yielding the final refined force field.

The final scale factors of the force field obtained using this method are presented in Table 5-1 along with the scale factors suggested by Fogarasi and Pulay for cyclobutane (12). It is worth noting that their scaling factors are used for adjusting their theoretical 4-21G force field evaluated for experimental geometries and so are somewhat different from ours where optimized geometries are used. The groupings of scale factors used into stretching, bending and torsion are the same as suggested by Blom and Altona (72), and also by Pulay et al. (12, 73). The C-Cl stretching and CCCl deformation scale factors are taken to be the same as for C-S stretching and CCS deformation, respectively, and not adjusted further. This procedure works because both S and Cl are the second-row atoms they are expected to behave in the same way for a specified basis set.

The vibrational frequencies, infrared intensities, and PED analysis predicted for gauche-EtSH calculated at both 3-21G and 6-31G** levels, with the force constants scaled by the factors given in Table 5-1, are listed in Table 5-2 and 5-3, respectively, together with the experimental values (28). With these scale factors, an excellent reproduction of the frequencies is achieved for this molecule with either basis set. In the 3-21G calculation, an average deviation in frequencies from the experimental values is 10.53% for frequencies calculated with unscaled force constants after direct evaluation of the ab initio force constants, while use of a single scale factor of 0.89^2 on the force constants brings down the average deviation to 2.07% (Table 3-13).

Further improvement is achieved when the set of scale factors given in Table 5-1 is employed, yielding an average deviation of 0.53% (Table 5-2). It should be noted that the average deviations are evaluated only for calculated wavenumbers greater than 500 cm^{-1} to avoid misinterpretation of a large percentage deviation due to small errors in the prediction of the lower frequency modes.

A similar trend of improvement is also observed for calculations made with the 6-31G** basis set. The average deviation in predicted frequencies is brought down from 10.88% for the direct evaluation to 1.42% (Table 3-14) with a single scaling factor of 0.89^2, and then is brought down further by the set of scale factors from Table 5-1 to only 0.51% as seen in Table 5-3.

It is very encouraging to realize that very small average deviations of 0.37% and 0.31% could be achieved from the 3-21G and 6-31G** calculations, respectively, if the value for the CH2 rock is excluded. A large negative deviation (3.50%) in these values suggest that the CH2 rock force constant need to be scaled by a different, larger scale factor than is used for the CH3 rocks. During adjustment of the scale factors, excellent agreement is obtained when the CH2 rock force constants calculated with both basis sets are scaled by 0.850.

Comparison of Table 5-3 (frequencies calculated using the 3-21G force constants with different scaling factors) to Table 3-13 (calculated using the 3-21G force constants with one single scaling factor of 0.89^2) shows no significant changes in the intensities and PEDs for any of the normal modes. Similar results are also observed for the 6-31G** calculation when Table 5-4 is compared with Table 3-14. Hence we conclude for these molecules that the use of several different scaling factors as recommended by Fogarasi and Pulay (12) adjusts the calculated frequencies to better agreement with experiment, without any significant effect on predicted intensities or PEDs.

Table 5-1: Scale Factors[a] Used for Adjusting the Theoretical Force Constants.

	3-21G	6-31G**	Pulay[b] 4-21G
Stretching:			
C-H str	0.804	0.817	0.850
S-H str	0.962	0.793	
C-C str	0.910	0.880	0.910
C-Cl str, C-S str	1.060	0.850	-
Bending:			
C-H wag	0.795	0.770	0.740
CH3 def, sciss, rock, twist	0.770	0.797	0.803
SCC def, CCCl def	0.830	0.821	-
HSC bend, CSC bend	0.879	0.821	-
Torsion:			
S-H tors, S-C tors, C-C tors	0.797	0.774	-

[a] These scale factors are calculated as described in the text. (For comparison the single scale factor is $0.89^2 = 0.792$)

[b] Optimized scale factors for cyclobutane (ref 12).

Table 5-2: Harmonic Vibrational Frequencies, Infrared Frequencies and Potential Energy Distribution Analysis (PED) Predicted for gauche-EtSH Calculated from an Empirically Scaled Force Field[a] (3-21G).

normal coord	wavenumbers, cm^{-1} exptl[b]	scl[c]	diff	A, km/mol	PED[d,e]
1	2980	2988	8	9.5	CH2 a-str(94-)
2	2967	2939	-28	26.1	CH2 s-str(55+) CH3 opl a-str(30-) CH3 ipl a-str(14+)
3	2930	2934	4	16.6	CH3 opl a-str(63+) CH2 s-str(31+)
4	2902	2918	16	6.5	CH3 ipl a-str(80+) CH2 s-str(13-)
5	2875	2869	-6	22.1	CH3 s-str(94-)
6	2571	2571	0	28.5	S-H str(100-)
7	1462	1464	2	3.5	CH3 ipl a-def(87+)
8	1452	1462	10	11.8	CH3 opl a-def(86+)
9	1437	1441	4	6.6	CH2 sciss(96-)
10	1377	1387	10	6.6	CH3 s-def(100-)
11	1269	1268	-1	30.5	CH2 wag(87-)
12	1246	1239	-7	1.0	CH2 twist(64-) CH3 opl rock(25-)
13	1093	1090	-3	11.8	HSC bend(28-) CH3 opl rock(18+) CH2 rock(17-) CH2 twist(12-) CH3 ipl rock(12+)
14	1051	1042	-9	1.3	CH3 ipl rock(41+) C-C str(23-) CH3 opl rock(10-)

---

continued

Table 5-2 -- continued

normal coord	wavenumbers, cm^{-1} exptl[b]	scl[c]	diff	A, km/mol	PED[d,e]
15	970	972	2	13.1	C-C str(64-) CH3 ipl rock(19-)
16	867	865	-2	14.6	HSC bend(52-) CH3 opl rock(24-) CH2 twist(14+)
17	740	715	-25	1.7	CH2 rock(60+) CH3 opl rock(13+) HSC bend(12-) C-S str(10-)
18	658	659	1	13.1	C-S str(78-)
19	319	320	1	1.0	SCC def(89-)
20	241	242	1	2.5	C-C tors(91+)
21	191	190	-1	31.5	H-S tors(94-)
			ΣA_i	259.7 km/mol	

Average Deviation[f] = 0.53%

---

[a] $F_{scl} = C^{1/2}F_{th}C^{1/2}$ (Eq. 5-1).

[b] From ref. 28.

[c] These frequencies are evaluated by scaling the theoretical force constants using the set of scaling factors proposed in Table 5-1.

[d] Percentage contributions greater than or equal to 10% are given in parentheses.

[e] Definitions of symmetry coordinates are the same as given by Shimanouchi et al. (66). The + and - signs give the relative phases of each symmetry coordinate in the normal coordinate (see ref 66). str = stretch; def = deformation; tors = torsion; scis = scissors; ipl = in plane; opl = out of plane.

[f] See footnote e in Table 4-3.

Table 5-3. Harmonic Vibrational Frequencies, Infrared Intensities and Potential Energy Distribution Analysis(PED) Predicted for gauche-EtSH Calculated from an Empirically Scaled Force Field[a] (6-31G**).

normal coord	wavenumbers, cm^{-1} exptl[b]	scl[c]	diff	A, km/mol	PED[d,e]
1	2980	2971	-9	37.3	CH2 a-str(74-) CH3 opl a-str(26-)
2	2967	2948	-19	13.8	CH3 opl a-str(59-) CH2 a-str(20+) CH3 ipl a-str(17+)
3	2930	2940	10	42.7	CH3 ipl a-str(74-) CH3 opl a-str(15-)
4	2902	2917	15	15.3	CH2 s-str(91+)
5	2875	2879	4	32.7	CH3 s-str(97-)
6	2571	2571	0	14.7	S-H str(100+)
7	1462	1452	-10	2.1	CH3 ipl a-def(87-)
8	1452	1447	-5	6.9	CH3 opl a-def(92-)
9	1437	1438	1	1.5	CH2 sciss(89-)
10	1377	1385	8	2.0	CH3 s-def(93-)
11	1269	1269	0	28.8	CH2 wag(83-)
12	1246	1246	0	1.2	CH2 twist(69+) CH3 opl rock(22+)
13	1093	1104	11	12.9	HSC bend(28-) CH2 rock(21-) CH3 opl rock(19+) CH2 twist(10-) CH3 ipl rock(10+)
14	1051	1051	0	0.3	C-C str(37+) CH3 ipl rock(31-)

---

continued

Table 5-3 -- continued

normal coord	wavenumbers, cm^{-1} exptl[b]	scl[c]	diff	A, km/mol	PED[d,e]
15	970	970	0	5.7	C-C str(43+) CH3 ipl rock(29+) CH2 wag(12-)
16	867	859	-8	9.3	HSC bend(52-) CH3 opl rock(24-) CH2 twist(15+)
17	740	713	-27	1.0	CH2 rock(59+) CH3 opl rock(17-) HSC bend(11+)
18	658	658	0	6.5	C-S str(79+)
19	319	320	1	1.5	SCC def(85-)
20	241	242	1	2.3	C-C tors(88-)
21	191	190	-1	20.7	H-S tors(90-)
			ΣA_i	259.3 km/mol	

Average Deviation[f] = 0.51%

[a-f] As in Table 5-2.

CHAPTER 6
PREDICTION OF INFRARED SPECTRA USING A SCALED-TRANSFERABLE FORCE FIELD WITH DIRECT TRANSFER OF POLAR TENSORS

In this chapter, the use of different scale factors and the transferability of internal coordinate force constants and polar tensors from a high level calculation, 6-31G**, for smaller model compounds is tested for diethyl sulfide and dichlorodiethyl sulfide. These predicted spectra are then compared with the "experimental" result (frequencies and PEDs) calculated using the set of force constants recommended by Shimanouchi et al. (66) as transferable force constants for molecules of this type.

In this study, the internal coordinate force constants of model compounds (trans-EtSH or trans-ClEtSH) which were calculated at the 6-31G** level (except for the CSC bending and CS torsion, which were taken from the results of an ab initio calculation of test molecules at the 3-21G level) were transferred to the test molecules (diethyl sulfide or mustard) and scaled according to Eq. 5-1 using scaling factors from Table 5-1. The atomic polar tensors (APTs) of the test molecules are obtained by transforming the APTs of their model compounds. These methods of transforming force constants and polar tensors have already been discussed in Chapter 4.

6.1 Diethyl Sulfide

Vibrational frequencies, infrared intensities, and potential energy distributions (PEDs) calculated for all-trans-diethyl sulfide using the 6-31G** parameters calculated for trans-EtSH adjusted by use of the proposed set of scale factors for force constants given in Table 5-1 are presented in Table 6-1. There they are compared with the frequencies and PEDs calculated using the force constants recommended by Shimanouchi et al. (66). The simulated bar IR spectrum predicted in Set A, Table 6-1 for this compound is shown in Fig. 6-1 to 6-4.

In examining the comparison between the PEDs (Table 6-1), we see that the general agreement is actually very good. As can be expected for calculations made by transferring parameters at this SCF level (6-31G**) from model compounds, scaled by simple scale factors, there are number of differences. The major discrepancy between the two calculations for the CH stretching region (2980 - 2840 cm^{-1}) is that our calculation predicts that the CH2 asymmetric stretching has a higher frequency than CH3 asymmetric stretching. The same phenomenon was also observed in the direct ab initio calculation for diethyl sulfide at the 3-21G level (see Set B in Table 4-3).

For the CH2 and CH3 bending modes (1500 - 1200 cm^{-1}) the agreement both for frequencies and PEDs, is excellent. The CH2 rocking frequencies (771 and 759 cm^{-1}) are again underestimated for this molecule, just as was the case for EtSH. If a larger scale factor of 0.850 is used (instead of 0.797) for the CH2 rocking force constants, the frequencies predicted for these modes then become 784 and 774 cm^{-1} in excellent agreement with experimental result of 787 and 778 cm^{-1}, respectively. The CC and CS stretching frequencies seem to be in an excellent agreement with the experimental Set B. This means that the inclusion of polarization functions in the 6-31G** calculation, together with the scaling factors from Table 5-1, really improve the agreement with experiment for all modes involving the heavy atoms. For example, the predicted SCC deformation mode at 341 cm^{-1} agrees with the experimental value surprisingly well (within 8 cm^{-1}). The other modes in this region below 400 cm^{-1} (namely, the CSC bend, CC and CS torsions) are predicted somewhat lower in frequency than the experimental Set B values. Actually, we can't say which set is better since the "experimental" frequencies listed in Set B are not observed experimental values, but are calculated from the force constants given by Shimanouchi et al. (66) for an interpretation of experimental spectrum of these kind of molecules.

The average deviation (0.70%) between the frequencies from the two calculations is very promising. This value is even more encouraging when the CH2 rocking mode force constants are scaled by 0.850, which brings down the deviation to only 0.59%.

6.2 2,2'-Dichlorodiethyl Sulfide

An examination of the comparison between our calculated spectrum from scaled transferred force constants (Set A) and the "experimental" spectrum (Set B) calculated as before from Shimanouchi force constants (66) for 2,2'-dichlorodiethyl sulfide shown in Table 6-2 indicates the same general agreement for this more complicated molecule as we found above for diethyl sulfide. The simulated bar IR spectrum predicted in Set A, Table 6-2 for this compound is presented in Fig. 6-5 to 6-8.

In the CH stretching region (3020-2900 cm^{-1}), the CH2 asym stretch of -CH2S- is predicted in Set A to have a higher frequency than CH2 sym stretch of -CH2Cl, while the case is reversed in Set B. For the CH bending modes in the 1500-1100 cm^{-1} region, the agreement is quite acceptable. Compared with the 3-21G calculation (Table 4-4), the frequencies predicted in Set A for CC, CS, CCl stretching modes agree very well with "experimental" values. As previously discussed in the diethyl sulfide and EtSH, the CH2 rocking for this compound is again underestimate due to the use of the single small scaling factor (0.797) for all CH2 rocking modes. In the lower frequency region of heavy atoms bending, the predicted frequencies in our Set A calculation again seem to be somewhat lower than those from Set B. The largest deviation in frequency between Set A and Set B in this region is in the prediction of CSC bending. This result is already expected since its force constant was not transferred from the model compound but was obtained from the 3-21G calculation and so expected to be inaccurate.

Table 6-1: Vibrational Frequencies, Infrared Intensities, and Potential Energy Distributions (PEDs) for all-trans-Diethyl Sulfide Calculated using the Scaled-Transferred Force Constants and Polar Tensors (trans-EtSH, 6-31G**), Compared with "Experimental" Values Calculated from the Shimanouchi Set of Empirical Transferable Force Constants.

set A transferred[a]			set B "experimental"[b]		set C experimental[g]	
wave-numbers[c] cm^{-1}	A, km/mol	PED[d,e]	wave-numbers[c] cm^{-1}	PED[d,e]	wave-numbers cm^{-1}	assignments
2971[d]	83.2	CH2 a-str(74), CH3 opl a-str(26)	2963[d]	CH3 opl a-str(92)		--
2949[d]	83.9	CH3 ipl a-str(96)	2962[d]	CH3 ipl a-str(99)		--
2948[d]	10.5	CH3 opl a-str(74), CH2 a-str(26)	2943[d]	CH2 a-str(95)		--
2916[d]	50.0	CH2 s-str(96)	2906[d]	CH2 s-tr(98)		--
2885[d]	55.2	CH3 s-str(99)	2880[d]	CH3 s-str(95)		--
1457[d]	2.4	CH3 ipl a-def(69), CH2 sciss(21)	1464[d]	CH3 ipl a-def(64), CH2 sciss(20)	1478 vw 1458 s	CH3 ipl def CH3 ipl def
1450[d]	8.1	CH2 sciss(72), CH3 ipl a-def(16)	1463[d]	CH3 opl a-def(82)	1454 s,sh 1450 s	CH3 opl def CH3 opl def

----

continued

Table 6-1 -- continued

set A transferred[a]			set B "experimental"[b]		set C experimental[g]	
wave-numbers[c] cm^{-1}	A, km/mol	PED[d,e]	wave-numbers[c] cm^{-1}	PED[d,e]	wave-numbers cm^{-1}	assignments
			1442	CH2 sciss(54), CH3 ipl a-def(22)	1444 s	CH2 sciss
1449[d]	12.0	CH3 opl a-def(92)				
			1431	CH2 sciss(50), CH3 s-def(34)	1438 s	CH2 sciss
			1388	CH3 s-def(86)	1380 s,sh	CH3 s-def
1386[d]	4.2	CH3 s-def(94)				
			1378	CH3 s-def(68), CH2 sciss(34)	1375 s	CH3 s-def
1270	37.9	CH2 wag(84)	1273	CH2 wag(84)	1299 vw	CH2 wag
1261	59.5	CH2 wag(84)	1270	CH2 wag(84)	1286 vs	CH2 wag
1236[d]	0.6	CH2 twist(57), CH3 opl rock(29)	1256[d]	CH2 twist(66), CH3 opl rock(6)	1264 w,sh 1256 vs	CH2 twist CH2 twist
1087	0.2	CH3 ipl rock(43), C-C str(36)	1075	C-C str(40), CH3 ipl rock(32)	1080 vw	C-C str
1044	0.0	C-C str(46), CH3 ipl rock(42)	1046	CH3 ipl rock(42), C-C str(42)	1042 vw	CH3 ipl rock

----
continued

Table 6-1 -- continued

set A transferred^{a}			set B "experimental"^{b}		set C experimental^{g}	
wave-numbers^{c} cm^{-1}	A, km/mol	PED^{d,e}	wave-numbers^{c} cm^{-1}	PED^{d,e}	wave-numbers cm^{-1}	assignments
1036	0.0	CH2 twist(32), CH2 rock(28), CH3 opl rock(23)	1041	CH3 opl rock(40), CH2 rock(30)	1042 vw	CH3 opl rock
1022	0.1	CH2 twist(32), CH3 opl rock(26), CH2 rock(25)	1032	CH3 opl rock(40), CH2 twist(30)	1028 vw	CH3 opl rock
974[d]	4.5	C-C str(53), CH3 ipl rock(23)	982[d]	C-C str(50), CH3 ipl rock(28)	993 s 986 s	CH3 ipl rock C-C str
771	4.2	CH2 rock(54), CH3 opl rock(35)	787	CH2 rock(64), CH3 opl rock(38)	798 vw	CH2 rock
759	2.0	CH2 rock(59), CH3 opl rock(32)	778	CH2 rock(66), CH3 opl rock(36)	798 vw	CH2 rock
688[d]	11.0	C-S str(93)	688[d]	C-S str(96)	693 s	C-S str
341	4.3	SCC def(92)	349	SCC def(104)	348 vw	SCC def
315	0.8	CSC bend(29), SCC def(40), C-S str(22)	339	CSC bend(27), SCC def(26), C-S str(18)	332 w	SCC def

----

continued

Table 6-1 -- continued

set A transferred[a]			set B "experimental"[b]		set C experimental[g]	
wave-numbers[c] cm^{-1}	A, km/mol	PED[d,e]	wave-numbers[c] cm^{-1}	PED[d,e]	wave-numbers cm^{-1}	assignments
232[d]	0.3	C-C tors(95)	251[d]	C-C tors(96)	273 vw 262 vw	C-C tors C-C tors
130	0.5	CSC bend(61), SCC def(38)	153	CSC bend(78), SCC def(28)	126 vw,sh	CSC bend
70[d]	1.5	C-S tors(95)	85[d]	C-S tors(98)	72 vw	C-S tors

ΣA_i 437.5 km/mol

Average Deviation[f] = 0.70%

---

[a] These values were evaluated using the 6-31G** force constants (adjusted by use of the set of scale factors presented in Table 5-1) and polar tensors calculated for model compounds.

[b] These values were calculated using the transferable empirical set of force constants from Shimanouchi et al. (66).

[c] [d] = "degenerate modes"; two modes are calculated to have this frequency.

[d-f] See footnotes c-e in Table 4-3.

[g] These values were taken from ref. 20; experimental IR in crystalline state.

Table 6-2: Vibrational Frequencies, Infrared Intensities, and Potential Energy Distribution Analysis (PED) for all-trans-2,2'-Dichlorodiethyl Sulfide Calculated using the Scaled-Transferable Force Constants and Polar Tensors (trans-ClEtSH, 6-31G**), Compared with "Experimental" Values Calculated from the Shimanouchi set of Transferable Force Constants.

set A transferred^{a}			set B experimental^{b}	
wave-numbers^{c}	A, km/mol	PED^{d,e}	wave-numbers^{c}	PED^{d,e}
3019[d]	17.2	CH2' a-str(90), CH2 a-str(10)	3005[d]	CH2' a-str(98)
2989[d]	5.8	CH2 a-str(90), CH2' a-str(10)	2956[d]	CH2' s-str(99)
2957[d]	38.0	CH2' s-str(97)	2944[d]	CH2 a-str(98)
2936[d]	22.9	CH2 s-str(99)	2905[d]	CH2 s-str(99)
			1439	CH2 sciss(68), CH2' sciss(26)
1454[d]	2.3	CH2 sciss(62), CH2' sciss(28)		
			1434	CH2' sciss (80)
			1428	CH2' sciss(66), CH2 sciss(22)
1451[d]	13.9	CH2' sciss(61), CH2 sciss(39)		
			1410	CH2 sciss(76)
1304[d]	7.1	CH2' wag(55), CH2 wag(37)	1306[d]	CH2' wag(76), CH2 wag(22)

----

continued

Table 6-2 -- continued

set A transferred^{a}			set B experimental^{b}	
wave-numbers^{c}	A, km/mol	PED^{d,e}	wave-numbers^{c}	PED^{d,e}
1266[d]	0.0	CH2 twist(45), CH2' twist(38)	1282[d]	CH2 twist(42), CH2' twist(38)
1208[d]	113.9	CH2 wag(64), CH2' wag(36)	1218[d]	CH2 wag(84), CH2' wag(24)
1134	2.5	CH2' twist(57), CH2 twist(37)	1147[d]	CH2' twist(50), CH2 twist(48)
1118	1.5	CH2' twist(46), CH2 twist(43)		
1062	0.2	C-C str(80)	1043	C-C str(74)
1041	3.7	C-C str(88)	1014	C-C str(88)
976[d]	0.9	CH2 rock(36), CH2' rock(32), CH2 twist(13)	984[d]	CH2' rock(44), CH2 rock(40)
810	4.9	C-S str(43), SCC def(20)	791	C-S str(52), C-Cl str(20)
770	2.8	CH2 rock(43), CH2' rock(39)	756[d]	CH2 rock(48), CH2' rock(46)

----
continued

Table 6-2 -- continued

set A transferred[a]			set B experimental[b]	
wave-numbers[c]	A, km/mol	PED[d,e]	wave-numbers[c]	PED[d,e]
765	16.0	C-S str(38), C-Cl str(29)	756	C-S str(64), SCC def(9)
746	2.2	CH2 rock(45), CH2' rock(43)		
731	107.2	C-Cl str(52), C-S str(48)	723	C-Cl str(68), C-S str(24)
712	36.9	C-Cl str(70), C-S str(32)	696	C-Cl str(70), C-S str(30)
341	0.7	SCC def(38), CCCl def(24), C-Cl str(20)	361	CSC bend(49), CCCl def(50)
316	1.3	CSC bend(38), CCCl def(53)	348	SCC def(36), C-Cl str(18)
209	0.1	SCC def(30), C-S str(26)	218	C-S str(22), SCC def(22)
203	11.8	CCCl def(54), SCC def(44)	198	CCCl def(66), SCC def(58)

----

continued

Table 6-2 -- continued

set A transferred[a]			set B experimental[b]	
wave-numbers[c]	A, km/mol	PED[d,e]	wave-numbers[c]	PED[d,e]
105[d]	14.9	C-C tors(87)	130	C-C tors(84)
			117	C-C tors(64), C-S tors(24)
57	1.4	CSC bend(47), SCC def(38)	75	C-S tors(74), C-C tors(24)
42	0.0	C-S tors(84)	60	CSC bend(58), SCC def(18), CCCl def(18)
24	0.0 -----	C-S tors(100)	43	C-S tors(90)
ΣA_i	429.1			

Average Deviation[f] = 0.70%

[a-f] As in Table 6-1; a prime symbol (CH2') refers to vibrations of Cl$\underline{CH}_2$- groups.

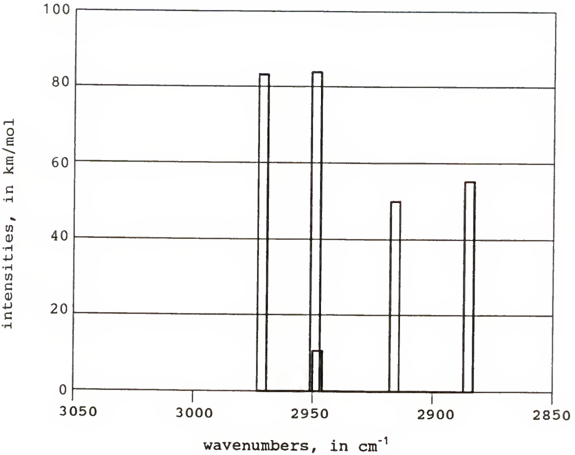

Figure 6-1. Simulated bar IR spectrum (3050-2850 cm^{-1}) of diethyl sulfide (Set A) predicted using the 6-31G** parameters calculated for trans-EtSH adjusted by use of the set of scale factors for force constants given in Table 5-1. The height of each bar is equal to the intensity in Table 6-1, while the wavenumber is the value listed in the same table.

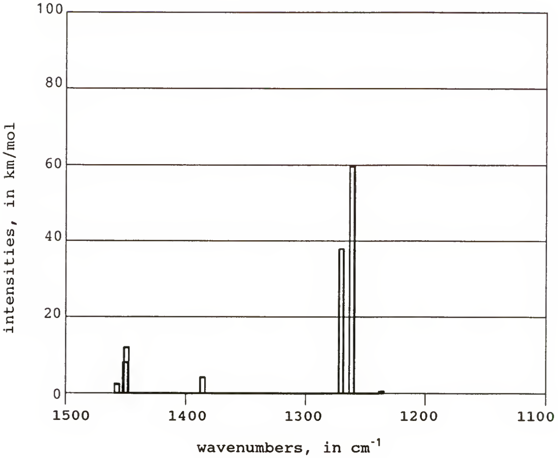

Figure 6-2. Simulated bar IR spectrum (1500 - 1100 cm^{-1}) of diethyl sulfide (Set A). (See caption to Fig 6-1.)

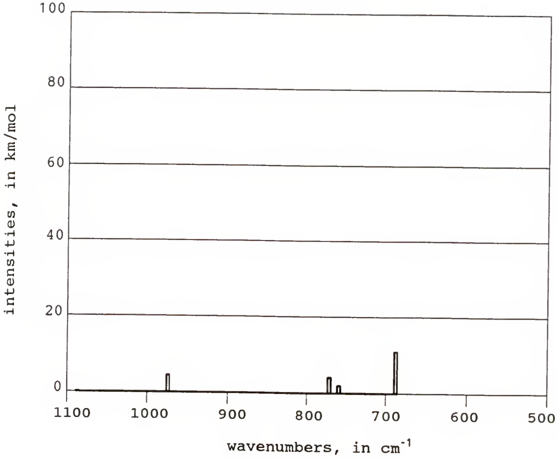

Figure 6-3. Simulated bar IR spectrum (1100-500 cm^{-1}) of diethyl sulfide (Set A). (See caption to Fig. 6-1.)

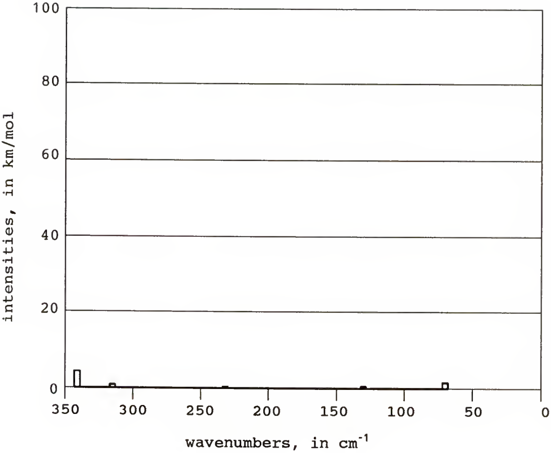

Figure 6-4. Simulated bar IR spectrum (350 - 0 cm^{-1}) of diethyl sulfide (Set A). (See caption to Fig 6-1.)

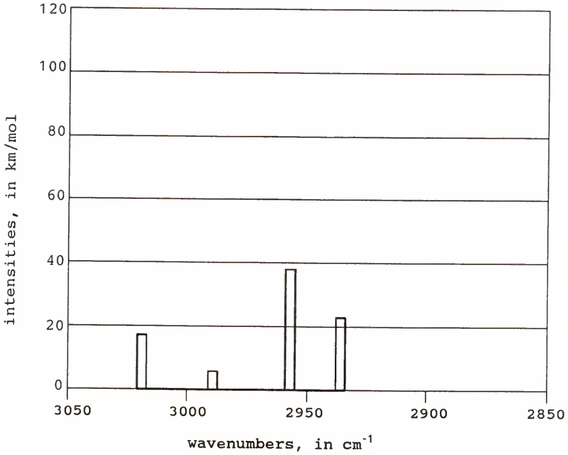

Figure 6-5. Simulated bar IR spectrum (3050-2850 cm^{-1}) of dichlorodiethyl sulfide (Set A) predicted using the 6-31G** parameters calculated for trans-ClEtSH adjusted by use of the set of scale factors for force constants given in Table 5-1. The height of each bar is equal to the intensity in Table 6-2, while the wavenumber is the value listed in the same table.

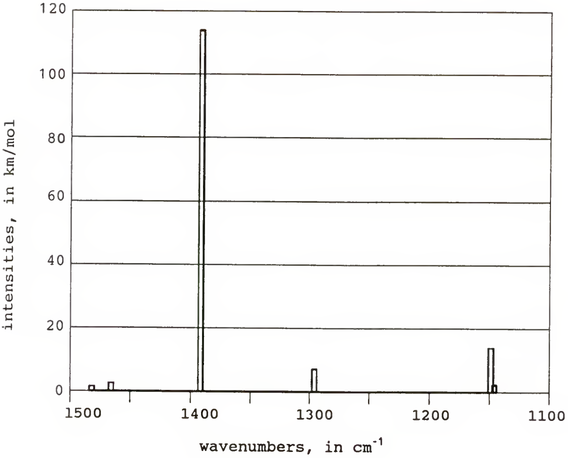

Figure 6-6. Simulated bar IR spectrum (1500 - 1100 cm^{-1}) of dichlorodiethyl sulfide (Set A). (See caption to Fig 6-5.)

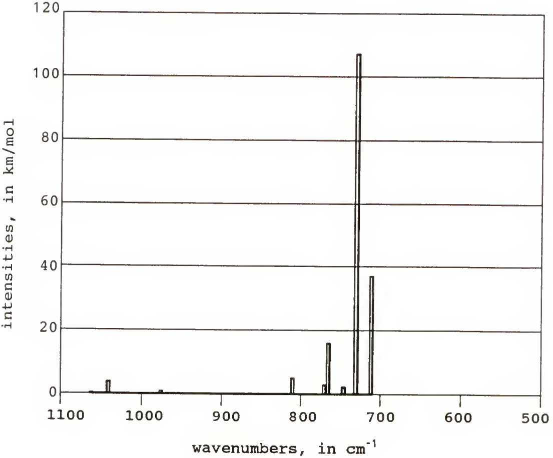

Figure 6-7. Simulated bar IR spectrum (1100 - 500 cm^{-1}) of dichlorodiethyl sulfide (Set A). (See caption to Fig 6-5.)

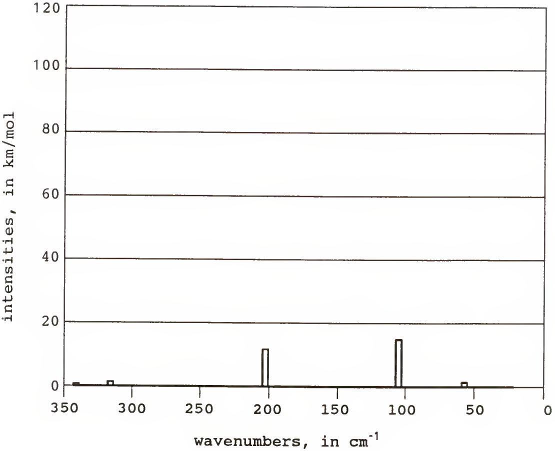

Figure 6-8. Simulated bar IR spectrum (350 - 0 cm^{-1}) of dichlorodiethyl sulfide (Set A). (See caption to Fig 6-5.)

CHAPTER 7
PARTITION OF POLAR TENSOR INVARIANTS

7.1 Introduction to Principal Component Analysis

Principal component analysis (PCA) is a multivariate technique for examining relationships among several quantitative variables. It is used for summarizing data and detecting linear relationships. Plots of principal components are especially valuable tools in exploratory data analysis. Principal components can be used to reduce the number of variables in regression, clustering, and so on.

PCA was originated by Pearson (75) in 1901 and later developed by Hotelling (76) in 1933. The model for PCA has been described previously in the chemical literature (77-79). Principal components have a variety of useful properties (80):

1- The eigenvectors are orthogonal, so the principal components represent jointly perpendicular directions through the space of the original variables.

2- The principal component scores are jointly uncorrelated.

3- The first principal component has the largest variance of any unit-length linear combination of the observed variables. The j^{th} principal component has the largest variance of any unit-length linear combination orthogonal to the first j-1 principal components. The last principal component has the smallest variance of any linear combination of the original variables.

4- The first j principal components are the best linear predictors of the original variables among all possible sets of j variables, although any non-singular linear transformation of the first j principal components would provide equally good prediction.

5- In geometric terms, the j-dimensional linear subspace spanned by the first j principal components gives the best possible fit to the data points as measured by the sum of squared perpendicular distances from each data point to the subspace.

The purpose of the PCA is to derive a small number of linear combinations (principal components) of a set of variables that retain as much of the information in the original variables as possible. Often a small number of principal components can be used in place of the original variables for plotting, regression, clustering, and so on. PCA can also be viewed as an attempt to uncover approximate linear dependencies among variables.

Principal component analysis is often followed by rotation of the components. Rotation is the application of a non-singular linear transformation to components to aid interpretation.

In principal component analysis (PCA), new coordinate axes, the PC axes, are obtained from the original ones by rotation. The first axis (PC1) corresponds to the direction of maximum variance in the original data and therefore contains the largest fraction of the total statistical information that could be compressed into a single dimension. The second PC axis (PC2) is orthogonal to the first and is directed along the maximum residual variance. The other axes (PC3, PC4,..) are obtained likewise.

The purpose of employing the PCA method is to reduce the dimensions of the information contained in the original multivariate data. PC plots turn out to be the most informative two-dimensional projections of the whole data set, and examination of the most significant of them will show most of the structure (if any) underlying the original polar tensor data. Analysis into principal components therefore yields a fairly good picture of the entire data set. This method is employed extensively and has already been discussed by Bruns and coworkers (36, 39, 81).

The invariants of a set of n atomic polar tensors from an n-atom polyatomic molecule can be arranged in a matrix Y of order n x m, where each row contains the m invariants of a single APT. Decomposition of this data matrix into principal components is represented by the matrix equation (39)

$$Y = Y_{av} + TB + E \qquad (7\text{-}1)$$

where Y_{av} contains the averages of the invariants over all tensors. Each row of B corresponds to one principal component and contains its "loading", that is, the direction cosines locating the PC axis in the original frame. The matrix B then defines how much of each invariant goes into each principal component. On the other hand, each row of T contains the "scores" of a polar tensor, which are its coordinates on the PC axes defined by B. There are as many columns in T, and rows in B, as there are principal components.

The part of the data matrix Y that is not described by the PC model Y_{av} + TB is contained in the residual matrix E. In the calculation of each principal component E is minimized in a least-squares sense. The values of its elements decrease as the number of principal components increases and the information still present in E is progressively transferred to Y_{av} + TB.

Before performing a PC decomposition it is usual to scale all the variables to unit variance, to avoid giving undue importance to the variables having the largest variation in the original data (36, 39).

7.2 Definitions of the Invariants

An atomic polar tensor (2) contains the derivatives of the three cartesian components of the molecular dipole moment with respect to the three cartesian displacement of the atom in question (Please refer to Eq. 2-29). These nine values can be regarded as the coordinates of a point representing the APT in 9-dimensional space. However, as they depend on the molecular orientation in the cartesian frame of reference, these coordinates are not convenient for a direct comparison of APTs from different molecules.

The orientation problem is easily solved by using APT invariants instead of the elements themselves. The invariants (X, $\bar{P}$, and β) of each atomic polar tensors have been defined by several authors (2, 3, 6, 9, 39, 63). For a given APT, their values are unaffected by the orientation of the cartesian coordinate system. The first invariants is the effective charge, X, which was first defined by King, Mast, and Blanchette (64), and its relationship to the APTs was given by Newton and Person (9). The effective charge is related to the length of the tensor and is given by Eq. 2-43. X_α is a very interesting quantity because it can be directly calculated from the sum of the intensities (3), when data for isotopic species are also available. The relation between the intensity sums and X is defined by Eq. 2-44.

Two other useful invariant properties are the mean dipole derivative, $\bar{P}_\alpha$, and the anisotropy, β_α, of the α^{th} APT (2, 9). The former is defined by

$$\bar{P}_\alpha = (1/3)\ \text{Trace}\ P_X^\alpha \qquad (7\text{-}2)$$

The squared anisotropy is defined by

$$\beta_\alpha^2 = (1/2)\ [(P_{xx} - P_{yy})^2 + (P_{yy} - P_{zz})^2 + (P_{zz} - P_{xx})^2 + 3(P_{xy}^2 + P_{yz}^2 + P_{xz}^2 + P_{zx}^2 + P_{yx}^2 + P_{zy}^2)] \qquad (7\text{-}3)$$

with $P_{uv} = \partial P_u / \partial v$. This parameter is a measure of the deviation of a polar tensor from a constant, diagonal tensor $\bar{P}_\alpha$.

However, only two of the invariant properties are independent and the relationship (9) between the three invariants (X, $\bar{P}$, and β) is given by

$$\beta_\alpha^2 = (9/2)\ (X_\alpha^2 - \bar{P}_\alpha^2) \qquad (7\text{-}4)$$

Two more invariants (39) can be obtained from the secular of an APT, which can be written as

$$f(\lambda) = \lambda^3 - (\mathrm{Tr\ Px}) * \lambda^2 + C * \lambda - D = 0 \qquad (7\text{-}5)$$

λ standing for the eigenvalues of the APT. Since the coefficients of the secular equation are not affected by unitary transformations, (Tr Px), C and D are invariants under a rotation of the cartesian frame. Tr Px, the polar tensor's trace, is simply three times the mean dipole moment derivative already recognized as an invariant, but C and D are two new invariants (39). D represents the determinant of the APT and C is the sum of the minors of the diagonal elements of the APT determinant. For an APT having P_{zx} and P_{xz} as the only nonzero off-diagonal elements, we have

$$C = P_{yy}P_{zz} + P_{xx}P_{zz} - P_{zx}P_{xz} + P_{xx}P_{yy} \qquad (7\text{-}6)$$

Instead of employing directly the values of C and D we shall use $\sqrt{C}$ and $\sqrt[3]{D}$, to make all invariants have the same dimension, namely charge (e). For the invariants β, X and C, defined by quadratic equations, their absolute values will always be used. Hence only $\bar{P}$ and $\sqrt[3]{D}$ have possible negative sign. Taken together, $\bar{P}$, X, β, $\sqrt{C}$ and $\sqrt[3]{D}$ represent an APT as a point in five dimensions.

7.3 Application of Principal Component Analysis in Partitioning the Invariants

In this work, the PCA is used to study similarities and differences of the polar tensors for carbon and hydrogen atoms from different molecules and also in the same molecules with different electronic/chemical environments. In this analysis, the invariants of polar tensors are used as variables instead of the elements themselves, to avoid the problems arising from different orientations of the cartesian reference frames.

The invariants for carbon and hydrogen atoms obtained from the 3-21G calculation of the APTs for the molecules of our study (14) are listed in Table 7-1 and 7-2, respectively.

The complete list of all invariants ($\bar{P}$, β, X, $\sqrt[3]{D}$ and $\sqrt{C}$) for all atoms in these series are presented in Appendix D.

7.3.1 Carbon Invariants

There are six sulphur-containing molecules used in this study: trans-EtSH (ET), gauche-EtSH (ETG), trans-ClEtSH (CL), all-trans-diethyl sulfide (DI), all-trans-2,2'-dichlorodiethyl sulfide or mustard gas (MU), and all-trans-2-chlorodiethyl sulfide which consists of ethyl (ES) and chloroethyl fragments (ESX). (See Fig 2-1 and 2-2).

From these calculations fourteen different carbon atom polar tensors calculated at the 3-21G level are used in this analysis. These carbon atoms are labelled by either 2 or 3, where C2 is the methylene carbon attached to sulphur atom (-$\underline{C}H_2$S-) and C3 is the terminal carbon (-$\underline{C}H_2CH_2$S-). (See Fig 2-2).

The input datafile containing all five invariants for the 14 different carbons is prepared on VAX/VMS to be used in SAS principal component analysis using PRINCOMP procedure (80). The output of the program consists of the simple statistics (mean and standard deviation), correlation matrix, eigenvalues and also the eigen-vectors of rotation. Here we shall explain some of the output for the sake of clarity.

The Pearson's product moment correlation coefficients (75, 76), called the correlation matrix, is used to determine the strength of a relationship between two variables. It is well known that the largest value, +1, is obtained when all points in the data set lie on a straight line. Its minimum value, 0, occurs when the data points are essentially randomly distributed throughout a two-variable plot or appear in certain types of nonlinear patterns. The correlation matrix for these 14 carbon atoms is given in Table 7-3.

These three invariants, $\bar{P}$, X, and ß, are highly correlated with each other and have correlation coefficients greater than 0.97, while $\sqrt{C}$ is correlated with them with correlation coefficients greater than 0.88. The worst correlation coefficient of 0.43 is between $\sqrt[3]{D}$ and ß. It is worth while to note that there is nothing wrong with a small correlation coefficient, but this unique characteristic ($\sqrt[3]{D}$) should be used as a fingerprint for an APT for this kind of carbon atom calculated at this SCF level (with 3-21G basis set).

The eigenvalues (listed in the SAS-PCA output) indicate that one or two principal components provide a good summary for the data; one components (PC1) accounts for 85% of the standardized variance and two components (PC1 and PC2) explain 99%. Subsequent components (PC3, PC4, and PC5) contribute less than 0.5% each. The first eigenvector, corresponding to 85% of the variance in the whole set is found to be

$$PC1 = 0.48\bar{P} + 0.47X + 0.46\beta + 0.33\sqrt[3]{D} + 0.48\sqrt{C}$$

It shows approximately equal loading on all variables except $\sqrt[3]{D}$, which contributes only 11% (= 0.33^2) to the component. PC1 can be regarded approximately as an arithmetic average of all invariants (except $\sqrt[3]{D}$). The second principal component, which represents about 14% of the total variance, is dominated by the cube root of the determinant ($0.866^2 = 75\%$).

$$PC2 = -0.16\bar{P} - 0.24X - 0.37\beta + 0.87\sqrt[3]{D} + 0.16\sqrt{C}$$

Figure 7-1 is a plot of PC2 against PC1. It shows that PC2 discriminates very well the behavior of C2 ($-\underline{C}H_2S-$ or methylene carbon) from that of the terminal carbon C3 ($\underline{C}H_3CH_2S-$ or $Cl\underline{C}H_2CH_2S-$) atoms due to their differences in the value of $\sqrt[3]{D}$ and β. It is also very interesting to see that PC1 in the positive part of PC2 divides C3 atoms into two groups, those from the ethyl fragments (CH_3CH_2S-) and those from the chloroethyl fragments ($ClCH_2CH_2S-$), by a wide margin.

Almost all of the C2 atoms are located at the bottom-left part of the plot. This part is more interesting where it shows that the APT of the C2 atom in trans-EtSH is different (higher value of PC1) from that for C2 atoms of diethyl sulfide. The same information is also obtained by comparing the "mass-weighted effective charge squared" (2-6, 34) or MWECS where the value for the C2 atom of trans-EtSH ($0.40\ e^2u^{-1}$) is higher than the value for C2 of diethyl sulfide ($0.028\ e^2u^{-1}$). (For convenience of the reader, the values of MWECS ($3X_\alpha^2/m_\alpha$) for all atoms are presented in Appendices D-1 and D-2.) Therefore, we should not expect good transferability of C2 polar tensors between these two molecules. On the other hand, the transference would be better between C2 from ClEtSH and those from mustard gas because these points are located very close to each other in the PCA plot.

In the case of C3 atoms, PC1 separates the C3 atom of EtSH from that for diethyl sulfide and also the C3 atom of ClEtSH from those for mustard gas with equal distances between each of them. However, this separation shown in Fig. 7-1 is smaller than for the C2 case. For C3 atoms, the PC1 values for atoms in smaller model compounds are lower than those for their larger counterparts. A similar pattern also could be observed by looking at their MWECS values (in Appendices D-1 and D-2); 0.001 e^2u^{-1} for C3 in EtSH compared with 0.002 e^2u^{-1} for C3 in diethyl sulfide, and 0.103 e^2u^{-1} for C3 in ClEtSH compared with 0.112 e^2u^{-1} for C3 atoms in mustard gas. Since the separation shown in Fig. 7-1 is very small, it can be concluded that the polar tensors for C3 atoms of EtSH and ClEtSH are not as much affected as are the C2 atoms when the H(S) atom is replaced by a CH_3CH_2- (for diethyl sulfide) or $ClCH_2CH_2$- group (for mustard gas).

7.3.2 Hydrogen Invariants

Twenty-three different hydrogen polar tensors are used in this analysis. Four different classes of hydrogen atoms from the molecules involved in this study are hydrogen in methylene groups (H5 & H6), the out-of-plane methyl hydrogen atoms (H7 & H8), the in-plane methyl hydrogen atom (H9), and the thiol hydrogen (H4). The last type will be briefly discussed here because it is not involved in the transference of APTs from model compounds (EtSH and ClEtSH) to their larger counterparts (diethyl sulfide, monochlorodiethyl sulfide, and mustard). Figure 7-2 shows the plot of the first two principal components of invariants for all 23 hydrogen atoms. It shows that the thiol hydrogens (at PC1 > +3.0) are really very different in their behavior from the other hydrogen atoms, which are located in the range of $2.0 > PC1 > -2.0$. This plot neatly proves that the thiol hydrogens (H-S) APTs are significantly different from other hydrogens (methylene or methyl). This result is what we would expect from atoms in chemical environments.

The correlation coefficients of the invariants for all 20 hydrogens bonded to C atoms are presented in Table 7-4. In Figure 7-3, which contains 97% of the total variance, these 20 hydrogen atoms have been grouped into five obvious clusters, i.e., three groups from $\underline{H}C\underline{H}_2C\underline{H}_2S$- hydrogens [in-plane(H9), out-of-plane methyl hydrogen (H7 and H8), and methylene hydrogen (H5 and H6)] and two groups from $ClC\underline{H}_2C\underline{H}_2S$- hydrogens [methylene hydrogens (H5 and H6) and chloromethyl hydrogen (H7 and H8)].

The first principal component, PC1, which describes 65% of the variance, contains X, β, $^3\!\sqrt{D}$ and $\sqrt{C}$ in approximately equal parts, plus a very small (2%) contribution from $\bar{\bar{P}}$. This components separates the in-plane (H9) from out-of-plane (H7 and H8) hydrogens of $\underline{H}C\underline{H}_2CH_2S$- fragments as well as $HC\underline{H}_2C$- from $ClC\underline{H}_2C$- hydrogens as seen in Fig. 7-3.

The second component, PC2, containing 32% of the variance, consists primarily 56% (= 0.75^2) of $\bar{P}$ out of phase with an equal part, 18% each, of X and $^3\sqrt{D}$. Figure 7-3 also shows that PC2 discriminates very well the -C$\underline{H}_2$S- hydrogens (H5 and H6) of CH_3CH_2S- fragments from those in $ClCH_2CH_2S$- fragments, and it also discriminates the in-plane hydrogens from those out-of-plane. This discrimination is actually due to the differences in those three invariants, especially in $\bar{P}$ as seen in Fig. 7-3.

Within the same group, it is very obvious that PC1 of each methylene hydrogen ($-CH_2S-$) in smaller model compounds differs from the values for those atoms in their larger counterparts. For example, the PC1 value of ET_H5 is -1.06 compared to -1.64 of DI_H5, and the PC1 value of CL_H5 is -1.29 compared to -2.06 of MU_H5. On the other hand, it seems that values of PC1 for methyl hydrogens (H7, H8, H9) are not very much affected when H(S) is replaced by a larger group such as an ethyl or chloroethyl fragment.

From these PCAs, we could conclude that the APTs of the carbon atom, and those for hydrogen atoms in the methyl groups (CH_3C-) are not as much affected as are the atoms in the methylene groups ($-CH_2S-$) when a larger molecule is constructed by combining two smaller ones.

7.4 Similarities and Differences of Polar Tensors Calculated at Two Different Levels.

What are the differences between APTs for these atoms calculated at the 3-21G and then at the 6-31G** level? This might be the toughest question to answer just by looking at the elements of the polar tensors in cartesian coordinates because of their dependency on the orientation of the molecule in these axes. As previously mentioned, this problem is easily overcome by studying the invariants of polar tensors. As mentioned above the dimension of the APT decreases from 9 to 5 and then from 5 to 2 when the PCA is applied. In this study, discussion will be concentrated on the APTs for carbon and hydrogen atoms calculated in these series.

7.4.1 Carbon Polar Tensors

In Figure 7-4, which contains 99% of the total variance, the carbon atoms have been grouped into three classes: methyl carbon ($\underline{C}H_3CH_2S-$), methylene carbon ($-\underline{C}H_2S-$), and chloromethyl carbon ($Cl\underline{C}H_2CH_2S-$).

The first principal component, PC1, which describes 84% of the variance in the whole set, contains $\bar{\bar{P}}$, X, β, and $\sqrt{C}$ in almost equal parts, plus a smaller contribution from $\sqrt[3]{D}$. The three groups observed in the plot are clearly separated by this component. It should be noticed that C2 of ethyl is grouped together with C2 of the chloroethyl fragment. This shows the weakness of the effect of chlorination at the methyl carbon on the APTs of the C2 atoms. Since the chlorine atom is substituted at the C3 atom, the separation between these two C3 APTs (ethyl and chloroethyl) is very clear along this PC1 component.

Probably the most interesting feature about this plot (Fig. 7-4) is the dependence on the second principal component, PC2, which explains 15% of the total variance. This component is dominated by $\sqrt[3]{D}$ ($0.84^2 = 71\%$) plus a smaller contribution ($0.42^2 = 18\%$) from β. Along this component, the 3-21G polar tensor invariants are well-separated from those calculated with the 6-31G** basis set. In each case, we should notice that the 6-31G** values are always located at some higher values of PC2 than are the 3-21G values. Hence we conclude for these molecules that the main difference between the 3-21G and 6-31G** calculation of APTs is in the value of $\sqrt[3]{D}$.

Another interesting bit of information obtained from the dependence on this second component PC2 is that the C3 atoms are not as much affected as are the C2 atoms. This very large effect on the APTs for C2 atoms and on those for the C3 atom of the chloroethyl group could be a result of the poor prediction of S and Cl atom properties with the 3-21G calculation. As discussed previously in Chapter 3, the addition of polarization functions, for example in the 6-31G** basis set, will improve considerably the prediction properties associated with the S, Cl (and other second row) atoms.

From this PCA plot, it could be concluded that the differences between polar tensors from these two calculations are due to the underestimated (or negative) value of $\sqrt[3]{D}$ in the 3-21G calculation. These differences are due to the polarization functions included in the 6-31G** basis set which affect the S and Cl atoms and also their neighboring atoms. Another important fact about this plot is that the values of the $\bar{P}$, X, ß, and $\sqrt{C}$ invariants for the carbon atom polar tensors are basis set independent.

7.4.2 Hydrogen Polar Tensors

Figure 7-5 is the plot of the first two principal components of the APT invariants (calculated with 6-31G** and 3-21G) for the 20 hydrogen atoms attached to carbon in these molecules which contains 95% of the original information. In this plot the hydrogen atoms have been grouped into four obvious clusters: in-plane methyl hydrogens (H9), out-of-plane methyl hydrogens (H7, H8), and methylene hydrogens (H5, H6) of CH_3CH_2S- ; and hydrogen atoms of $ClCH_2CH_2S$- fragments.

The first principal component, PC1, which explains 54% of the variance in the whole set, contains X, ß, $\sqrt[3]{D}$, and $\sqrt{C}$ in almost equal parts. Along this component, the hydrogen atoms are divided into two large groups; methyl hydrogens (HCH_2C-) in the positive direction and methylene hydrogens (-CH_2S-) in the negative direction. There are two well-separated groups on the positive side which belong to the in-plane and out-of-plane methyl hydrogens. Methylene hydrogens of the ethyl fragments and all hydrogens from chloroethyl fragments are separated into two groups on the negative side of PC1. It is worthwhile to note that one of the gauche methylene hydrogen (ETG_H5 & ETG6_H5) is separated from the remaining group of CH2 hydrogen atoms and it appears together with the chloroethyl hydrogens. From the optimized geometry, it is found that this hydrogen is nearly trans (-174.6° with 3-21G and -174.0° with 6-31G** basis) to the thiol hydrogen (See Table 3-1 and Fig. 2-2).

The second principal component, PC2, which contains 41% of the variance, is composed mostly of $\bar{P}$ (44%) and ß (28%). The other three invariants (X, $\sqrt[3]{D}$, and $\sqrt{C}$) contribute a total of only 28%. As previously discovered for the carbon atom case in Fig. 7-4, this component (PC2) is also the one that responsible for the separation of the hydrogen APTs calculated with these two different basis sets.

The same pattern as for the carbon atoms APTs is again repeated here for the hydrogen atoms where the APTs from the 6-31G** calculation are always located at higher PC2 values than are those from the 3-21G calculation. This means that the 3-21G basis set underestimates the values of the mean dipole moment and of the anisotropy of hydrogen atom polar tensors in this series. The plot (Fig. 7-5) shows that the separations among invariants calculated for methylene hydrogens (-C$\underline{H}_2$S-) and those for chloromethyl hydrogens (ClC$\underline{H}_2$CH$_2$S-) are larger compared to separation of the invariants for the methyl hydrogens (CH_3CH_2S-) (H7, H8 & H9). Possibly the reason is the differences in the quality of prediction of properties for S and Cl atoms with these two basis sets, which may also affect prediction of properties for their neighboring atoms. Another important fact obtained from the plot in Fig. 7-5 is that the three invariants (X, $\sqrt[3]{D}$ and $\sqrt{C}$) which dominate PC1, are basis set independent.

7.5 Comments on the Atom Anisotropy, Effective Charges, and Mean Dipole Moment Derivatives in Vibrational Intensity Analysis

The analysis of integrated intensities in terms of atomic polar tensors (8, 9) and effective atomic charges (4) has revealed a hitherto unnoticed order in the structural parameters that control vibrational transition moments. Kim and King (82) have shown that the value of the atom anisotropy (ß) relative to the effective charge (X) is a very useful parameter in characterizing molecular structure through analysis of the vibrational intensities.

The atomic polar tensor for atom n in a molecule is defined as the conjugate (transpose) gradient of the molecular dipole moment vector P written as Eq. 2-29, and the square of the effective charge is defined as one-third of the sum of the squares of the polar tensor components as given in Eq. 2-43. The other two scalar quantities are the mean dipole derivative (Eq. 7-2) and the atom anisotropy (Eq. 7-3 or Eq. 7-4). Using the relationship between the three invariants and rearranging Eq. 7-4

$$X_n^2 = (2/9)\ \beta_n^2 + (\bar{P}_n)^2 \tag{7-7}$$

and then dividing by X^2

$$1 = (\sqrt{2/3})^2 (\beta_n/X_n)^2 + (\bar{P}_n/X_n)^2 \tag{7-8}$$

Defining

$$\alpha_n = (\sqrt{2/3})\ (\beta_n/X_n) \tag{7-9}$$

β_n and X_n are taken as absolute values, so that α_n ranges from 0 to 1, and

$$\gamma_n = (\bar{P}_n/X_n) \tag{7-10}$$

Since $\bar{P}_n$ can be negative, γ_n ranges from -1 to +1.
We can rewrite Eq. 7-8 as

$$1 = \alpha_n^2 + \gamma_n^2 \tag{7-11}$$

the equation for a circle plotted as α_n against γ_n as coordinates.

These new parameters α_n and γ_n have been proved (82) to be useful in characterizing chemical bonds in terms of atomic properties. In their studies for various compounds, Kim and King (KK) concluded that the values of α_n are close to zero for molecules intuitively regarded as ionic in that they dissociate in water. On the other hand, the values of α_n are rather close to 1 for the molecules considered to be covalent.

In Figure 7-6 is the plot (as a circle) of the values of α_n against the values of γ_n for all hydrogen and chlorine atoms for these molecules calculated at the 3-21G level. The values of α_n and γ_n for all atoms are presented in Appendices F and G, respectively. The plot separates the Cl atoms very well from the H atoms. The data represented by the filled squares in Fig. 7-6 show that the values of α_n for the Cl atoms fall in the region of 0.55 to 0.58. This means that the Cl atoms in these molecules seem to have bonding intermediate (slightly more covalent) in character between ionic and covalent. These values are consistent with the reported values (82) for α_n values from flourine atoms (around 0.50).

All methylene hydrogen atoms ($-CH_2-$), represented in Fig. 7-6 as filled triangles, are divided into two main groups: one group with α_n at around 0.90 belongs to $CH_3C\underline{H}_2S-$ fragments and the other one with α_n values around 0.98 belongs to $ClCH_2C\underline{H}_2S-$ fragments.

At the top of the plot in Fig. 7-6, where the α_n values are closer to 1, there are several groups of atoms that almost overlap with each other. However, a careful investigation will help in separating them into four groups according to their γ_n values. From the left, hydrogen atoms from $ClCH_2C\underline{H}_2S$- fragments (as mentioned above), in-plane hydrogens of $\underline{H}CH_2CH_2S$- thiol hydrogens (H-S-), out-of-plane hydrogens of $ClC\underline{H}_2CH_2S$-, and out-of-plane hydrogens of $HC\underline{H}_2CH_2S$- fragments. This plot shows that these hydrogen atoms, located at the top of the plot, are bonded to carbon atoms more covalently than are the H atoms in the methylene group in the $CH_3C\underline{H}_2S$- fragments.

Generally speaking, this plot in Fig. 7-6 seems to give similar information as was found from the Principal Component Analysis (PCA) as shown in Fig. 7-3, but with additional important information about the nature of the chemical bonds involved. In other words, this plot should also be used in determining the possibility of transfering APT's parameters from one system to another system depending on their chemical similarities.

Table 7-1: The Invariants (in e) of Polar Tensors for 14 Carbon Atoms from this Study Calculated at the 3-21G Level.

C atom[a,b]	$\bar{P}$	χ	β	$\sqrt[3]{D}$	$\sqrt{C}$
ETG_C2	0.250	0.395	0.650	0.103	0.260
ET_C2	0.254	0.402	0.661	-0.156	0.235
DI_C2	0.203	0.335	0.566	-0.190	0.131
ES_C2	0.223	0.403	0.713	-0.227	0.114
ETG_C3	-0.007	0.085	0.180	0.039	0.077
ET_C3	0.021	0.070	0.142	0.045	0.029
DI_C3	0.029	0.099	0.200	0.062	0.061
ES_C3	0.021	0.124	0.260	0.058	0.045
CL_C2	0.173	0.297	0.513	-0.126	0.143
MU_C2	0.135	0.275	0.508	-0.187	0.178
ESX_C2	0.109	0.203	0.363	-0.148	0.084
CL_C3	0.469	0.640	0.926	0.304	0.612
MU_C3	0.502	0.670	0.942	0.341	0.679
ESX_C3	0.515	0.698	0.999	0.339	0.680

[a] ET = trans-EtSH, ETG = gauche-EtSH, DI = diethyl sulfide, CL = ClEtSH, MU = mustard gas, ES (= CH_3CH_2S-) and ESX (= $ClCH_2CH_2S$-) are the fragments of monochloro-diethyl sulfide.

[b] C2 = -$\underline{C}H_2S$-, C3 = -$\underline{C}H_2CH_2S$-

Table 7-2: The Invariants (in e) of Polar Tensors for 23 Hydrogen Atoms from this Study Calculated at the 3-21G Level.

H atoms[a,b]	$\bar{P}$	X	β	$\sqrt[3]{D}$	$\sqrt{C}$
ETG_H5	0.006	0.069	0.145	0.022	0.082
ET_H5	-0.044	0.101	0.192	0.082	0.080
DI_H5	-0.047	0.099	0.186	0.084	0.060
ES_H5	-0.041	0.095	0.182	0.084	0.064
ETG_H6	-0.042	0.100	0.193	0.081	0.082
ETG_H7	-0.001	0.099	0.210	-0.074	0.109
ET_H7	0.015	0.094	0.198	-0.084	0.104
DI_H7	0.013	0.097	0.205	-0.086	0.107
ES_H7	0.018	0.097	0.202	-0.087	0.102
ETG_H8	0.014	0.092	0.193	-0.081	0.102
ETG_H9	-0.009	0.122	0.258	-0.097	0.146
ET_H9	-0.003	0.112	0.237	-0.094	0.137
DI_H9	-0.019	0.124	0.261	-0.089	0.147
ES_H9	-0.014	0.118	0.249	-0.085	0.142
CL_H5	-0.010	0.079	0.167	0.048	0.092
MU_H5	-0.011	0.071	0.149	0.060	0.081
ESX_H5	-0.014	0.070	0.145	0.061	0.079
CL_H7	0.006	0.073	0.153	-0.041	0.084
MU_H7	0.007	0.074	0.157	-0.048	0.087
ESX_H7	0.003	0.075	0.159	-0.041	0.089

[a] As in Table 7-1.

[b] H5, H6 = $-C\underline{H}_2S-$; H7, H8 = $-C\underline{H}_2CH_2S-$; H9 = $\underline{H}CH_2CH_2S-$

Table 7-3: Correlation Coefficients for the Invariants of APTs of 14 Carbon Atoms from this Study Calculated at the 3-21G level.

	$\bar{P}$	X	β	$\sqrt[3]{D}$	$\sqrt{C}$
$\bar{P}$	1.00				
X	0.99	1.00		SYM	
β	0.97	0.99	1.00		
$\sqrt[3]{D}$	0.58	0.53	0.43	1.00	
$\sqrt{C}$	0.95	0.93	0.88	0.76	1.00

Table 7-4: Correlation Coefficients for the Invariants of APTs of 20 Hydrogen Atoms Bonded to C Atoms from this Study Calculated at the 3-21G Level.

	$\bar{P}$	X	β	$\sqrt[3]{D}$	$\sqrt{C}$
$\bar{P}$	1.00				
X	-0.27	1.00		SYM	
β	-0.08	0.98	1.00		
$\sqrt[3]{D}$	-0.73	-0.41	-0.58	1.00	
$\sqrt{C}$	0.31	0.72	0.85	-0.80	1.00

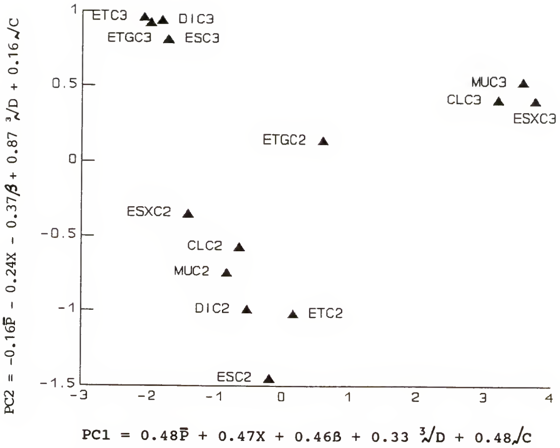

Figure 7-1. Plot of the first two principal components for the invariants of polar tensors for 14 carbon atoms in from this study calculated at the 3-21G level.

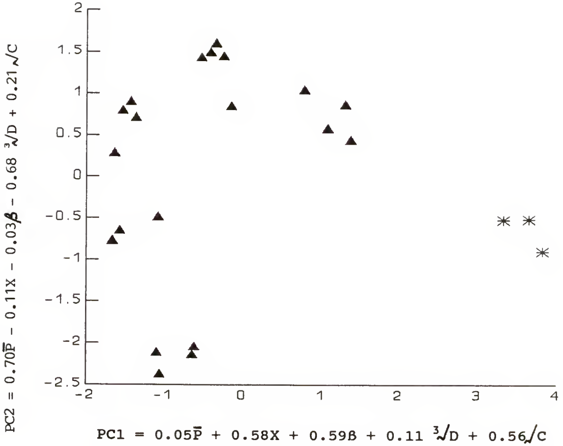

Figure 7-2. Plot of the first two principal components of the invariants of polar tensors for 23 H atoms from this study caculated at the 3-21G level. Hydrogen atoms bonded to carbon are indicated by filled triangles and hydrogen atoms bonded to sulphur are indicated by stars.

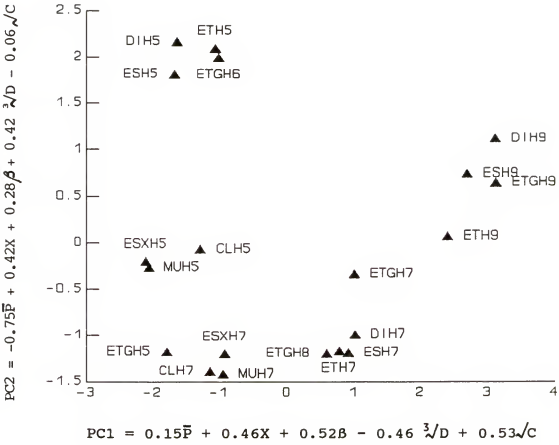

Figure 7-3. Plot of the first two principal components of the invariants of polar tensors for 20 hydrogen atoms bonded to C atoms from this study calculated at the 3-21G level.

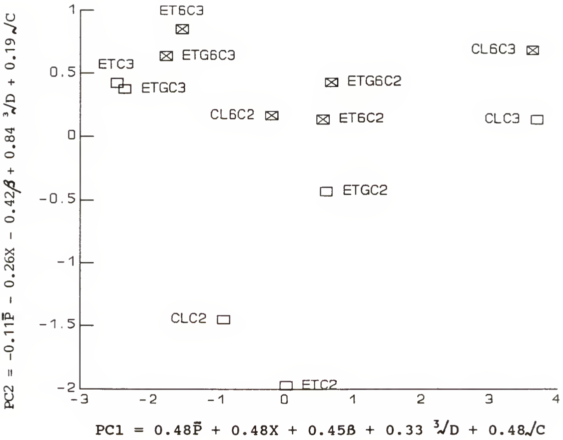

Figure 7-4. Plot of the first two principal components for the invariants of polar tensors for carbon atoms in ClEtSH and EtSH calculated at two different levels: 3-21G (empty squares) and $6\text{-}31G^{**}$ (squares with an x inside).

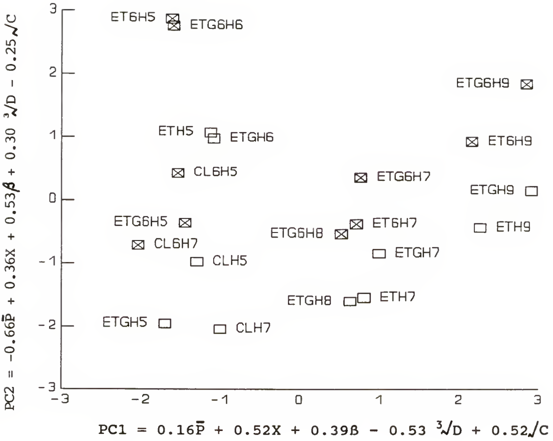

Figure 7-5. Plot of the first two principal components for the invariants of polar tensors for hydrogens in ClEtSH and EtSH calculated the two different levels: 3-21G (empty squares) and $6\text{-}31G^{**}$ (squares with an x inside).

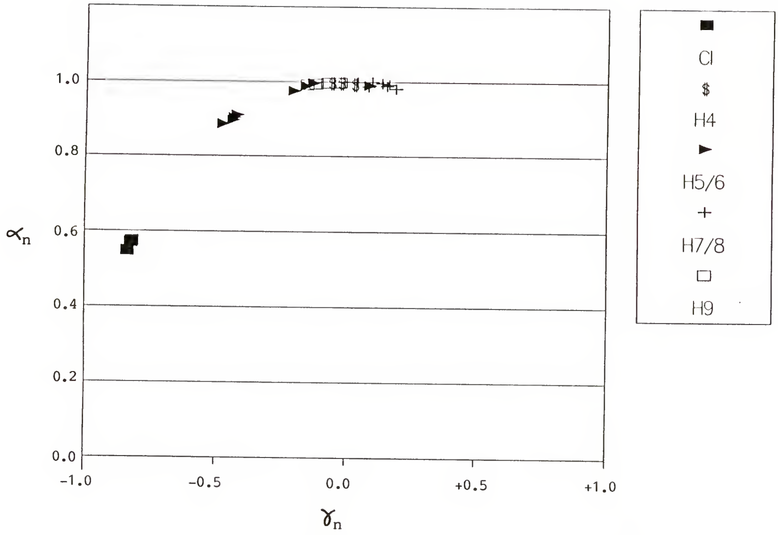

Figure 7-6. Plot of α_n against γ_n in accordance with Eq. 7-11, for all hydrogen and chlorine atoms for the mustard series of molecules calculated at the 3-21G level.

CHAPTER 8
SUMMARY

The present work tests the use of ab initio self consistent field calculations of force constants and intensity parameters, combined with a normal coordinate analysis, to predict and interpret infrared spectra for a series of molecules containing S and Cl atoms bonded to $-CH_2-CH_2-$ hydrocarbon portions. The series of molecules that were studied is: trans and gauche ethanethiol (CH_3CH_2SH or EtSH), 2-chloroethanethiol ($ClCH_2CH_2SH$ or ClEtSH), diethyl sulfide ($(CH_3CH_2)_2S$), 2-chlorodiethyl sulfide ($ClCH_2CH_2SCH_2CH_3$), and 2,2'-dichlorodiethyl sulfide ($(ClCH_2CH_2)_2S$ or mustard). These molecules were selected not only because of the poisonous properties of mustard gas, which prohibit detailed experimental studies, but also because they provide an opportunity for studies of the similarities and differences of the spectral properties of the CH_2 group when a Cl atom is substituted for an H atom.

The effects of Cl substitution on the frequency and intensity for each normal mode, and on the total intensity sum for each molecule are analyzed. Since the ab initio calculations for several of the molecules were done using two different basis sets, (3-21G and 6-31G**), the effect of adding polarization functions to the basis set on the calculated frequencies and intensities of compounds including hypervalent atoms could be examined thoroughly. The calculation of the energy of trans and gauche EtSH conformations with the 3-21G basis set yields a very good estimate of the energy difference (0.26 kcal/mol) between the two conformers involving rotation of the S-H group around the C-S bond. This estimate is in surprisingly excellent agreement with the experimental measurement of 0.3 kcal/mol (28). With a larger basis set (6-31G**), the difference in energy is predicted to be smaller (0.17 kcal/mol). However, the latter calculation is superior in predicting the total dipole moments of the two conformers of EtSH. Both calculations predicted optimized geometries in very good agreement with experiment. Because the properties for these two components are in such good agreement with experimental values, we expected that the predicted vibrational spectra might also be in agreement with experimental values.

At the beginning of Chapter 3, the various performances of the two basis sets were assessed. The initial comparison of the predicted geometries and frequencies with the observed value shows that the 6-31G** calculation gives better agreement than does the 3-21G calculation, especially for properties (such as S-H or C-Cl bond lengths) related to S and Cl atoms. The 3-21G calculation overestimates the C-S and C-Cl bond lengths and hence is found to underestimate their force constants (and thus the frequencies of the corresponding stretching vibrations). The potential energy distribution analysis determine the contributions (the PED) from each symmetry coordinate to the potential energy associated with each normal coordinate. The intensity analysis can be thought of as the corresponding description of the contributions from each symmetry coordinate to the intensity of each normal mode. It is worth noting that the intensity of a normal mode does not depend solely on the intensity parameters (atomic polar tensors or APTs) but also on the amplitude of the vibrational motion. This implies that the ab initio calculation must be able to produce a very good approximation for the APTs and also for the force constants. The intensity analysis technique was developed to explain why the intensity of a particular mode is sometimes predicted to be drastically different for a different calculation where the basis set is changed, even though the total intensity sum may be predicted to be nearly the same in both calculations.

The method of transferring parameters (geometries, force constants, and polar tensors) calculated (or measured) for a small model compound to predict the spectrum of a large molecule containing the small molecule as a fragment is tested here. In this study, we have transferred the ab initio value of force constants calculated in internal coordinate space and the calculated atomic polar tensors in cartesian coordinate space (both calculated at the 3-21G level) from trans-EtSH to the all- trans conformer of diethyl sulfide. Comparing these frequencies predicted with the transferred force constants with the ones obtained from the direct ab initio calculation (also at the 3-21G level) shows excellent agreement, i.e. frequencies within ±0.45%. The small deviation is probably due to the difference in the equilibrium geometry for the diethyl sulfide from that predicted by directly transferring from ethanethiol, and also to the neglect of the force constant cross terms that couple the vibrations between the two halves of the molecule. However, these cross terms are expected to be very small (and also predicted to be very small in the direct 3-21G calculation) since sulphur is a very big atom and it vibrationally isolates the two halves of the diethyl sulfide molecule.

The intensity prediction for diethyl sulfide using transferred APTs from EtSH is also in very good agreement with that from the direct calculation. Using the transferred polar tensors, the intensity sum is calculated to be about 10.9 km/mol higher than that found from the direct calculation (378.2 km/mol).

When the same technique of transferring parameters is applied to mustard, the frequencies and total intensity sum agree even better with the direct calculation than was found for diethyl sulfide.

When the calculated frequencies are compared with the experimental values, we conclude, in agreement with others

(12-13), that the ab initio calculation always produces the frequencies that are about 10-11% higher than the experimental values. Therefore, a single scaling factor of 0.89 (13) is used to estimate the experimental frequencies from the calculated ones. This single scaling factor seems to work quite well for these molecules in empirically correcting errors due to the limitation of the basis sets and to the neglect of electron correlation. It successfully reduces the average deviation in the predicted frequencies compared to experimental frequencies from 11% (ab initio) for EtSH to only 2.07% for the 3-21G calculation and to 1.44% for the $6\text{-}31G^{**}$ calculation. The larger error in the 3-21G calculation (2.07%) is primarily contributed from nonsystematic errors in predicting the frequencies of the normal modes related to the S atom which suggests that a different scaling factor (larger) is needed to convert the predicted frequencies for these modes to experimental values.

By examining the deviations from the experimental values for predicted frequencies associated with each different group of internal coordinates (C-S stretch, CH_2 wagging, etc.) for EtSH, a set of transferable scaling factors was obtained. The grouping of the force constant scaling factors used here is the same as that suggested by Fogarasi and Pulay (12). When this set of scaling factors is applied to predicted force constants for EtSH itself, excellent agreement is achieved for almost all modes (the average deviation is ±0.53% for 3-21G and ±0.51 for 6-31G** calculations).

Perhaps the most interesting subject was the comparison of the frequencies calculated using our best transferable set of force constants (calculated for EtSH and ClEtSH at the 6-31G** level and scaled by our set of transferable scaling factors) for diethyl sulfide and mustard with the "experimental" values calculated using the transferable set of "experimental" force constants suggested by Shimanouchi et al. (66). A very good agreement is obtained for diethyl sulfide and also for mustard gas. However, if a different scale factor (about 0.85) is used to scale the force constants for the CH_2 rocking motion, an even better agreement (±0.59%) could be achieved.

In Chapter 7, five invariants of the calculated atomic polar tensors ($\bar{P}$, X, ß, $\sqrt{C}$, $\sqrt[3]{D}$) for all atoms of each molecule are resolved into two principal components (PC1 and PC2), following a standard PCA program (80). A plot of the components (PC2 against PC1) shows that the C and H atoms of the $-SCH_2-$ group for EtSH and for diethyl sulfide are different. This result could explain why the total intensity sum calculated for diethyl sulfide using the transferred polar tensors from EtSH differs from the value from the direct calculation by 10.9 km/mol. Nevertheless, a smaller deviation is observed for the corresponding C and H atoms in ClEtSH and in mustard from the same plot. This finding is consistent with the small difference in their intensity sums (only about 2.9 km/mol).

Another important feature about the PCA plot is the partitioning of the invariants to show the factors that contribute to the difference in the APTs calculated with the two different basis sets (3-21G and 6-31G**). In fact, the difference of APTs between the two calculations (3-21G and 6-31G**) arise almost entirely from the calculated differences in C and H atoms of the $-SCH_2-$ group for these two calculations. The APTs of the CH3- group show less basis set dependence, probably because the CH3- group is far from the S atom.

APPENDIX A
FLOWCHARTS OF ICA1 PROGRAM

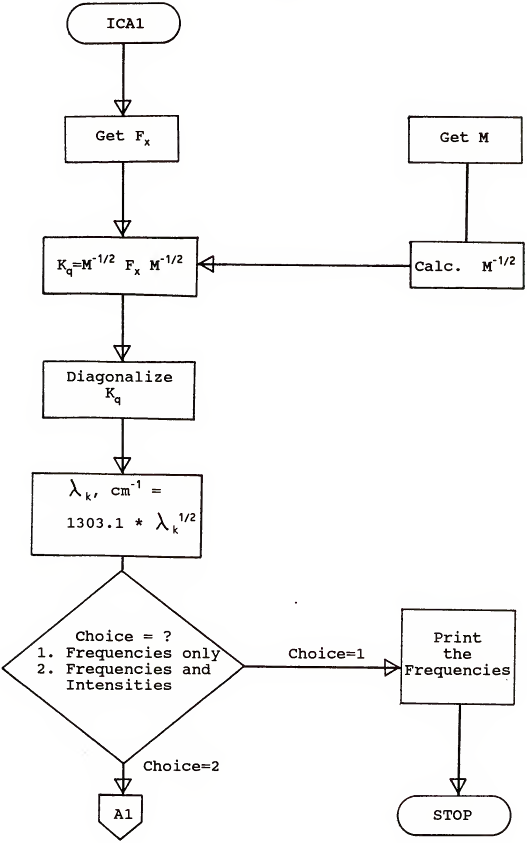
ICA1
Get F_x
Get M
$K_q=M^{-1/2}\ F_x\ M^{-1/2}$
Calc. $M^{-1/2}$
Diagonalize K_q
λ_k, cm^{-1} = 1303.1 * $\lambda_k^{1/2}$
Choice = ?
1. Frequencies only
2. Frequencies and Intensities
Choice=1
Print the Frequencies
Choice=2
A1
STOP

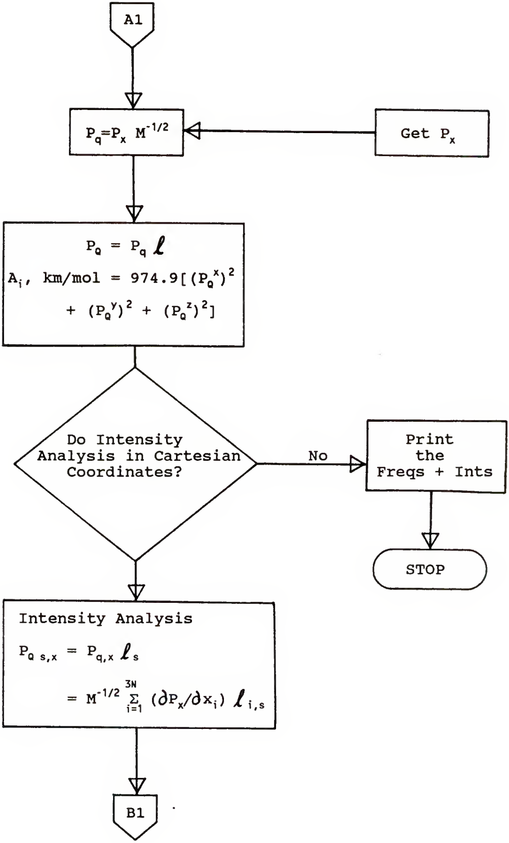
A1
$P_q = P_x M^{-1/2}$
Get P_x
$P_Q = P_q \ell$
A_i, km/mol $= 974.9[(P_Q^x)^2 + (P_Q^y)^2 + (P_Q^z)^2]$
Do Intensity Analysis in Cartesian Coordinates?
No
Print the Freqs + Ints
STOP
Intensity Analysis
$P_{Q\,s,x} = P_{q,x} \ell_s = M^{-1/2} \sum_{i=1}^{3N} (\partial P_x/\partial x_i) \ell_{i,s}$
B1

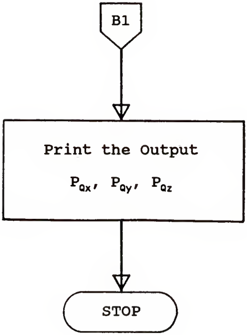
B1
Print the Output
P_{Qx}, P_{Qy}, P_{Qz}
STOP

APPENDIX B
FLOWCHARTS OF ICA2 PROGRAM

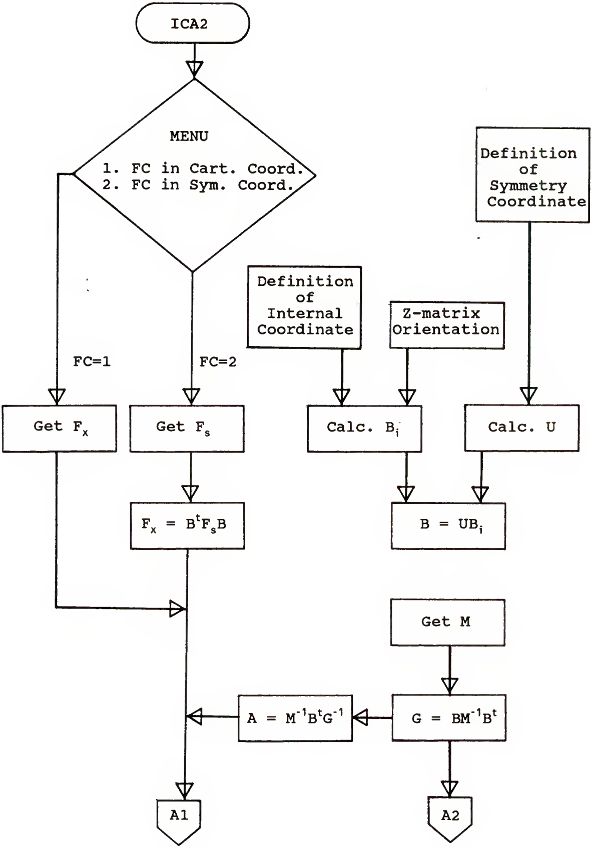
ICA2
MENU
1. FC in Cart. Coord.
2. FC in Sym. Coord.
FC=1
FC=2
Definition of Internal Coordinate
Z-matrix Orientation
Definition of Symmetry Coordinate
Get F_x
Get F_s
Calc. B_i
Calc. U
$F_x = B^tF_sB$
$B = UB_i$
Get M
$A = M^{-1}B^tG^{-1}$
$G = BM^{-1}B^t$
A1
A2

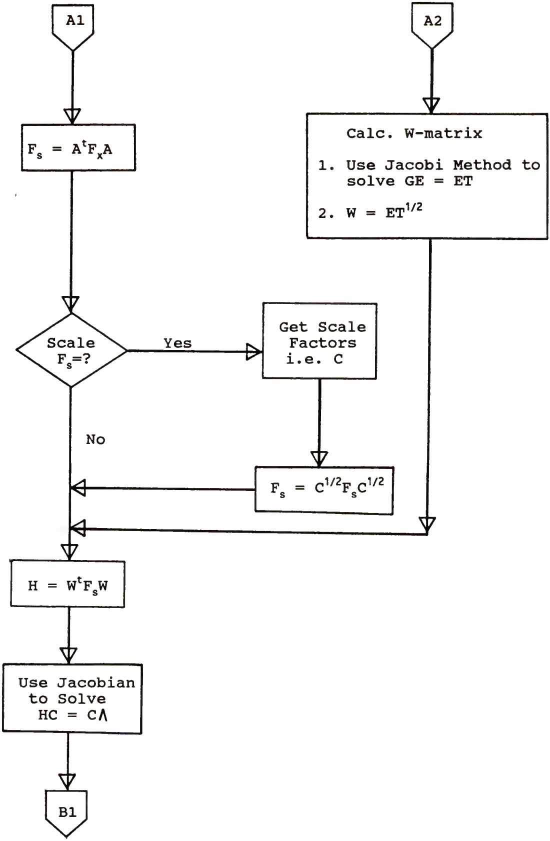
A1
A2
$F_s = A^t F_x A$
Calc. W-matrix
1. Use Jacobi Method to solve GE = ET
2. $W = ET^{1/2}$
Scale F_s=?
Yes
Get Scale Factors i.e. C
No
$F_s = C^{1/2} F_s C^{1/2}$
$H = W^t F_s W$
Use Jacobian to Solve $HC = C\Lambda$
B1

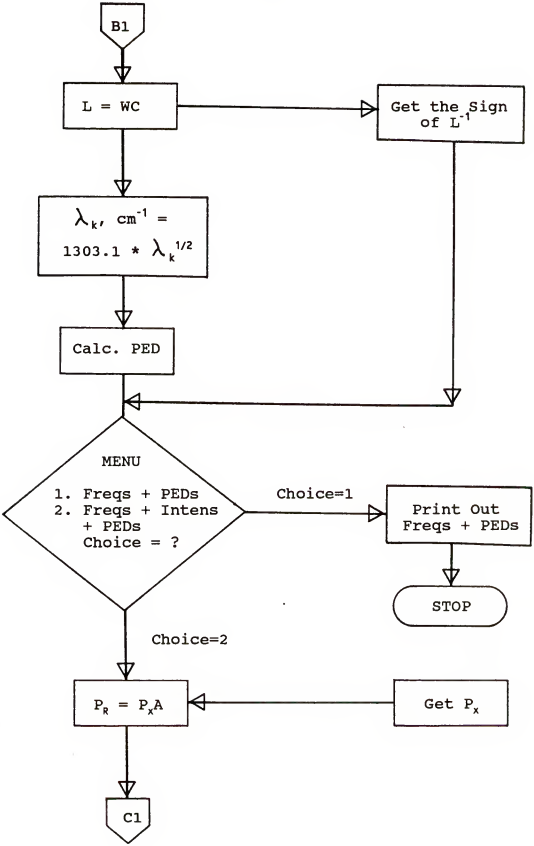
B1
L = WC
Get the Sign of L^{-1}
λ_k, cm^{-1} = 1303.1 * $\lambda_k^{1/2}$
Calc. PED
MENU
1. Freqs + PEDs
2. Freqs + Intens + PEDs
Choice = ?
Choice=1
Print Out Freqs + PEDs
STOP
Choice=2
$P_R = P_xA$
Get P_x
C1

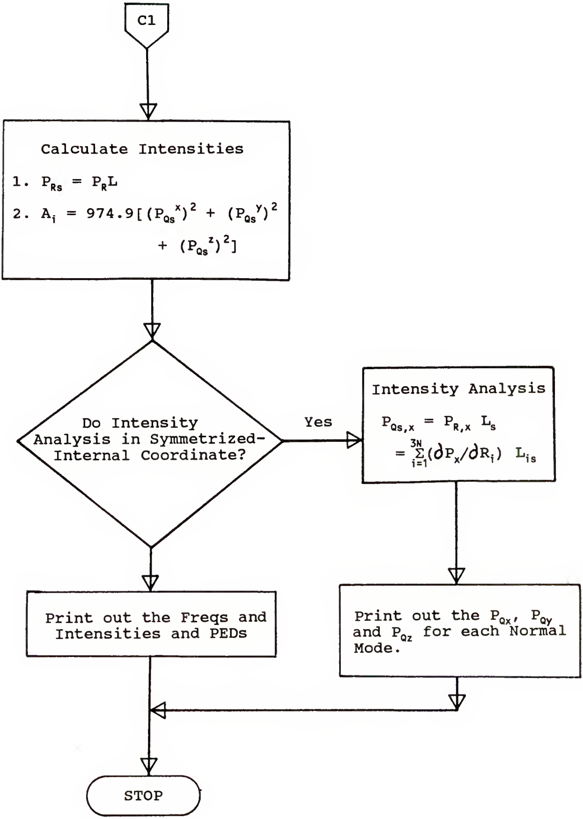
C1
Calculate Intensities
1. $P_{Rs} = P_R L$
2. $A_i = 974.9[(P_{Qs}^x)^2 + (P_{Qs}^y)^2 + (P_{Qs}^z)^2]$
Do Intensity Analysis in Symmetrized-Internal Coordinate?
Yes
Intensity Analysis
$P_{Qs,x} = P_{R,x} L_s = \sum_{i=1}^{3N}(\partial P_x/\partial R_i) L_{is}$
Print out the Freqs and Intensities and PEDs
Print out the P_{Qx}, P_{Qy} and P_{Qz} for each Normal Mode.
STOP

APPENDIX C

COMPONENTS OF DIPOLE MOMENT DERIVATIVES WITH RESPECT TO INTERNAL COORDINATES (P_R) FOR 2-CHLOROETHANETHIOL CALCULATED AT THE 6-31G** LEVEL.

			P_R (e)	
		X	Y	Z
1	S(CH2) s-str	0.0729	0.0000	-0.1040
2	S(CH2) sciss	0.0375	0.0000	0.0268
3	S(CH2) a-str	0.0000	-0.0803	0.0000
4	S(CH2) rock	0.0000	0.1472	0.0000
5	S(CH2) wag	0.0262	0.0000	-0.1165
6	S(CH2) twist	0.0000	0.0451	0.0000
7	SCC def	0.2980	0.0000	0.2038
8	Cl(CH2) s-str	-0.0569	0.0000	0.0823
9	Cl(CH2) sciss	-0.0420	0.0000	-0.0154
10	Cl(CH2) a-str	0.0000	-0.0495	0.0000
11	Cl(CH2) rock	0.0000	0.1155	0.0000
12	Cl(CH2) wag	0.0349	0.0000	-0.0907
13	Cl(CH2) twist	0.0000	-0.0586	0.0000
14	CCCl def	-0.3498	0.0000	-0.1513
15	C-Cl str	-0.1783	0.0000	-0.7760
16	C-S str	0.0225	0.0000	0.2267
17	C-C str	0.0521	0.0000	0.0208
18	H-S tors	0.0000	0.2005	0.0000
19	C-C tors	0.0000	0.2117	0.0000
20	HSC bend	-0.1166	0.0000	0.0582
21	S-H str	0.0915	0.0000	0.0507

APPENDIX D
INVARIANTS OF ATOMIC POLAR TENSORS

APPENDIX D-1
MASS-WEIGHTED SQUARED EFFECTIVE CHARGES ($3\ \chi^2/m$, in e^2u^{-1}) FOR ALL ATOMS OF CH_3CH_2S- FRAGMENTS

	EtSH				diethyl sulfide	mono-chloro-DS
	gauche		trans		trans	trans
Atoms	6-31G**	3-21G	6-31G**	3-21G	3-21G	3-21G
S-1	0.006	0.010	0.005	0.009	0.010	0.010
C-2	0.030	0.040	0.031	0.040	0.028	0.041
C-3	0.003	0.002	0.004	0.001	0.002	0.004
H-4	0.054	0.080	0.052	0.081	--	--
H-5	0.020	0.014	0.042	0.030	0.029	0.027
H-6	0.041	0.030	0.042	0.030	0.029	0.027
H-7	0.033	0.029	0.029	0.027	0.028	0.028
H-8	0.027	0.025	0.029	0.027	0.028	0.028
H-9	0.055	0.044	0.044	0.037	0.046	0.042

APPENDIX D-2
MASS-WEIGHTED SQUARED EFFECTIVE CHARGES
(3 X^2/m, in e^2u^{-1}) FOR ALL ATOMS OF $ClCH_2CH_2S$- FRAGMENTS

	ClEtSH		mustard	mono-chloro-DS
	trans		trans	trans
Atoms	6-31G**	3-21G	3-21G	3-21G
S-1	0.005	0.007	0.010	0.010
C-2	0.019	0.022	0.019	0.010
C-3	0.091	0.103	0.112	0.122
H-4	0.047	0.073	--	--
H-5/6	0.025	0.019	0.015	0.015
H-7/8	0.017	0.016	0.017	0.017
Cl-9	0.022	0.027	0.031	0.033

APPENDIX D-3
MEAN DIPOLE MOMENT DERIVATIVES ($\bar{P}$, in e) FOR ALL ATOMS OF CH_3CH_2S- FRAGMENTS

	EtSH				diethyl sulfide	mono-chloro-DS
	gauche		trans		trans	trans
Atoms	6-31G**	3-21G	6-31G**	3-21G	3-21G	3-21G
S-1	-0.157	-0.208	-0.155	-0.203	-0.289	-0.274
C-2	0.253	0.250	0.255	0.254	0.203	0.223
C-3	0.088	-0.007	0.109	0.021	0.029	0.021
H-4	-0.003	-0.003	-0.006	-0.009	--	--
H-5	-0.025	0.006	-0.068	-0.044	-0.047	-0.041
H-6	-0.066	-0.042	-0.068	-0.044	-0.047	-0.041
H-7	-0.030	-0.001	-0.017	0.015	0.013	0.018
H-8	-0.016	0.014	-0.017	0.015	0.013	0.018
H-9	-0.044	-0.009	-0.033	-0.003	-0.019	-0.014

APPENDIX D-4
MEAN DIPOLE MOMENT DERIVATIVES ($\bar{P}$, in e) FOR ALL ATOMS OF $ClCH_2CH_2S$- FRAGMENTS

	ClEtSH		mustard	mono-chloro-DS
	trans		trans	trans
Atoms	6-31G**	3-21G	3-21G	3-21G
S-1	-0.136	-0.169	-0.264	-0.274
C-2	0.197	0.173	0.135	0.109
C-3	0.469	0.469	0.502	0.515
H-4	0.005	0.005	--	--
H-5/6	-0.038	-0.010	-0.011	-0.014
H-7/8	-0.024	0.006	0.007	0.003
Cl-9	-0.411	-0.470	-0.496	-0.511

APPENDIX D-5
ANISOTROPY VALUES (ß, in e) FOR ALL ATOMS OF CH_3CH_2S- FRAGMENTS

	EtSH				diethyl sulfide	mono-chloro-DS
	gauche		trans		trans	trans
Atoms	6-31G**	3-21G	6-31G**	3-21G	3-21G	3-21G
S-1	0.400	0.516	0.375	0.496	0.288	0.404
C-2	0.502	0.650	0.509	0.661	0.566	0.713
C-3	0.154	0.180	0.131	0.142	0.200	0.260
H-4	0.286	0.348	0.281	0.350	--	--
H-5	0.168	0.145	0.208	0.192	0.186	0.182
H-6	0.207	0.193	0.208	0.192	0.186	0.182
H-7	0.216	0.210	0.206	0.198	0.205	0.202
H-8	0.200	0.193	0.206	0.198	0.205	0.202
H-9	0.273	0.258	0.248	0.237	0.261	0.249

APPENDIX D-6
ANISOTROPY VALUES (ß, in e) FOR ALL ATOMS OF $ClCH_2CH_2S$- FRAGMENTS

	ClEtSH		mustard	mono-chloro-DS
	trans		trans	trans
Atoms	6-31G**	3-21G	3-21G	3-21G
S-1	0.370	0.457	0.416	0.404
C-2	0.419	0.513	0.508	0.363
C-3	0.799	0.926	0.942	0.999
H-4	0.265	0.332	--	--
H-5/6	0.175	0.167	0.149	0.145
H-7/8	0.151	0.153	0.157	0.159
Cl-9	0.615	0.654	0.739	0.753

APPENDIX D-7

EFFECTIVE CHARGES (X, in e) FOR ALL ATOMS OF CH_3CH_2S- FRAGMENTS

	EtSH				diethyl sulfide	mono-chloro-DS
	gauche		trans		trans	trans
Atoms	6-31G**	3-21G	6-31G**	3-21G	3-21G	3-21G
S-1	0.245	0.320	0.235	0.310	0.319	0.334
C-2	0.347	0.395	0.350	0.402	0.335	0.403
C-3	0.114	0.085	0.126	0.070	0.099	0.124
H-4	0.135	0.164	0.132	0.165	--	--
H-5	0.083	0.069	0.119	0.101	0.099	0.095
H-6	0.118	0.100	0.119	0.101	0.099	0.095
H-7	0.106	0.099	0.099	0.094	0.097	0.097
H-8	0.096	0.092	0.099	0.094	0.097	0.097
H-9	0.136	0.122	0.122	0.112	0.124	0.118

APPENDIX D-8
EFFECTIVE CHARGES (X, in e) FOR ALL ATOMS OF $ClCH_2CH_2S-$ FRAGMENTS

	ClEtSH		mustard	mono-chloro-DS
	trans		trans	trans
Atoms	6-31G**	3-21G	3-21G	3-21G
S-1	0.221	0.274	0.329	0.334
C-2	0.279	0.297	0.275	0.203
C-3	0.602	0.640	0.670	0.698
H-4	0.125	0.157	--	--
H-5/6	0.091	0.079	0.071	0.070
H-7/8	0.075	0.073	0.074	0.075
Cl-9	0.503	0.562	0.606	0.622

APPENDIX D-9
CUBIC ROOTS OF POLAR TENSORS DETERMINANT ($\sqrt[3]{D}$, in e) FOR ALL ATOMS OF CH_3CH_2S- FRAGMENTS

	EtSH				diethyl sulfide	mono-chloro-DS
	gauche		trans		trans	trans
Atoms	6-31G**	3-21G	6-31G**	3-21G	3-21G	3-21G
S-1	0.197	0.258	0.192	0.257	-0.254	-0.198
C-2	0.185	0.103	0.140	-0.156	-0.190	-0.227
C-3	0.085	0.039	0.114	0.045	0.062	0.058
H-4	0.101	0.092	0.112	0.117	--	--
H-5	0.053	0.022	0.085	0.082	0.084	0.084
H-6	0.086	0.081	0.085	0.082	0.084	0.084
H-7	-0.049	-0.074	-0.062	-0.084	-0.086	-0.087
H-8	-0.061	-0.081	-0.062	-0.084	-0.086	-0.087
H-9	-0.068	-0.097	-0.069	-0.094	-0.089	-0.085

APPENDIX D-10
CUBIC ROOTS OF POLAR TENSOR DETERMINANT ($\sqrt[3]{D}$, in e) FOR ALL ATOMS OF $ClCH_2CH_2S$- FRAGMENTS

	ClEtSH		mustard	mono-chloro-DS
	trans		trans	trans
Atoms	6-31G**	3-21G	3-21G	3-21G
S-1	0.187	0.233	-0.165	-0.198
C-2	0.108	-0.126	-0.187	-0.148
C-3	0.346	0.304	0.341	0.339
H-4	0.111	0.127	--	--
H-5/6	0.065	0.048	0.060	0.061
H-7/8	0.053	-0.041	-0.048	-0.041
Cl-9	-0.327	-0.387	-0.399	-0.412

APPENDIX D-11
SQUARE ROOTS OF THE SUMS OF THE POLAR TENSOR MINORS ($\sqrt{C}$, in e) FOR ALL ATOMS OF CH_3CH_2S- FRAGMENTS

	EtSH				diethyl sulfide	mono-chloro-DS
	gauche		trans		trans	trans
Atoms	6-31G**	3-21G	6-31G**	3-21G	3-21G	3-21G
S-1	0.153	0.212	0.162	0.207	0.472	0.420
C-2	0.360	0.260	0.340	0.235	0.131	0.114
C-3	0.145	0.077	0.191	0.029	0.061	0.045
H-4	0.128	0.172	0.138	0.179	--	--
H-5	0.085	0.082	0.023	0.080	0.060	0.064
H-6	0.026	0.082	0.023	0.080	0.060	0.064
H-7	0.103	0.109	0.107	0.104	0.107	0.102
H-8	0.105	0.102	0.107	0.104	0.107	0.102
H-9	0.137	0.146	0.131	0.137	0.147	0.142

APPENDIX D-12

SQUARE ROOTS OF THE SUMS OF THE POLAR TENSOR MINORS ($\sqrt{C}$, in e) FOR ALL ATOMS OF THE $ClCH_2CH_2S$- FRAGMENTS

	ClEtSH		mustard	mono-chloro-DS
	trans		trans	trans
Atoms	6-31G**	3-21G	3-21G	3-21G
S-1	0.115	0.142	0.390	0.420
C-2	0.269	0.143	0.178	0.084
C-3	0.671	0.612	0.679	0.680
H-4	0.127	0.166	--	--
H-5/6	0.073	0.092	0.081	0.079
H-7/8	0.074	0.084	0.087	0.089
Cl-9	0.618	0.723	0.751	0.775

APPENDIX E
MULLIKEN NET ATOMIC CHARGES

APPENDIX E-1
MULLIKEN NET ATOMIC CHARGES (q, in e) CALCULATED FOR ALL ATOMS OF CH_3CH_2S- FRAGMENTS

	EtSH				diethyl sulfide	mono-chloro-DS
	gauche		trans		trans	trans
Atoms	6-31G**	3-21G	6-31G**	3-21G	3-21G	3-21G
S-1	-0.021	0.021	-0.021	0.016	0.251	0.261
C-2	-0.374	-0.667	-0.362	-0.659	-0.669	-0.664
C-3	-0.327	-0.585	-0.350	-0.596	-0.595	-0.599
H-4	0.045	0.064	0.043	0.064	--	--
H-5	0.155	0.261	0.148	0.251	0.240	0.248
H-6	0.151	0.254	0.148	0.251	0.240	0.248
H-7	0.117	0.209	0.134	0.227	0.223	0.227
H-8	0.134	0.228	0.134	0.227	0.223	0.227
H-9	0.120	0.215	0.126	0.219	0.214	0.221

APPENDIX E-2
MULLIKEN NET ATOMIC CHARGES (q, in E) CALCULATED FOR ALL ATOMS OF $ClCH_2CH_2S$- FRAGMENTS

	ClEtSH		mustard	mono-chloro-DS
	trans		trans	trans
Atoms	6-31G**	3-21G	3-21G	3-21G
S-1	-0.009	0.036	0.272	0.261
C-2	-0.368	-0.660	-0.663	-0.669
C-3	-0.305	-0.533	-0.537	-0.528
H-4	0.058	0.085	--	--
H-5/6	0.173	0.282	0.277	0.270
H-7/8	0.186	0.296	0.295	0.292
Cl-9	-0.095	-0.083	-0.081	-0.097

APPENDIX F
VALUES OF ALPHA [OR ($\sqrt{2/3}$)ß/X)]

APPENDIX F-1
VALUES OF ALPHA [OR ($\sqrt{2/3}$)β/X] FOR ALL ATOMS OF CH_3CH_2S- FRAGMENTS

	EtSH				diethyl sulfide	mono-chloro-DS
	gauche		trans		trans	trans
Atoms	6-31G**	3-21G	6-31G**	3-21G	3-21G	3-21G
S-1	0.770	0.760	0.752	0.754	0.426	0.570
C-2	0.682	0.776	0.686	0.775	0.796	0.834
C-3	0.637	0.998	0.490	0.956	0.952	0.988
H-4	0.999	1.000	1.004	1.000	--	--
H-5	0.954	0.991	0.824	0.896	0.886	0.903
H-6	0.827	0.910	0.824	0.896	0.886	0.903
H-7	0.961	1.000	0.981	0.993	0.996	0.982
H-8	0.982	0.989	0.981	0.993	0.996	0.982
H-9	0.946	0.997	0.958	0.998	0.992	0.995

APPENDIX F-2
VALUES OF ALPHA [OR ($\sqrt{2/3}$)β/X] FOR ALL ATOMS OF $ClCH_2CH_2S$- FRAGMENTS

	ClEtSH		mustard	mono-chloro-DS
	trans		trans	trans
Atoms	6-31G**	3-21G	3-21G	3-21G
S-1	0.789	0.786	0.596	0.570
C-2	0.708	0.814	0.871	0.843
C-3	0.626	0.682	0.663	0.675
H-4	0.999	0.997	--	--
H-5/6	0.907	0.997	0.989	0.976
H-7/8	0.949	0.988	1.000	0.999
Cl-9	0.576	0.549	0.575	0.571

APPENDIX G
VALUES OF GAMMA (OR $\overline{P}/X$)

APPENDIX G-1
VALUES OF GAMMA (OR $\overline{P}/X$) FOR ALL ATOMS OF CH_3CH_2S- FRAGMENTS

	EtSH				diethyl sulfide	mono-chloro-DS
	gauche		trans		trans	trans
Atoms	6-31G**	3-21G	6-31G**	3-21G	3-21G	3-21G
S-1	-0.641	-0.650	-0.660	-0.655	-0.906	-0.820
C-2	0.729	0.633	0.729	0.632	0.606	0.553
C-3	0.772	-0.082	0.865	0.300	0.293	0.169
H-4	-0.022	-0.018	-0.045	-0.055	--	--
H-5	-0.301	0.087	-0.571	-0.436	-0.475	-0.432
H-6	-0.559	-0.420	-0.571	-0.436	-0.475	-0.432
H-7	-0.283	-0.010	-0.172	0.160	0.134	0.186
H-8	-0.167	0.152	-0.172	0.160	0.134	0.186
H-9	-0.324	-0.074	-0.270	-0.027	-0.153	-0.119

APPENDIX G-2
VALUES OF GAMMA (OR $\bar{P}/X$) FOR ALL ATOMS OF $ClCH_2CH_2S-$ FRAGMENTS

	ClEtSH		mustard	mono-chloro-DS
	trans		trans	trans
Atoms	6-31G**	3-21G	3-21G	3-21G
S-1	-0.615	-0.617	-0.802	-0.820
C-2	0.706	0.582	0.491	0.537
C-3	0.779	0.733	0.749	0.738
H-4	0.040	0.032	--	--
H-5/6	-0.418	-0.127	-0.155	-0.200
H-7/8	-0.320	0.082	0.095	0.040
Cl-9	-0.817	-0.836	-0.818	-0.822

REFERENCES

1. J. H. Schachtschneider and R. G. Snyder, Spectrochim. Acta, 19, 117 (1963).

2. W. B. Person in "Vibrational Intensities in Infrared and Raman Spectroscopy," W. B. Person and G. Zerbi, Eds. (Elsevier Scientific Publishing Co., Amsterdam, 1982), Chap. 4.

3. W. T. King and G. B. Mast, J. Mol. Spectrosc., 80, 2521 (1976).

4. J. C. Decius and G. B. Mast, J. Mol. Spectrosc., 70, 294 (1978).

5. J. C. Decius, J. Mol. Spectrosc., 57, 348 (1975).

6. M. Gussoni and S. Abbate, J. Chem. Phys., 65, 3439 (1976).

7. L. A. Gribov, "Intensity Theory for Infrared Spectra of Polyatomic Molecules" (English translation) (Consultants Bureau, New York, 1964).

8. J. F. Biarge, J. Herranz, and J. Morcillo, An. R. Soc. Esp. Fis. Quim., A57, 81 (1961).

9. W. B. Person and J. H. Newton, J. Chem. Phys., 61, 1040 (1974); 64, 3036 (1976).

10. R. J. Bartlett in "Geometrical Derivatives of Energy Surfaces and Molecular Properties," P. Jorgensen and J. Simons, Eds. (NATO ASI series; D. Reidel: Boston, 1986) p 35.

11. W. J. Hehre, L. Radom, P. V. R. Schleyer, and J. A. Pople, "Ab Initio Molecular Orbital Theory" (Wiley: New York, 1985).

12. G. Fogarasi and P. Pulay in "Vibrational Spectra and Structure," J. R. Durig, Ed. (Elsevier: Amsterdam, 1985) Vol. 14 and references therein.

13. J. A. Pople, H. B. Schlegel, R. Krishnan, D. J. DeFrees, J. S. Binkley, M. J. Frisch, and R. A. Whiteside, R. F. Hout and W. J. Hehre, Int. J. Quantum Chem., S15, 269 (1981).

14. C. Sosa, R. J. Bartlett, K. KuBulat, and W. B. Person, J. Phys. Chem., 93, 577 (1989).

15. G. S. Pearson, Chemistry in Britain, 24 (7), 657 (1988).

16. L. Leadbeater, Chemistry in Britain, 24 (7), 683 (1988).

17. S. D. Christesen, private communication.

18. C. Sosa, R. J. Bartlett, K. KuBulat, W. B. Person, and S. D. Christesen, unpublished manuscript.

19. C. Sosa, R. J. Bartlett, K. KuBulat, and W. B. Person, unpublished manuscript.

20. M. Ohta, Y. Ogawa, H. Matsuura, I. Harada and T. Shimanouchi, Bull. Chem. Soc. Jpn., 50, 380 (1977).

21. L. D. Hoffland, R. J. Piffath, and J. B. Bouck, Opt. Eng., 24 (6), 982 (1985).

22. T. Shimanouchi, Y. Ogawa, M. Ohta, H. Matsuura, and I. Harada, Bull. Chem. Soc. Jpn., 49, 2999 (1976).

23. M. Hayashi, Y. Shiro, M. Murakami, and H. Murata, Bull. Chem. Soc. Jpn., 38, 1740 (1965).

24. (a) R. G. Azrak and E. B. Wilson, J. Chem. Phys., 52, 5299 (1970).
(b) A. Almenningen, O. Bastiansen, L. Fernholt, and K. Hedberg, Acta Chem. Scand., 25, 1946 (1971).

25. M. Hayashi, H. Imaishi, and K. Kuwada, Bull. Chem. Soc. Jpn., 47, 2382 (1974).

26. J. Nakagawa, K. Kuwada, and M. Hayashi, Bull. Chem. Soc. Jpn., 49, 3420 (1976).

27. R. E. Schmidt and C. R. Quade, J. Chem. Phys., 62, 3864 (1975).

28. D. Smith, J. P. Devlin, and D. W. Scott, J. Mol. Spectrosc., 25, 174 (1968).

29. D. W. Scott and G. A. Crowder, J. Mol. Spectrosc., 26, 477 (1968).

30. F. Inagaki, I. Harada, and T. Shimanouchi, J. Mol. Spectrosc., 46, 381 (1973).

31. M. Ohsaku, J. Mol. Struct., 138, 283 (1986).

32. J. P. McCullough, H. L. Finke, D. W. Scott, M. E. Gross, J. F. Messerly, R. E. Pennington, and G. Waddington, J. Am. Chem. Soc., 76, 4796 (1954).

33. P. Pulay in "Modern Theoretical Chemistry," H. F. Schaefer III, Ed. (Plenum Press, New York, 1977), Vol. 4.

34. W. B. Person and K. KuBulat, J. Mol. Struct., 173, 357 (1988).

35. W. B. Person and J. Overend, J. Chem. Phys. 66, 1443 (1977); B. J. Kroh, W. B. Person, and J. Overend, J. Chem. Phys., 65, 969 (1976).

36. B. B. Neto, M. N. Ramos, and R. E. Bruns, J. Chem. Phys., 85, 4515 (1986).

37. I. Scott-Lebron, Ph.D. Dissertation, University of Florida, 1986.

38. P. J. Zavala, Ph.D. Dissertation, University of Florida, 1988.

39. B. B. Neto, M. M. C. Ferreira, and R. E. Bruns, private communication between W. B. Person and R. E. Bruns.

40. W. B. Person and K. KuBulat, unpublished manuscript.

41. J. A. Pople, R. Krishnan, H. B. Schlegel, and J. S. Binkley, Int. J. Quantum Chem., S13, 225 (1979).

42. J. S. Binkley, J. A. Pople, and W. J. Hehre, J. Am. Chem. Soc., 102, 939 (1980).

43. (a) P. C. Hariharan and J. A. Pople, Chem. Phys. Lett., 66, 217 (1972).
(b) M. M. Francl, W. J. Pietro, W. J. Hehre, J. S. Binkley, M. S. Gordon, D. J. DeFrees, and J. A. Pople, J. Chem. Phys., 77, 3654 (1982).

44. J. S. Binkley, M. J. Frisch, D. J. DeFrees, K. Raghavachari, R. A. Whiteside, H. B. Schlegel, E. M. Fluder, and J. A. Pople. GAUSSIAN 82. (Carnegie-Mellon University: Pittsburgh, 1983).

45. E. B. Wilson, J. C. Decius, and P. C. Cross "Molecular Vibrations" (McGraw-Hill, New York, 1955).

46. R. J. Bartlett, G. D. Purvis III, G. B. Fitzgerald, R. J. Harrison, Y. S. Lee, W. D. Laidig, S. J. Cole, D. H. Magers, E. A. Salter, G. W. Trucks, C. Sosa, M. Rittby, and S. Pal. ACES (Advanced Concepts in Electronic Structure). Quantum Theory Project, University of Florida: Gainesville, FL, 1987.

47. A. Komornicki and J. W. McIver, Jr., J. Chem, Phys., 70, 2014 (1979).

48. J. Gerratt and I. M. Mills, J. Chem. Phys., 49, 1719 (1968).

49. R. D. Amos, Chem. Phys. Lett., 108, 185 (1984).

50. Y. Yamaguchi, M. Frisch, J. Gaw, H. F. Schaefer, and J. S. Binkley, J. Chem. Phys., 84, 2262 (1986).

51. C. Sosa and H. B. Schlegel, J. Chem. Phys., 86, 6937 (1987).

52. S. Califano, "Vibrational States" (John Wiley and Sons, New York, 1976).

53. S. Chin, Ph.D. Dissertation, University of Florida, 1984.

54. T. Miyazawa, J. Chem. Phys., 29, 246 (1958).

55. W. B. Person and B. Crawford, Jr., J. Chem. Phys., 26, 1295 (1957).

56. J. H. Wilkinson, "The Algebraic Eigenvalue Problem," (Oxford University Press, 1965) p 266.

57. M. Szczesniak, K. Szczepaniak, J. S. Kwiatkowski, K. KuBulat, and W. B. Person, J. Am. Chem. Soc., 110, 8319 (1988).

58. T. Tipton, D. A. Stone, K. KuBulat, and W. B. Person, J. Phys. Chem., 93, 2917 (1989).

59. a) J. S. Kwiatkowski, K. KuBulat, W. B. Person, and R. J. Bartlett, J. Mol. Struct., in press.
b) W. B. Person, J. S. Kwiatkowski, K. KuBulat, and G. S. Sanchez, unpublished manuscript.

60. M. Szczesniak, K. Szczepaniak, J. Leszczynski, K. KuBulat, and W. B. Person, unpublished manuscript.

61. M. Szczesniak, K. Szczepaniak, A. Jaworski, K. KuBulat, and W. B. Person, unpublished manuscript.

62. G. Keresztury and G. Jalsovszky, J. Mol. Struct., 10, 304 (1971).

63. W. T. King in "Vibrational Intensities in Infrared and Raman Spectroscopy," W. B. Person and G. Zerbi, Eds. (Elsevier Scientific Publishing Co., Amsterdam, 1982), Chap. 6.

64. W. T. King, G. B. Mast, and P. P. Blanchette, J. Chem. Phys., 56, 440 (1972); 58, 1272 (1973).

65. a) K. KuBulat and W. B. Person, unpublished manuscript.
b) J. H. Schachtschneider, Technical Report, Shell Development Co. (Emerville, CA, 1969).

66. (a) T. Shimanouchi, H. Matsuura, Y. Ogawa, and I. Harada, J. Phys. Chem. Ref. Data, 7, 1323 (1978); 9, 1149 (1980).
(b) H. Matsuura and M. Tasumi in "Vibrational Spectra and Structure", J. R. Durig, Ed. (Amsterdam, 1983), Vol. 12.

67. D. C. McKean, J. E. Boggs, and L. Schafer, J. Mol. Struct., 116, 313 (1984).

68. E. E. Ball, M. A. Ratner, and J. R. Sabin, Chem. Scr., 12, 128 (1977), and references therein.

69. G. Fogarasi and P. Pulay, J. Mol. Struct., 141, 145 (1986).

70. P. Pulay, Mol. Phys., 17, 197 (1969).

71. P. Pulay and W. Meyer, J. Mol. Spectrosc., 40, 59 (1971).

72. C. E. Blom and C. Altona, Mol. Phys., 31, 1377 (1976).

73. F. Torok, A. Hegedus, K. Kosa, and P. Pulay, J. Mol. Struct., 32, 93 (1976).

74. G. Fogarasi and P. Pulay, J. Mol. Struct., 39, 275 (1977).

75. K. Pearson, Phil. Mag., 6(2), 559 (1901).

76. H. Hotelling, J. Edu. Psy., 24, 417 (1933).

77. S. Wold and K. Anderson, J. Chromatogr., 80, 43 (1973).

78. P. H. Weiner and J. F. Parcher, Anal. Chem., 45, 302 (1973).

79. R. N. Carey, S. Wold, and J. O. Westgard, Anal. Chem., 47, 1824 (1975).

80. SAS Institute Inc. "SAS^R User's Guide: Statistics, Version 5 Edition." Carey, NC: SAS Institute Inc., 1985.

81. O. M. Herrera, R. E. Bruns, and B. B. Neto, J. Chem. Phys., in press.

82. K. Kim and W. T. King, J. Chem. Phys., 80, 983 (1984).

BIOGRAPHICAL SKETCH

KuHalim Bin KuBulat was born in Sanglang (Perlis), Malaysia, on June 13, 1957. He completed high school at the Alam Shah Boarding School (Malaysia) in April, 1976. In April, 1980 he received a B.Sc.(Hons.) in chemistry from the University Kebangsaan Malaysia (UKM). He was employed as a chemist at the Malaysian Department of Chemistry from April, 1980 to December, 1980. He then joined the Faculty of Science (Department of Chemistry), UKM as an assistant lecturer. He entered the graduate school at the University of Florida and received his Ph.D. in physical chemistry in May, 1989. He is required to serve UKM upon completing his study. KuHalim KuBulat is married to Suraya Ibrahim.

I certify that I have read this study and that in my opinion it conforms to acceptable standards of scholarly presentation and is fully adequate, in scope and quality, as a dissertation for the degree of Doctor of Philosophy.

Willis B. Person, Chairman
Professor of Chemistry

I certify that I have read this study and that in my opinion it conforms to acceptable standards of scholarly presentation and is fully adequate, in scope and quality, as a dissertation for the degree of Doctor of Philosophy.

Alan Katritzky
Kenan Professor of Chemistry

I certify that I have read this study and that in my opinion it conforms to acceptable standards of scholarly presentation and is fully adequate, in scope and quality, as a dissertation for the degree of Doctor of Philosophy.

William Weltner, Jr.
Professor of Chemistry

I certify that I have read this study and that in my opinion it conforms to acceptable standards of scholarly presentation and is fully adequate, in scope and quality, as a dissertation for the degree of Doctor of Philosophy.

Robert J. Hanrahan
Professor of Chemistry

I certify that I have read this study and that in my opinion it conforms to acceptable standards of scholarly presentation and is fully adequate, in scope and quality, as a dissertation for the degree of Doctor of Philosophy.

Thomas L. Bailey

Thomas Bailey
Professor of Physics

This dissertation was submitted to the Graduate Faculty of the Department of Chemistry in the College of Liberal Arts and Sciences and to the Graduate School and was accepted as partial fulfillment of the requirements for the degree of Doctor of Philosophy.

MAY 1989

Dean, Graduate School